# Evaluation of Various References and Perturbation Terms of the Thermodynamic Perturbation Theory of the First Order

BY

MOHAMMED F. AL KHATER

A Thesis Presented to the
DEANSHIP OF GRADUATE STUDIES

**KING FAHD UNIVERSITY OF PETROLEUM & MINERALS**

DHAHRAN, SAUDI ARABIA

In Partial Fulfillment of the
Requirements for the Degree of

**MASTER OF SCIENCE**

**In**

**Chemical Engineering**

**May 2016**

KING FAHD UNIVERSITY OF PETROLEUM & MINERALS

DHAHRAN- 31261, SAUDI ARABIA

**DEANSHIP OF GRADUATE STUDIES**

This thesis, written by **MOHAMMED F. AL KHATER** under the direction of his thesis advisor and approved by his thesis committee, has been presented and accepted by the Dean of Graduate Studies, in partial fulfillment of the requirements for the degree of **MASTER OF SCIENCE IN CHEMICAL ENGINEERING.**

Dr. Nayef M. Al-Saifi

(Advisor)

Dr. Mohammed Ba-Shammakh
Department Chairman

Dr. Eid M. AL-Mutairi
(Member)

Dr. Salam A. Zummo
Dean of Graduate Studies

Dr. Housam Binous

(Member)

16/5/16

Date

عمادة الدراسات العليا
DEANSHIP OF GRADUATE STUDIES

*Dedicated to my family, friends and instructors.*

# Acknowledgments

First of all, I thank Allah for all his bounties including completing this work.

I would like to acknowledge my advisor Dr.Nayef AL-Saifi for his tremendous support and guidance during my research period. The knowledge and the skills he delivered to me helped me a lot in getting this work done.

I also thank my thesis committee members: Dr.Eid AL-Mutairi and Dr.Housam Binous for their support and guidance.

I want also to acknowledge my colleague Mr.Yousef AL-Sunni for his help and support in this work.

I would like to thank my father, my family and my friend Mr.Nayef Jalkhaf for their encouragement and support during my study.

Finally, I want to acknowledge King Fahd University of Petroleum and Minerals and the department of chemical engineering for facilitating this research.

# Table of contents

# List of tables

# List of figures

# Abstract

**Full Name : MOHAMMED FAHAD AL KHATER**

**Thesis Title : Evaluation of Various References and Perturbation Terms of the Thermodynamic Perturbation Theory of the First Order**

**Major Field : Chemical Engineering**

**Date of Degree : May, 2016**

Thermodynamic perturbation theories have been widely accepted as a platform of theory-based equations of state. In this work, the mathematical structure of Wertheim's first order thermodynamic perturbation theory (TPT1) is investigated for its role in the existence of the non-physical pressure-volume-temperature (PVT) behavior. The study is focused on references constructed based on Lennard-Jones and Mie potentials. Two versions of TPT1 are utilized for this purpose; namely the soft-SAFT and SAFT-VR Mie. In addition, a new version denoted by SAFT-LJ3 is constructed based on the Lennard-Jones model of (Mecke et al., 1996). The study is carried out by evaluating the volume root loci of the three models. The variation of volume root loci with temperature and pressure is illustrated using bifurcation diagrams. The bifurcation diagrams are generated by the arc-length continuation method with the aid of Wagon's method. The mathematical structures of these models are evaluated for spherical and non-spherical molecules. The SAFT-VR Mie equation of state is examined for the existence of multiple phase separation regions.

The study reveals that all the three models exhibit non-physical branches demonstrated in volume-temperature bifurcation diagrams at fixed pressure. Unlike the

SAFT-VR Mie, the soft-SAFT and SAFT-LJ3 models exhibit non-physical volume-temperature branches within the region of practical applications. The number of the non-physical branches is higher for non-spherical particles due to the addition of the chain part representing the size of particles. This problem is attributed to the empirical nature of the pair-correlation function at contact that is utilized in the chain term. Irrespective of the accuracy, the generated PVT behavior of the SAFT-LJ3 is more realistic that that of the soft-SAFT.

For spherical molecules, the SAFT-VR Mie exhibits higher non-physical branches compared to the SAFT-LJ3 and soft-SAFT although they are far from the practical region. The investigation of the SAFT-VR Mie reveals that the model is not free from exhibiting additional phase separation regions as it was expected. It was found that the SAFT-VR Mie accommodates an artificial phase separation region termed as liquid-solid demixing region due to the non-existence of its critical point. The study reveals that it is possible to discard all non-physical regions in the SAFT-VR Mie due to the fact that these regions are located above a packing fraction value of 0.494. In addition, the non-physical branches in the SAFT-LJ3 and soft-SAFT cannot be eliminated without a modification in the mathematical structure.

# ملخص الرسالة

**الاسم الكامل:** محمد بن فهد بن خاطر الخاطر.

**عنوان الرسالة:** تقييم لعدة حدود في نظرية الاضطراب من الدرجة الأولى.

**التخصص:** الهندسة الكيميائية.

**تاريخ الدرجة العلمية:** 2016 م

**تعتبر نظرية الاضطراب واحدة من أهم النظريات المستخدمة في علم الديناميكا الحرارية حيث اشتق منها عدة معادلات للحالة تعرف بمجموعها بنظريات الترابط الإحصائي للموائع. بالرغم من دقة هذه النظريات في حساب خصائص الموائع إلا أن هذه النظريات ولشدة تعقيد عباراتها الرياضية قد تؤدي إلى نتائج وهمية. هذا البحث يسلط الضوء على مجموعة من نظريات الترابط الإحصائي المبنية على نموذجي "لينارد جونز" و "ماي" للطاقة الكامنة للجزيئات. توصل البحث إلى أن جميع هذه النظريات تقوم بإعطاء نتائج وهمية للحجم المولي للموائع كما تم طرح بعض الحلول لتفادي هذه المشكلة عند استخدام هذه النظريات في برامج المحاكاة.**

# Chapter 1

## 1.1 Introduction

For long decades, the calculations of thermodynamic properties and phase equilibrium have been limited to simple empirical equations of state such as Soave-Redlich-Kwong (Soave, 1972) and Peng-Robinson equations of state (Peng & Robinson, 1976). Despite the fact that these models have extensively been used in both academic and industrial purposes, their narrow applicability has raised the demand for an alternative approach. For instance, these empirical models are unsuccessful for polar and associative mixtures. This is evident due to the fact that these semi-empirical models are limited to molecules with repulsion and dispersion interactions. The polar and associative interactions are more complex and cannot be treated empirically. This is why theoretical models, which are usually developed by statistical-mechanical approaches, have found growing attention. To account for polar and associative interactions in a proper way, it is first important to give accurate representation for repulsion and dispersion interactions.

Among various approaches in statistical mechanics, perturbation methods have shown immense interest among researchers due to its capability and flexibility to describe the molecular behavior for various interactions. Extensive work has been paid to perturbation theories which proved to be effective in improving the accuracy of thermodynamic properties calculations. Various perturbation theories have been proposed such as Barker-Henderson perturbation theory (Barker & Henderson, 1967), Weeks-Chandler-Anderson perturbation theory (WCA) (Weeks, Chandler, & Andersen, 1971) and Mansoori-Canfield (Mansoori & Canfield, 1969) and Rasaiah-Stell (Rasaiah & Stell, 1970)

perturbation theory (MCRS). Although these perturbation theories were successful, the main focus was also on repulsion and dispersion interactions. The problem of associative and other interactions remained without an efficient solution in perturbation theories.

In early eighties, Wertheim proposed an elegant perturbation theory (Wertheim, 1984b) which gave a proper treatment for association interactions and made the theory flexible to add other molecular interactions. The Wertheim's perturbation theory was extended by Chapman et al (Chapman, Gubbins, Jackson, & Radosz, 1989, 1990; Chapman, Jackson, & Gubbins, 1988) and resulted in the development of the so-called statistical association fluid theory (SAFT). Because of the flexibility of the Wertheim's perturbation theory, several versions of SAFT have been proposed by adopting various references and perturbation terms. For instance, the reference terms were hard sphere in CK-SAFT (Stanley H Huang & Maciej Radosz, 1990) and original SAFT (Chapman et al., 1990), hard-chain in PC-SAFT (Gross & Sadowski, 2001) and Lenard-Jones in soft-SAFT (F. J. Blas & Vega, 1997).

The use of a reference term in perturbation theories implies the availability of an accurate model and pair correlation function that represent the reference term. For instance, accurate and simple models and pair-correlation functions are available for hard sphere system (Carnahan & Starling, 1969; Goldman & White, 1988; Khoshkbarchi & Vera, 1997; Malijevsky & Veverka, 1999; Rambaldi, Salustri, & Benedetti, 2006; Wang, 2002; L. V. Yelash & Kraska, 2001). The hard sphere model is described, for example, by Carnahan-Starling equation of state (Carnahan & Starling, 1969) which proved to be accurate when compared to exact molecular simulation data. Similarly, an accurate pair-correlation function that describes the hard sphere system is available from the Percus-Yevick theory

(Percus & Yevick, 1958). These features of hard sphere systems do not exist for any other references. An exact pair-correlation function or model for Lennard-Jones doesn't exist although extensive effort has been paid for this purpose (Tang & Lu, 1997; Tang, Tong, & Lu, 1997). This is why many researchers shifted their attention to empirical methods to develop a Lennard-Jones model such as (J. K. Johnson, Zollweg, & Gubbins, 1993; Kolafa & Nezbeda, 1994; Lisal, Aim, Mecke, & Fischer, 2004; Mecke et al., 1996)

The use of these empirical models with the Wertheim's first order perturbation theory has shown improvement in the calculations of phase equilibria and thermodynamic properties (F. J. Blas & Vega, 1997; Kraska & Gubbins, 1996). This is expected due to the fact that the accuracy of any perturbation theory improves as the reference term could accurately describe the molecule interactions between molecules. For example, non-polar molecules accommodate repulsion and dispersion. The hard sphere reference represents only the repulsive term while the Lennard-Jones model describes both repulsion and dispersion.

However, the empirical nature of these the Lennard-Jones references is not expected to be without consequences. For example, due to the empirical approximation in the mathematical form of the dispersion term in the PC-SAFT EOS (Gross & Sadowski, 2001) which is based on square-well potential, it was found that the model exhibits multiple phase separation regions in addition to the ordinary phase separation region (Privat, Conte, Jaubert, & Gani, 2012; Privat, Gani, & Jaubert, 2010; L. Yelash, Müller, Paul, & Binder, 2005). Non-physical pressure-temperature-volume behavior has also found in the CK-SAFT (Stanley H Huang & Maciej Radosz, 1990) and simplified SAFT (Fu & Sandler, 1995) equations of state due to the empirical approximation in the dispersion term (Isa,

2015). This led to the increase of the number of the non-physical of volume roots in these models (Polishuk, 2010).

In this work, various Lennard-Jones models, namely soft-SAFT, SAFT-LJ3 which is developed in this work and based on (Mecke et al., 1996) and SAFT-VR Mie-LJ (12-6) have been investigated. Both soft-SAFT and SAFT-LJ3 are based on fitting of molecular simulation data and they adopt the same chain term (K. Johnson, Muller, & Gubbins, 1994). On the other hand, SAFT-VR Mie-LJ, which is a special case of the popular recent SAFT-VR Mie equation of state (Lafitte et al., 2013), is a more theory based model. Due to its flexibility and high accuracy compared to others, SAFT-VR Mie equation of state is given more attention in this work. The models analysis implemented in this work will mainly depend on the concept of generating the bifurcation diagrams of different components for each model and observing any non-physical solution behavior.

## 1.2 Objectives of this work

a) To study the mathematical structure of various reference and perturbation terms in TPT1.

b) To investigate the effect of different reference and perturbation terms on the solution behavior.

c) To compare the solution behavior of soft-SAFT, SAFT-LJ3 and SAFT-VR Mie-LJ equations of state.

d) To investigate the unrealistic PVT behavior for each SAFT model by constructing bifurcation diagrams.

e) To determine the range of applicability of each model.

f) To propose guidelines for obtaining safe results from using the SAFT models.

g) To suggest a criteria for efficient use of SAFT-VR Mie equation of state.

## 1.3 Approach

The various versions of the SAFT equation of state are coded using Wolfram Mathematica© and Matlab©. The adjustable parameters in each model are then determined for several components by fitting the model to experimental PVT data using an optimization code that adopts Simplex method. After that, the models, with the aid of arc-length continuation method, are used to generate the bifurcation diagrams of two classes of components: spherical and non-spherical. These bifurcation diagrams will give the full picture of the solution behavior of the SAFT models since they visualize the locus of the PVT solution of these models. After that, the bifurcation diagrams of various SAFT models are compared and the non-physical solution behavior is detected in each model. Based on this analysis, the range of applicability of each model is determined. Finally, some numerical techniques for avoiding the non-physical solutions are proposed.

## 1.4 The scope of the work

This work should give the awareness of the non-physical solution behavior issue associated with soft-SAFT, SAFT-LJ3 and SAFT-VR Mie-LJ equations of state. It clarifies the possible situations where these models could provide misleading results in phase equilibrium and thermodynamic properties calculations. Furthermore, the conclusions of this work should help in implementing these models in process simulators and using them efficiently without the need to determine all volume roots and to test their stabilities. Finally, this work addresses the room of improvement in SAFT equations of state that are based on Lennard-Jones.

## 1.5 Thesis organization

### 1.5.1 Chapter 2: First order thermodynamic perturbation theories (TPT1)

In this chapter, the fundamentals of perturbation theories are introduced and the application to statistical mechanics is clarified by a simple example of second virial coefficient calculation. Different thermodynamic perturbation theories and their applications in the literature are summarized. The mathematical structure of the first order thermodynamic perturbation theories is also explored. Finally, the expressions of the selected models are reported.

### 1.5.2 Chapter 3: Reliable techniques for the determination of volume root loci from complex thermodynamic models

This chapter summarizes the mathematical and numerical methods used in the analysis of the solution behavior of SAFT equations of state. It first starts by introducing the idea of the bifurcation diagrams and their interpretation. After that, the arc-length continuation method, which is a numerical method used to solve parametrized non-linear equations, is explained. Finally, a systematic algorithm for finding all the solutions of a non-linear equation is proposed and clarified by a simple example.

### 1.5.3 Chapter 4: Solution behavior of different LJ models

The analysis of the solution behavior of the selected Lennard-Jones models is conducted in this chapter. The bifurcation diagrams of both spherical and non-spherical components are generated and analyzed for the studied LJ models. The non-physical volume roots and two-phase regions are determined in each model. Finally, the effect of pressure on the solution behavior of these models is investigated.

### 1.5.4 Chapter 5: Solution behavior of SAFT-VR Mie EOS

The solution behavior of the general form of the SAFT-VR Mie equation of state is investigated in this chapter. The effect of the repulsive exponent in the Mie potential on the solution behavior is demonstrated.

### 1.5.5 Chapter 6: Conclusions and recommendations

This chapter summarizes the work stating the conclusions made about the solution behavior of the studied models. It also suggests some recommendations for making a safe and efficient use of these models.

# Chapter 2

# First order thermodynamic perturbation theories (TPT1)

## 2.1 Introduction

The development of equations of state has a long history. Since van der waals work, the equation of state has passed through many improvements. RK, SRK and Peng Robinson equations of state are examples of these improvements. Despite the fact that these models are still widely used, they do have serious limitations. For instance, these models are not applicable for polar and associative mixtures. For that reason, more accurate models have been proposed and they are mainly developed based on perturbation theories. The perturbation theories are the most commonly used approach to develop thermodynamic models.

During the past decades, many perturbation theories such as Barker-Henderson perturbation theory (Barker & Henderson, 1967), Weeks-Chandler-Anderson perturbation theory (WCA) (Weeks et al., 1971) and Mansoori-Canfield (Mansoori & Canfield, 1969) and Rasaiah-Stell (Rasaiah & Stell, 1970) perturbation theory (MCRS). The application of these theories was limited due to the fact that the proposed perturbation theories at that time only described the hard-core and dispersion terms, which are available in cubic equations of state. In fact, these theories are not expected to add a remarkable improvement to the calculations of thermodynamic properties and phase equilibrium compared to the well-known cubic equations of state which describe the properties of non-polar mixtures with reasonable accuracy.

In 1982, an elegant perturbation theory was proposed by considering the association interactions (Wertheim, 1984b). Such a theory represents a major improvement in thermodynamic modeling because the association interactions have not successfully been considered in the previous perturbation theories. The Wertheim's perturbation theory overcame the main challenge associated with previous models that were unable to provide reasonable approximation for association interactions. . The theory was extended by (Chapman et al., 1989, 1990) and resulted in the development of the so-called statistical association fluid theory (SAFT). The SAFT theory was accurately able to predict the properties of non-polar, polar, polymer and association mixtures. **Table 2.1** summarizes a broad range of SAFT applications to various kinds of mixtures. The success of the SAFT theory made it a good alternative to the empirical equations of state.

Because (Wertheim, 1984a, 1984b, 1986a, 1986b) made his theory general without specifying the reference or perturbation terms, various SAFT versions have appeared such as the original SAFT (Chapman et al., 1989), CK-SAFT (S. H. Huang & M. Radosz, 1990, 1991), simplified-SAFT (Fu & Sandler, 1995), soft-SAFT (F. J. Blas & Vega, 1997), Variable-Range-SAFT (SAFT-VR) (Gil-Villegas, Galindo, Whitehead, Jackson, & Burgess, 1997), SAFT-Yukawa dipole-dipole (SAFT-YDD) (Z.-P. Liu, Li, & Chan, 2001), Perturbed-Chain-SAFT (PC-SAFT) (Gross & Sadowski, 2001, 2002) and SAFT-VR Mie (Lafitte et al., 2013). The main difference between the various versions of the SAFT equation of state is the definition of the reference and perturbation terms.

The appearance of many versions of the SAFT equation of state raises questions about accuracy, applications and limitations of each version. The mathematical complexity and the increasing number of these models make it a difficult task to evaluate all these

models. However, these models could be classified according to their perturbation references and it would be possible to focus the attention on one type of references. The Lennard-Jones reference is more realistic than other references. This is why the SAFT versions based on the Lennard-Jones reference are selected for the study in this work although their mathematical formulations are complex. Before evaluating various types of Lennard-Jones based models, it would be necessary to shed light on the basic concepts of perturbation theories and how SAFT versions differ from each other.

**Table 2.1: Some Recent Applications of the SAFT Equations of state (Müller & Gubbins, 2000).**

| Application | Reference |
|---|---|
| **VLE of alkanes, organics, alcohols, acids, etc.** | (S. H. Huang & M. Radosz, 1990), (Gregg, Stein, Chen, & Radosz, 1993), (Byun, Hasch, & McHugh, 1996) and (W.-B. Liu, Li, & Lu, 1999) |
| **VLE of fluorohydrocarbons and refrigerants** | (Clements, Zafar, Galindo, Jackson, & McLure, 1997) |
| **VLE of aqueous alkanolamine solutions** | (Button & Gubbins, 1999) |
| **LLE for hydrocarbons, alcohols, solvating mixtures** | (Gregg et al., 1993) |
| **Fluid phase equilibria of aqueous mixtures** | (Economou & Donohue, 1992) |
| **Aqueous ionic fluids** | (W.-B. Liu et al., 1999) |
| **Phase behavior of reservoir fluids, bitumen and petroleum pitch** | (S. Huang & M. Radosz, 1991) |
| **SLE naphthalene, alkane, polyethylene solutions** | (Pan & Radosz, 1999) |
| **Phase behavior and solubility of polymer solutions and blends** | (Wu & Chen, 1994), (Lee, LoStracco, & McHugh, 1994), (Chen, Economou, & Radosz, 1992) and (Pradhan, Chen, & Radosz, 1994) |
| **Cloud points of polymer and copolymer solutions** | (Byun et al., 1996) |
| **Supercritical fluid extraction** | (Economou, Gregg, & Radosz, 1992) |

## 2.2 Perturbation theories

### 2.2.1 Main components of perturbation theory

Perturbation theory is a mathematical approach that is utilized to give an approximate solution of a problem when the exact solution is not available and cannot be obtained. This could be achieved by starting from an exact solution of a related problem (reference term). In this method, the reference term should dominate the solution while the perturbation term is usually small relative to the reference term. The perturbation term is obtained using Taylor series expansion of the actual expression. The order of perturbation is the number of terms of the truncated Taylor series. Theoretically, infinite perturbation order is needed to obtain the exact solution. However, in many situations, an excellent agreement with the exact solution could be gained with low orders of perturbation terms.

### 2.2.2 Application to statistical mechanical theories

It is well-known that an exact model that can describe the thermodynamic properties doesn't exist. However, an approximate solution could be obtained based on perturbation theories. The idea of most perturbation theories in statistical mechanics is based on splitting the pair-wise potential. The pair-wise potential is a model that describes the interactions between two molecules. The simplest pair-wise potential is the hard sphere model which does not describe the attractive forces between the molecules:

$$u_{hs}(r) = \begin{cases} \infty & , \ r < \sigma \\ 0 & , \ r > \sigma \end{cases} \tag{2.1}$$

where $\sigma$ is the diameter of the segment.

More realistic models that account for both repulsive and attractive forces are also available. Some common examples of these models are square-well potential, triangle-well potential, Lennard-Jones potential and Mie potential.

The mathematical representations of the intermolecular potentials for square-well potential and triangle-well potential are respectively given by:

$$u(r) = \begin{cases} \infty & , \ r < \sigma \\ -\varepsilon & , \ \sigma \leq r \leq R_{SW}\sigma \\ 0 & , \ r > R_{SW}\sigma \end{cases} \tag{2.2}$$

and

$$u(r) = \begin{cases} \infty & , \ r < \sigma \\ \varepsilon \dfrac{\dfrac{r}{\sigma} - R_{TW}}{R_{TW} - 1} & , \ \sigma \leq r \leq R_{TW}\sigma \\ 0 & , \ r > R_{TW}\sigma \end{cases} \tag{2.3}$$

where $\sigma$ is the diameter of the segment, $\varepsilon$ is the dispersion energy between segments, $R_{SW}$ and $R_{TW}$ are the well depths of square-well potential and triangle-well potential; respectively.

The intermolecular Mie potential, which is more realistic than the previous potentials, is described by:

$$u_{Mie}(r) = \frac{\lambda r}{\lambda r - \lambda a}\left(\frac{\lambda r}{\lambda a}\right)^{\frac{\lambda a}{\lambda r - \lambda a}} \varepsilon \left(\left(\frac{\sigma}{r}\right)^{\lambda r} - \left(\frac{\sigma}{r}\right)^{\lambda a}\right) \tag{2.4}$$

where $\sigma$ is the diameter of the segment, $\varepsilon$ is the dispersion energy between segments, $\lambda r$ is the repulsive exponent and $\lambda a$ is the attractive exponent. If $\lambda r$ is equal to 12 and $\lambda a$ is equal to 6, the intermolecular potential gives the Lennard-Jones potential.

In statistical mechanics, any of these potentials can be implemented as a reference term in perturbation theory to derive thermodynamic properties if its pair correlation function and an accurate related pressure-temperature-volume relation are available. The repulsive forces, which are described by the positive component in any of the above potentials, are accurately described by a hard sphere model. Fortunately, the hard sphere system is well-understood and could be represented by very accurate models. Due to the fact that the harsh repulsive forces dominate the structure of fluids (Chandler, 1978), it is evident that the hard sphere system could be used as a reference and the attractive forces could be used as a perturbation in perturbation methods.

To illustrate this concept, a simple example of application of perturbation theory is considered in calculating the second virial coefficient of the triangle-well potential. The second virial coefficient of the triangle-well fluids is calculated using perturbation theory with different perturbation orders and the accuracy is compared with the exact solution. The second virial coefficient is given by the following equation (Sandler, 2010):

$$B = 2\pi \int_0^\infty (1 - e^{-\frac{u(r)}{kT}}) r^2 dr \tag{2.5}$$

The intermolecular triangle potential is decomposed into a repulsive term (reference) and a perturbation term:

$$u(r) = u_{hs}(r) + x\, u_{per}(r) \tag{2.6}$$

where:

$$u_{hs}(r) = \begin{cases} \infty & , \ r < \sigma \\ 0 & , \ r > \sigma \end{cases} \tag{2.7}$$

and

$$u_{per}(r) = \begin{cases} 0 & , \ r < \sigma \\ \varepsilon \dfrac{\dfrac{r}{\sigma} - R_{TW}}{R_{TW} - 1} & , \ \sigma \le r \le R_{TW}\sigma \\ 0 & , \ r > R_{TW}\sigma \end{cases} \tag{2.8}$$

In this case, the truncated Taylor series expansion of the second virial coefficient in $x$ gives an approximate solution to the original integral. Obviously, if the value of $x$ is 1, the triangular potential is returned. **Figure 2.1** shows a comparison of reduced second virial coefficient obtained by different orders of perturbation with the exact answer As shown in the figure, as the order of perturbation increases, the accuracy of the perturbation theory becomes close to the exact answer. In this example, the first and second orders don't give accurate representation of the reduced virial coefficient. However, the accuracy becomes quite comparable with the exact when the order is four.

**Figure 2.1: Reduced second virial coefficient for Triangle-Well fluids where the solid line is the exact value and the dashed curves are approximates with different perturbation orders.**

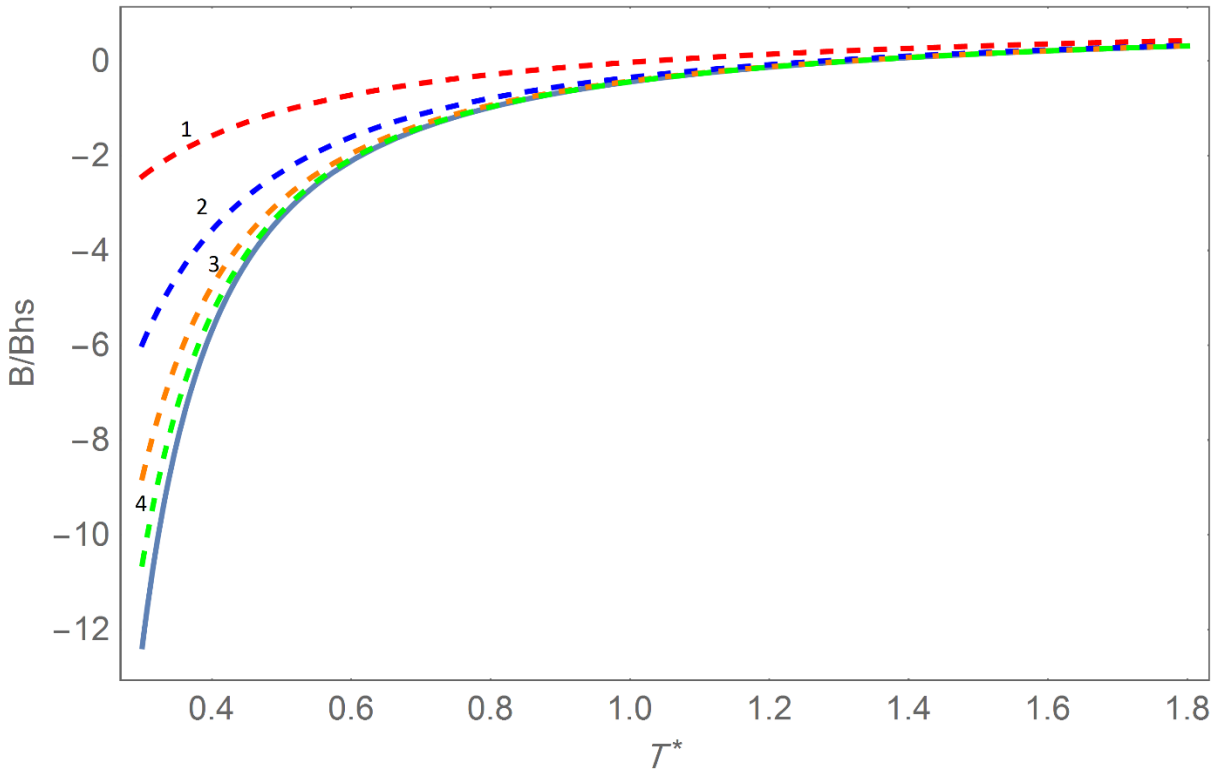


## 2.3 Thermodynamic models from perturbation theories

In models development, since the repulsive forces dominate the structure of fluid, the repulsive forces can be taken as a reference term in perturbation theories. As previously indicated, to select the reference term, two major quantities must accurately be available: radial distribution function (RDF) and equation of state based on a specific pair potential model. Since the RDF and the equation of state of the hard sphere potential are available with a very high accuracy, it has been used as a reference term in many models. Some other

potentials like Lennard-Jones potential and square-well potential have also been implemented in perturbation theories with the use of approximate solution to the RDF and equation of state.

The application of perturbation theories to describes fluid properties starts with expanding the partition function of the Helmholtz free energy in the canonical ensembles using Taylor series . Due to the variation in defining the reference and perturbation terms, various versions of TPT theory have been proposed. **Table 2.2** lists some of the common models and their reference terms.

**Table 2.2: Reference terms of some models.**

| Model | Reference Term |
|---|---|
| Original SAFT | Hard Sphere |
| Simplified SAFT | Hard Sphere |
| CK-SAFT | Hard Sphere |
| PC-SAFT | Hard Sphere + Chain |
| Soft SAFT | Lennard-Jones |
| SAFT-VR Mie | Mie Potential |

These models are expressed in terms of the Helmholtz free energies of various contributions like repulsion, dispersion, chain and association:

$$a^{res} = a^{hs} + a^{disp} + a^{chain} + a^{assoc} \tag{2.9}$$

In terms of compressibility factors, the above equation is given by:

$$Z = 1 + Z^{hs} + Z^{disp} + Z^{chain} + Z^{assoc} \tag{2.10}$$

In these expressions, the hard sphere term represents the effect of repulsive forces between the molecules while the dispersion term takes into account the contribution of the instantaneous induced dipole interactions. In fact, these two terms are already available in the cubic equations of state but with empirical formulation. Consequently, it can obviously be noticed that the major improvement made by the TPT is the consideration of the contribution arising from the association and size of molecules.

In addition, unlike cubic equations of state, every term in TPT is proposed based on theoretical foundations. The theoretical foundations could become stronger and more realistic if the Lennard-Jones potential is selected as a reference since Lennard-Jones models could accurately describe spherical systems.

## 2.4 Thermodynamic models based on Lennard-Jones

The fact that Lennard-Jones potential accurately describes the real molecular interaction has encouraged many researchers to develop fluid theories based on it. The Lennard-Jones potential gains its accuracy from two factors. The first one is its capability to describe the softness of molecules. This feature does not exist in simple potentials like hard sphere and square-well. The second factor is that it describes both repulsive and attractive forces.

In terms of perturbation theories, the Lennard-Jones potential has been implemented as a reference term in several models like soft-SAFT (F. J. Blas & Vega, 1997) and LJ-SAFT (Kraska & Gubbins, 1996). The main obstacle in using Lennard-Jones

potential as a reference term in perturbation theory is the lack of accurate RDF and equation of state that correspond to this potential. For that reason, most of the Lennard-Jones perturbation theories available in the literature adopt empirical RDF and equation of state that are based on fitting of molecular simulation data. For example, the soft-SAFT model uses the Lennard-Jones equation of state proposed by (J. K. Johnson et al., 1993):

$$A_{monomer} = \sum_{i=1}^{8} \frac{a_i \rho^{*i}}{i} + \sum_{i=1}^{6} b_i G_i \tag{2.11}$$

where $a_i$ and $b_i$ are temperature dependent coefficients and $G_i$ are density dependent coefficients. These coefficients are listed in the original work (J. K. Johnson et al., 1993). On the other hand, the equation of state used in LJ-SAFT is given by (Kolafa & Nezbeda, 1994):

$$\begin{aligned} A_{monomer} = kT/\varepsilon \left( 5/3 * \mathrm{Log}[1-\eta] + \frac{\eta(34 - 33\eta + 4\eta^2)}{6(1-\eta)^2} \right) \\ + \left( \mathrm{Exp}[-\gamma * (\rho)^2] * m * \mathrm{Nav} * \sigma^3/v * kT/\varepsilon * \mathrm{DB}[T] \right. \\ + \sum_{j=2}^{5} c_{0,j} * \rho^j + (kT/\varepsilon)^{-1/2} * \sum_{j=2}^{6} c_{-1,j} * \rho^j + (kT/\varepsilon)^{-2/2} \\ \left. * \sum_{j=2}^{6} c_{-2,j} * \rho^j + (kT/\varepsilon)^{-4/2} * \sum_{j=2}^{6} c_{-4,j} * \rho^j \right) \end{aligned} \tag{2.12}$$

where $\eta$ is packing fraction, k is Boltzmann constant, Nav is Avogadro's number, $c_{i,j}$ and $\gamma$ are fitting constants and $\mathrm{DB}[T]$ is the residual second virial coefficient and .

Both models utilize the RDF at contact proposed by (J. K. Johnson, Mueller, & Gubbins, 1994):

$$g_{LJ}(\sigma) = 1 + \sum_{i=1}^{5}\sum_{j=1}^{5} a_{i,j}\rho^{i}(kT/\varepsilon)^{1-j} \tag{2.13}$$

where $a_{i,j}$ are fitting constants.

Another Lennard-Jones equation of state that has been used in this work to develop a new Lennard-Jones model (SAFT-LJ3) is given by (Mecke et al., 1996):

$$A_{monomer} = \frac{4\zeta - 3\zeta^2}{(1-\zeta)^2} + \sum_{i=1}^{32} c_i (T^*/T_c^*)^{m_i} (\rho^*/\rho_c^*)^{n_i} e^{p_i(\rho^*/\rho_c^*)^{q_i}} \tag{2.14}$$

where $\zeta$ is packing fraction, $m_i$, $n_i$, $p_i$ and $q_i$ are fitting constants, $T_c^* = 1.328$ and $\rho_c^* = 0.3107$.

If the above three models are employed to Wertheim's first order thermodynamic perturbation theory (TPT1), three adjustable parameters are needed for non-associating components. The three adjustable parameters are the chain length (m), the diameter of the segment ($\sigma$) and the dispersion energy between segments ($\varepsilon$). The values of the adjustable parameters for soft-SAFT and SAFT-LJ3 equations of state used in this work are listed in **Table 2.3** and **Table 2.4** respectively.

**Table 2.3: Parameters for soft-SAFT equation of state.**

| Component | m | $\sigma$(A°) | $\varepsilon/k$ (K) |
|---|---|---|---|
| Methane | 1 | 3.722 | 147.3020 |
| Ethane | 1.5936 | 3.585 | 190.3750 |
| Propane | 1.9969 | 3.657 | 207.9678 |
| Octane | 3.5894 | 3.9265 | 261.49 |
| Argon | 1 | 3.405 | 117.21 |

**Table 2.4: Parameters for SAFT-LJ3 equation of state.**

| Component | m | $\sigma$(A°) | $\varepsilon/k$ (K) |
|---|---|---|---|
| Methane | 1 | 3.7155 | 140.57 |
| Ethane | 1.2466 | 3.9127 | 211.47 |
| Propane | 1.4176 | 4.1507 | 245.55 |
| Octane | 3.4098 | 3.9987 | 264.96 |
| Argon | 1 | 3.4 | 112.76 |

## 2.5 A thermodynamic model based on Mie potential

In 2006, the Mie potential was implemented in a perturbation theory (Lafitte, Bessieres, Piñeiro, & Daridon, 2006). A more accurate version of this model was recently published (Lafitte et al., 2013). This model has proved to be accurate in describing phase equilibria as well as the second derivative properties like heat capacity and speed of sound. The SAFT-VR Mie model is given by the following expressions (Lafitte et al., 2013):

$$a_{\text{res}} = a_{\text{MONO}} + a_{\text{CHAIN}} + a_{\text{ASSOC}} \tag{2.15}$$

where the monomer term is given by:

$$a_{\text{MONO}} = m_s(a_{\text{HS}} + \beta a_1 + \beta^2 a_2 + \beta^3 a_3) \tag{2.16}$$

where $m_s$ is the chain length and $\beta = 1/kT$.

The adopted hard-sphere term is given by (Carnahan & Starling, 1969):

$$a_{\mathrm{HS}} = \frac{4\eta - 3\eta^2}{(1-\eta)^2} \tag{2.17}$$

The dispersion term was expanded based on the Barker and Henderson perturbation theory into up to the third order. The first order expansion was given by:

$$a_1 = c\left({x_0}^{\lambda \mathrm{a}}(a_{\mathrm{s1}}[\eta, \lambda \mathrm{a}] + B[\eta, \lambda \mathrm{a}]) - {x_0}^{\lambda \mathrm{r}}(a_{\mathrm{s1}}[\eta, \lambda \mathrm{r}] + B[\eta, \lambda \mathrm{r}])\right) \tag{2.18}$$

where $c = \frac{\lambda \mathrm{r}}{\lambda \mathrm{r} - \lambda \mathrm{a}}\left(\frac{\lambda \mathrm{r}}{\lambda \mathrm{a}}\right)^{\frac{\lambda \mathrm{a}}{\lambda \mathrm{r} - \lambda \mathrm{a}}}$, $a_{\mathrm{s1}}$ and $B$ are algebraic expressions implemented in the first and second order expansion terms and $x_0$ is the reduced diameter.

The second order expansion was given by:

$$\begin{aligned} a_2 = .5K_{\mathrm{HS}}(1+X)\epsilon c^2 \Big({x_0}^{2\lambda \mathrm{a}}(a_{\mathrm{s1}}[\eta, 2\lambda \mathrm{a}] + B[\eta, 2\lambda \mathrm{a}]) \\ - 2{x_0}^{\lambda \mathrm{a} + \lambda \mathrm{r}}(a_{\mathrm{s1}}[\eta, \lambda \mathrm{a} + \lambda \mathrm{r}] + B[\eta, \lambda \mathrm{a} + \lambda \mathrm{r}]) \\ + {x_0}^{2\lambda \mathrm{r}}(a_{\mathrm{s1}}[\eta, 2\lambda \mathrm{r}] + B[\eta, 2\lambda \mathrm{r}])\Big) \end{aligned} \tag{2.19}$$

where $K_{\mathrm{HS}}$ is the isothermal compressibility of the hard-sphere reference fluid.

An empirical expression was utilized to define the third order expansion:

$$a_3 = -\epsilon^3 f_4[\alpha]\eta {x_0}^3 \mathrm{Exp}[f_5[\alpha]\eta {x_0}^3 + f_6[\alpha]\eta^2 {x_0}^6] \tag{2.20}$$

where $\alpha$ is van der Waals-like attractive constant and $f_i[\alpha]$ are mathematical expressions resulting from fitting of molecular simulation data.

Finally, the chain term was given by the following expression:

$$a_{\text{CHAIN}} = -(m_s - 1)\text{Log}[\text{gMie}[\sigma]] \tag{2.21}$$

where the RDF is given by:

$$\text{gMie}[\sigma] = \text{gdHS}[\sigma]\, e^{\beta\epsilon \text{g1}[\sigma]/\text{gdHS}[\sigma] + (\beta\epsilon)^2 \text{g2}[\sigma]/\text{gdHS}[\sigma]} \tag{2.22}$$

SAFT-VR Mie equation of state has five adjustable parameters: chain length ($m_s$), diameter of the segment ($\sigma$), dispersion energy between segments ($\epsilon$), repulsive exponent ($\lambda$r) and attractive exponent ($\lambda$a). When the values of attractive and repulsive exponents are 6 and 12 respectively, the model becomes a Lennard-Jones model (SAFT-VR Mie-LJ). The original work of SAFT-VR Mie can be consulted to get more details about the mathematical formulation of this model. The values of the adjustable parameters for SAFT-VR Mie-LJ and SAFT-VR Mie equations of state used in this work are listed in **Table 2.5** and **Table 2.6** respectively. Therefore, three main thermodynamic models based on Lennard-Jones are introduced in this chapter; namely soft-SAFT, SAFT-LJ3 and SAFT-VR Mie-LJ. The mathematical formulations of these models are completely different and complex.

**Table 2.5: Parameters for SAFT-VR Mie-LJ equation of state.**

| Component | m | $\sigma$(A°) | $\epsilon/k$ (K) | $\lambda$r | $\lambda$a |
|---|---|---|---|---|---|
| Methane | 1 | 3.7396 | 149.26 | 12 | 6 |
| Ethane | 1.4535 | 3.6978 | 201.4 | 12 | 6 |
| Octane | 3.3798 | 4.0122 | 267.89 | 12 | 6 |
| Argon | 1 | 3.4085 | 117.31 | 12 | 6 |

**Table 2.6: Parameters for SAFT-VR Mie equation of state.**

| Component | m | $\sigma$(A$^o$) | $\epsilon/k$ (K) | λr | λa |
|---|---|---|---|---|---|
| Methane | 1 | 3.7412 | 153.36 | 12.650 | 6 |
| Methane (10-6) | 1 | 3.7274 | 134.25 | 10 | 6 |
| Methane (20-6) | 1 | 3.7955 | 186.2 | 20 | 6 |
| Perfluoromethane | 1 | 4.3372 | 232.62 | 42.553 | 5.1906 |
| Ethane | 1.4373 | 3.7257 | 206.12 | 12.400 | 6 |
| Octane | 2.6253 | 4.4696 | 369.18 | 17.378 | 6 |
| Decane | 2.9976 | 4.5890 | 400.79 | 18.885 | 6 |

# Chapter 3

# Reliable techniques for the determination of volume root loci from complex thermodynamic models

## 3.1 Introduction

In the previous chapter, three different thermodynamic models based on the Lennard-Jones potential were introduced. The difference of the three models is not clear although various studies indicated that they are comparable in terms of accuracy (Felipe J. Blas & Vega, 1998). To use these models in process simulators, the accuracy is not a sufficient condition for critical evaluation of the models in practical applications. It is still not clear how the multiple volume roots vary with temperature and pressure. It is also not obvious if these models exhibit any non-physical behaviour like multiple phase separation regions. This is why it is important to study not only the accuracy but also the deficiency of the models caused by the mathematical formulations.

The mathematical forms were empirically constructed with complex terms in most of Lennard-Jones models. Thus, it is a difficult task to compare different Lennard-Jones models unless there is critical evaluation of the consequences of the empirical mathematical formulations. The initial step towards the evaluation is to determine how the volume roots vary with temperature and pressure. In this work, the bifurcation diagrams are implemented along with arc-length continuation method and a sophisticated solver for finding all the roots to develop a new technique for analysing the solution behaviour of such complicated models and determining the locus of the PVT solution.

## 3.2 Bifurcation diagrams

The bifurcation diagram is a visualisation of the solutions of parameterized non-linear equations. Although this technique is mainly related to dynamic systems, there is still a good reason to implement in thermodynamics which is an equilibrium science in general. The thermodynamic models that are based on canonical ensembles are expressed in terms of molar volume and temperature. For that reason, one of these variables can be taken as a bifurcation parameter. In this work, the temperature is taken as a bifurcation parameter and the volume roots are obtained accordingly at any certain pressure.

**Figure 3.1** shows a typical bifurcation diagram for a cubic equation of state. The red points are called "turning points" and they are located where the curve (branch) changes its direction. The two turning points represent the boundaries of the two-phase region. As the temperature increases, the molar volume reaches the ideal gas limit. The solution behaviour shown in **Figure 3.1** is the physical behaviour that any equation of state should exhibit. However, when the thermodynamic model gets more complex, the solution behaviour will most probably deviate from the physical behaviour.

**Figure 3.1: Bifurcation diagram from cubic equations of state.**

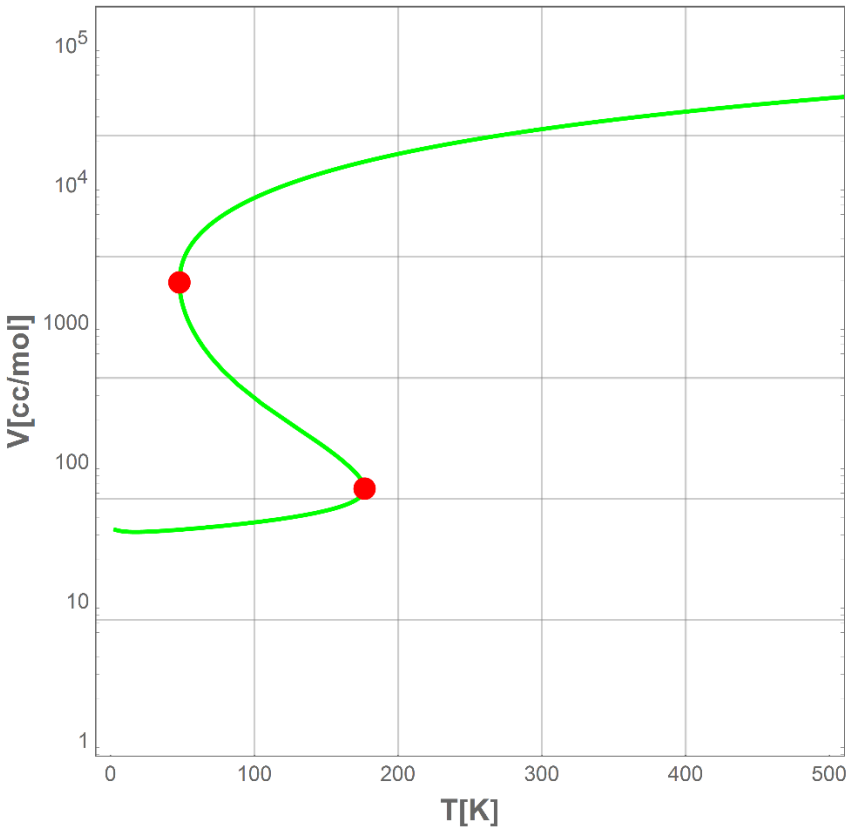


Depending on the mathematical structure and the nature of the non-linearity of the equation of state, several non-physical behaviours could appear in its bifurcation diagram. For instance, extra non-physical branches might show up in the bifurcation diagram resulting in a larger number of volume roots. The non-physical branches usually appear at low values of molar volume and they are independent of pressure in many cases. The other non-physical behaviour that can also occur in complex models is the co-existence of multiple two-phase regions of which only one represents the real vapour-liquid equilibrium region. The main issue about the non-physical two-phase regions is that they usually satisfy the mechanical stability making it a difficult task to describe the vapour-liquid equilibrium behaviour using these models since the mechanical stability must be tested in this case. The

bifurcation diagrams shown in **Figure 3.2** and **Figure 3.3** are examples of non-physical solution behaviours that are obtained from a more complex equation of state, SAFT-VR Mie.

**Figure 3.2: Bifurcation diagram containing extra non-physical branches.**

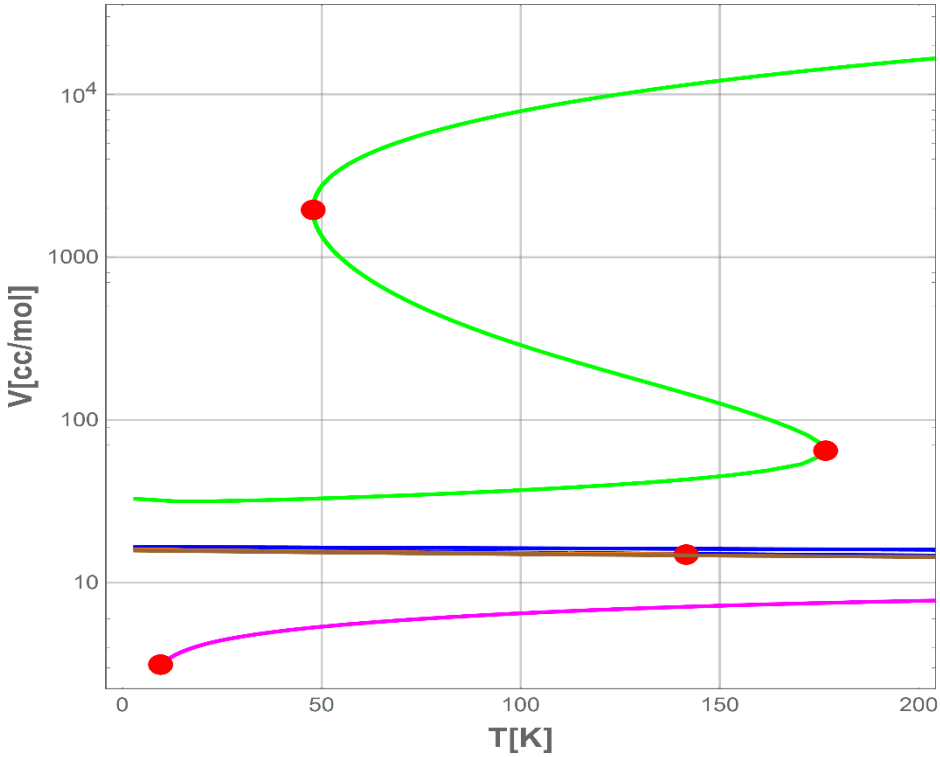

**Figure 3.3: Bifurcation diagram containing extra non-physical two-phase region.**

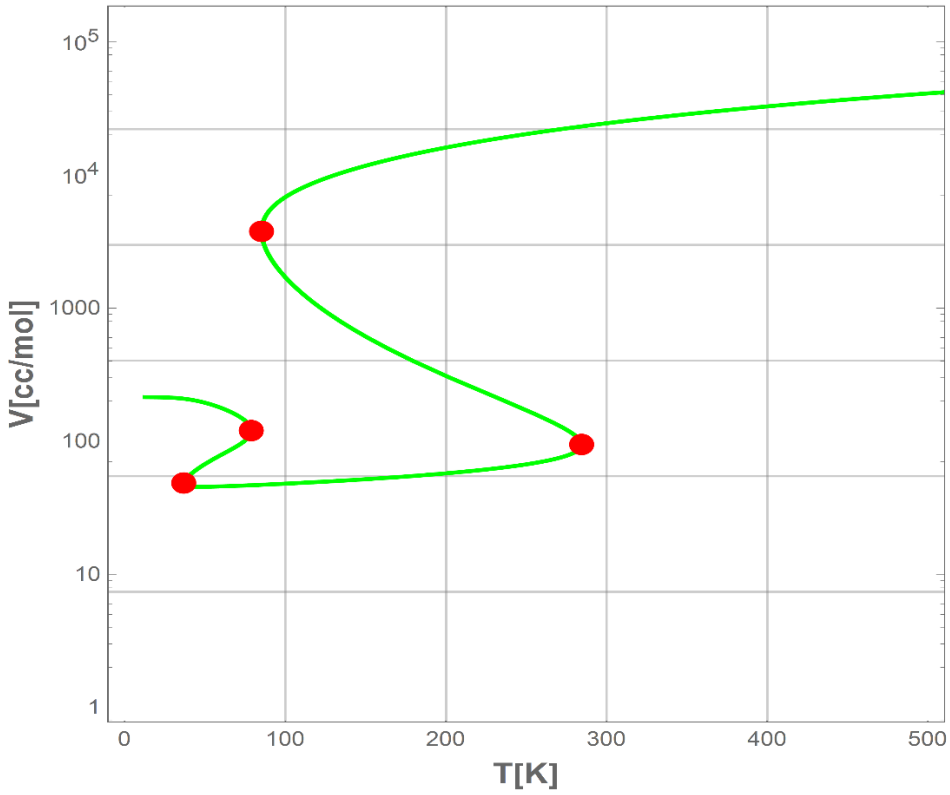


## 3.3 Continuation methods

"Over the past ten to fifteen years two new techniques have yielded extremely important contributions toward the numerical solution of nonlinear systems of equations. These two methods have been called by various names. One of the methods has been called the predictor-corrector or pseudo arc-length continuation method. This method has its historical roots in the imbedding and incremental loading methods which have been successfully used for several decades by engineers and scientists to improve convergence properties when an adequate starting value for an iterative method is not available" (Allgower & Georg, 1990). In this work, the arc-length continuation method is implemented to solve the non-linear equations of state at various conditions and generate

the bifurcation diagrams. The non-linear algebraic equation is re-written so that all variables (V & T) are parameterized with an independent variable (s) and it is then solved simultaneously with the auxiliary equation:

$$V'^2(s) + T'^2(s) = 1 \qquad (3.1)$$

The turning points are the extrema of the temperature:

$$T'(s) = 0 \qquad (3.2)$$

The NDSolve command in Mathematica® is used to solve the non-linear system of differential-algebraic equations. The most critical point in this method is to use appropriate initial conditions of V & T. Different initial conditions could result in different branches in the bifurcation diagram. In order to catch all the branches, all the volume roots corresponding to the initial condition of temperature must be implemented as initial conditions separately. For that reason, a sophisticated solver that is capable to find all volume roots is needed.

## 3.4 A systematic method for finding all volume roots

From the previous discussion, it is realized that studying the solution behaviour of any equation of state requires finding all the volume roots at any specific pressure and temperature. The set of temperature and all corresponding volume roots represent the initial condition required to generate the bifurcation diagram at any specific pressure using arc-length continuation method. Finding the volume roots at certain P & T is done using the

common numerical methods: Newton's method, Secant method, Trust Region method…etc. All these methods are iterative methods and their convergence highly depends on the initial guess value.

The trivial way of finding all the roots is to vary the initial guess and to try as many values as possible. Although this is the common technique for finding all the roots, it still has many limitations. First of all, it is not systematic so it can not be automated and it has to be done manually. Moreover, it does not guarantee finding all the roots especially when two consecutive roots are close to each other since it will be difficult to catch both of them using random initial guess values.

To overcome these limitations, there must be a systematic solver that has the capability of finding all the roots. Wagon has proposed a graphical method that implements the MeshFunctions option in Plot command in Mathematica® (Wagon, 2010). This method detects the values at which the curve crosses the horizontal axis and improve them using FindRoot command by taking them as initial guess values. The main problem with this method is that it only works in Mathematica® and can not be used in other platforms. In this work, Wagon's method is converted from a graphical method to a purely numerical method that can be implemented in any platform.

The first step is to create an array that covers the search interval with a certain step size. The second step is to evaluate the non-linear equation at all the values in the array and store their signs in another array. The third step is to detect the positions where the sign changes and collect their corresponding values from the first array (seeds). The seeds are then improved by implementing them as initial guess values in any numerical technique, Newton's method for example, in order to give the actual roots. To illustrate this method,

a simple example is considered. The roots of the function $Sin(x)$ are obtained in the interval: $10 \leq x \leq 50$.

First of all, the search array is created:

[10 , 11 , 12 , 13 , 14 , 15 , 16 , 17 , 18 , 19 , 20 , 21 , 22 , 23 , 24 , 25 , 26 , 27 , 28 , 29 , 30 , 31 , 32 , 33 , 34 , 35 , 36 , 37 , 38 , 39 , 40 , 41 , 42 , 43 , 44 , 45 , 46 , 47 , 48 , 49 ,50].

Next, $Sin(x)$ is evaluated at all the search points and the signs are detected:

[-1 , -1 , -1 , 1 , 1 , 1 , -1 , -1 , -1 , 1 , 1 , 1 , -1 , -1 , -1 , -1 , 1 , 1 , 1 , -1 , -1 , -1 , 1 , 1 , 1 , -1 , -1 , -1 , 1 , 1 , 1 , -1 , -1 , -1 , 1 , 1 , 1 , 1 , -1 , -1 , -1].

It is clear that the positions where the function changes its sign are:

[3 , 6 , 9 , 12 , 16 , 19 , 22 , 25 , 28 , 31 , 34 , 38].

The corresponding values from the search array (seeds) are:

[12 , 15 , 18 , 21 , 25 , 28 , 31 , 34 , 37 , 40 , 43 , 47].

Finally, seeds are improved by using them as initial guess values in Newton's method which will result in the actual roots:

[12.5664 , 15.708 , 18.8496 , 21.9911 , 25.1327 , 28.2743 , 31.4159 , 34.5575 , 37.6991 , 40.8407 , 43.9823 , 47.1239].

**Figure 3.4: Zeros of Sin(x) using modified Wagon's method.**

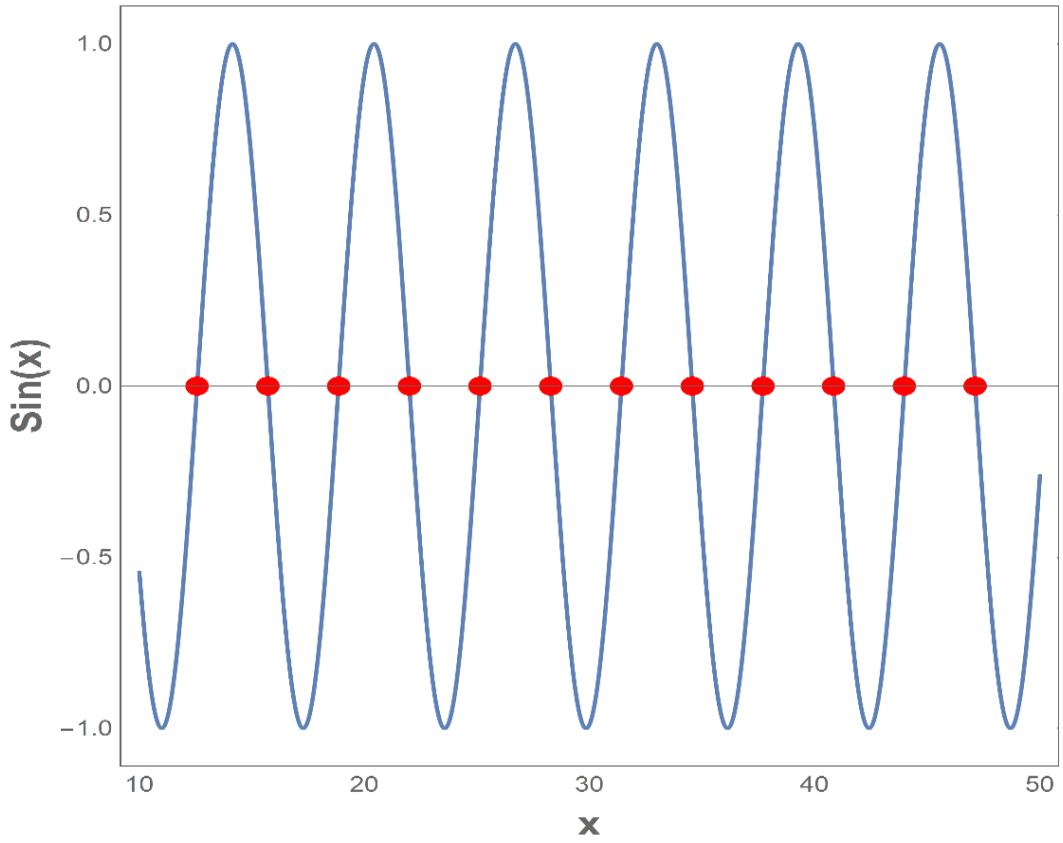


The combination of the Wagon's method and the arc-length continuation method makes it a reliable technique that could be utilized to determine the volume root loci from complex thermodynamic models. In the next two chapters, the proposed combination will be utilized to study SAFT-LJ based models and SAFT-VR Mie.

# Chapter 4

# Solution behavior of different LJ models

## 4.1 Introduction

Several Lennard-Jones models have been proposed in the literature. Most of these models were constructed based on adjusting molecular simulation data. Although these models are almost equivalent in terms of accuracy, they might differ in exhibiting artificial PVT behavior. The fact that these models are highly non-linear gives them a higher possibility of exhibiting non-physical solution behaviors. These non-physical behaviors might arise from exhibiting non-physical multi-phase separation regions. In addition, these models might have different non-physical volume roots at the same temperature and pressure. The non-physical behaviors represent a serious limitation in LJ models and make their application less efficient. For example, when these models are implemented in any process simulator, there is a possibility of getting wrong results since the equations of these models might converge to non-physical volume roots. An efficient procedure to determine and examine all volume roots is needed to avoid any complication in selecting the correct stable roots. Although several procedures have been proposed in the literature (Xu, Brennecke, & Stadtherr, 2002), their application is impractical in terms of computational time especially for complex models like SAFT-VR Mie equation of state. To propose a simple method, it is first necessary to understand how the PVT behavior of these models behaves at every possible state conditions. For that reason, the new numerical techniques that include generating the bifurcation diagrams, discussed in **Chapter 2**, are utilized to analyze the PVT solution behavior of different LJ models. In this chapter, the solution

behavior of three LJ models, which are soft-SAFT, SAFT-LJ3 and SAFT-VR Mie-LJ, are investigated and compared for several components.

## 4.2 Components classification

The solution behavior analysis of the LJ models in this chapter depends on generating the bifurcation diagrams of each model for different components. In order to get a clear picture of the PVT solution behavior of these models, the studied components should be selected in such a way that the effects of different terms of the TPT1 models are investigated. In this analysis, components are classified as spherical and non-spherical components. The term “spherical molecules” refers to those molecules having a chain length (m) equal to one. Methane, Perfluoromethane and Argon are some examples of molecules that could be approximated with m equals to one. The analysis of the bifurcation diagrams of these components will eliminate the effect of the chain term on the solution behavior and only show the effect of the combination of the hard sphere and dispersion terms. On the other hand, “non-spherical molecules” are those molecules having a chain length greater than one. Despite the fact that the contribution of the chain term in thermodynamic properties is minor for short chains, it can cause a remarkable change in the solution behavior. The bifurcation diagrams of non-spherical components will demonstrate the effect of including the chain term on the solution behavior of the LJ models. Finally, the analysis done in this work is limited to non-associating components.

## 4.3 Soft-SAFT

### 4.3.1 Spherical molecules

**Figure 4.1** shows the bifurcation diagram of methane at 1atm for soft-SAFT equation of state. The physical branch (green) exhibits four turning points. The first two turning points, on the right side, are the limits of the physical two-phase region. In this region, the model produces three volume roots on the physical branch. The lower volume root corresponds to the liquid phase while the upper one corresponds to the vapor phase. For any temperature between the two turning points, the intermediate root is mechanically unstable. On the other hand, the other two turning points, on the left side, represent a non-physical two-phase region. Although the range of this non-physical region is very small, it still can produce misleading results since it interferes with the physical two-phase region. **Table 4.1** summarizes the two saturation temperatures obtained for methane at 1atm and 5atm and their corresponding volume roots and fugacity coefficients.

The other branch (blue) is another example of non-physical solution behavior. It adds two more volume roots that do not have any physical meaning. In fact, this non-physical branch can lead to serious mistakes in calculations since it is very close to the physical branch making the possibility of capturing the wrong volume root high. It is clear from the bifurcation diagram in **Figure 4.1** that the soft-SAFT equation of state can give up to seven volume roots for methane at 1atm. Volume roots of methane at 1atm and 60K are listed in **Table 4.2**.

The same behavior is observed for other spherical molecules. For example, **Figure 4.2** shows the bifurcation diagram of argon at 1atm. It can be noticed that the solution

behavior is similar in methane and argon where one extra cyclic branch exists and this can be generalized for other spherical molecules.

**Figure 4.1: Bifurcation diagram of methane at 1atm for soft-SAFT equation of state.**

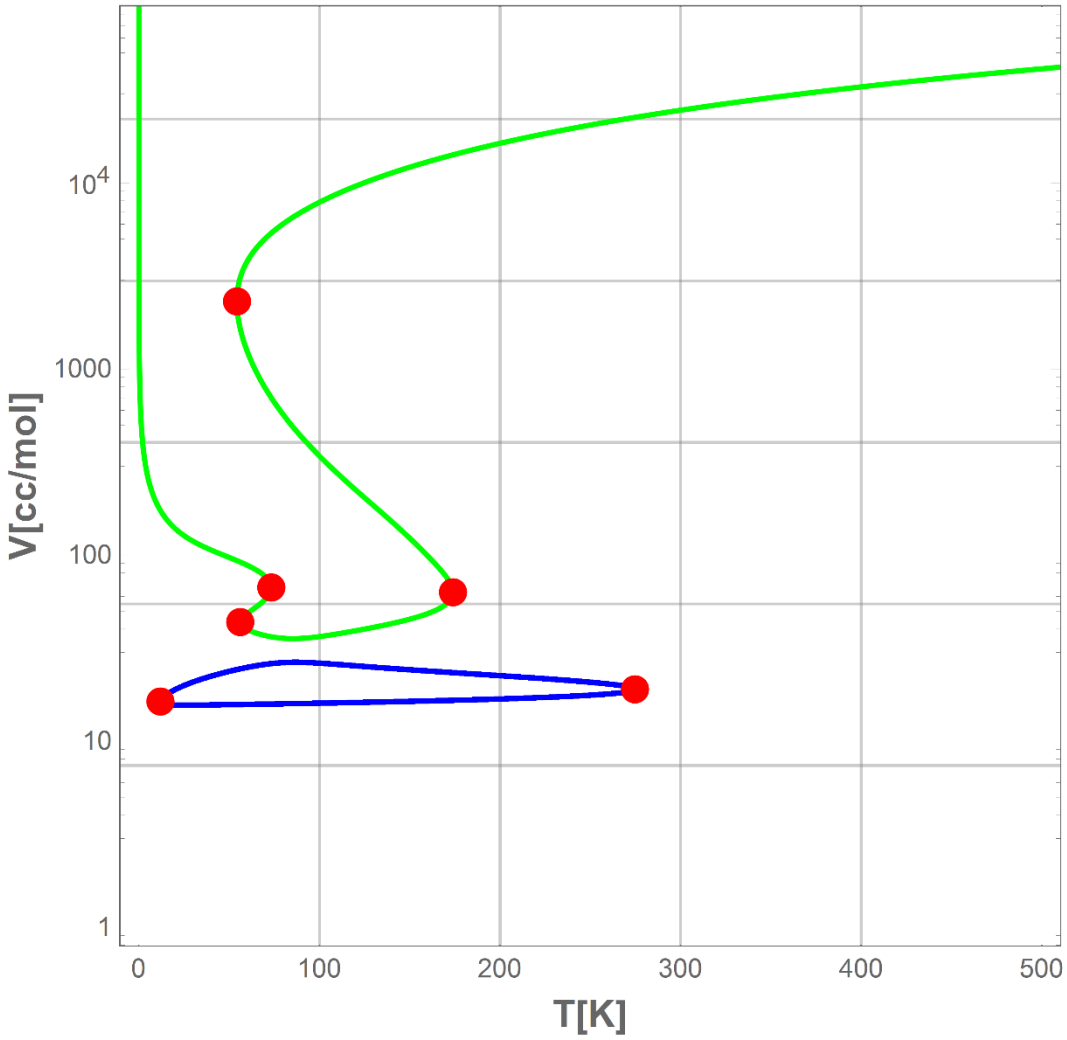

**Table 4.1: Saturation properties of methane at 1atm and 5atm using soft-SAFT.**

| P(atm) | Actual two-phase region | | | |
|---|---|---|---|---|
| | T(K) | $V_{liquid}$(cc/mol) | $V_{vapor}$(cc/mol) | Fugacity coefficient |
| 1 | 110.06 | 37.73 | 8749.35 | 0.9697 |
| 5 | 133.83 | 41.54 | 1982.78 | 0.9115 |
| P(atm) | Non-physical two-phase region | | | |
| | T(K) | $V_{liquid}$(cc/mol) | $V_{vapor}$(cc/mol) | Fugacity coefficient |
| 1 | 64.38 | 38.24 | 83.84 | 0.0087 |
| 5 | 64.26 | 38.27 | 83.59 | 0.0018 |

**Table 4.2: Volume roots (cc/mol) of methane at 1atm and 60K using soft-SAFT.**

| | |
|---|---|
| **V1** | 15.8 |
| **V2** | 24.9 |
| **V3** | 39.8 |
| **V4** | 48.6 |
| **V5** | 88.2 |
| **V6** | 1242.8 |
| **V7** | 3793.1 |

**Figure 4.2: Bifurcation diagram of argon at 1atm for soft-SAFT equation of state.**

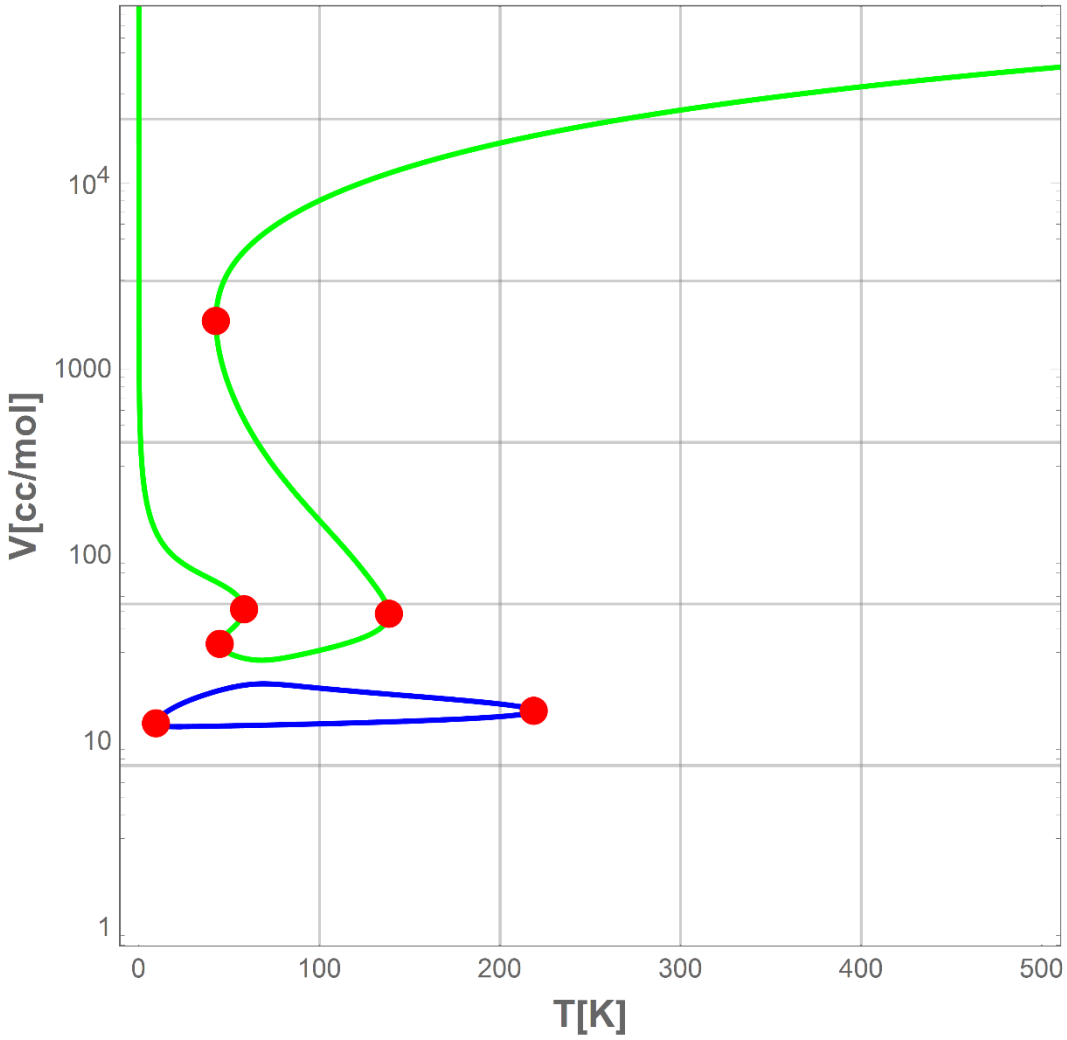


### 4.3.2 Non-spherical molecules

To get a clear picture of the PVT solution behavior of LJ chains, components of different chain lengths are considered. The first component is ethane which has a short

chain length (m). The study of such a component will clarify the effect of adding the chain term on the solution behavior. **Figure 4.3** shows the bifurcation diagram of ethane at 1atm.

**Figure 4.3: Bifurcation diagram of ethane at 1atm for soft-SAFT equation of state.**

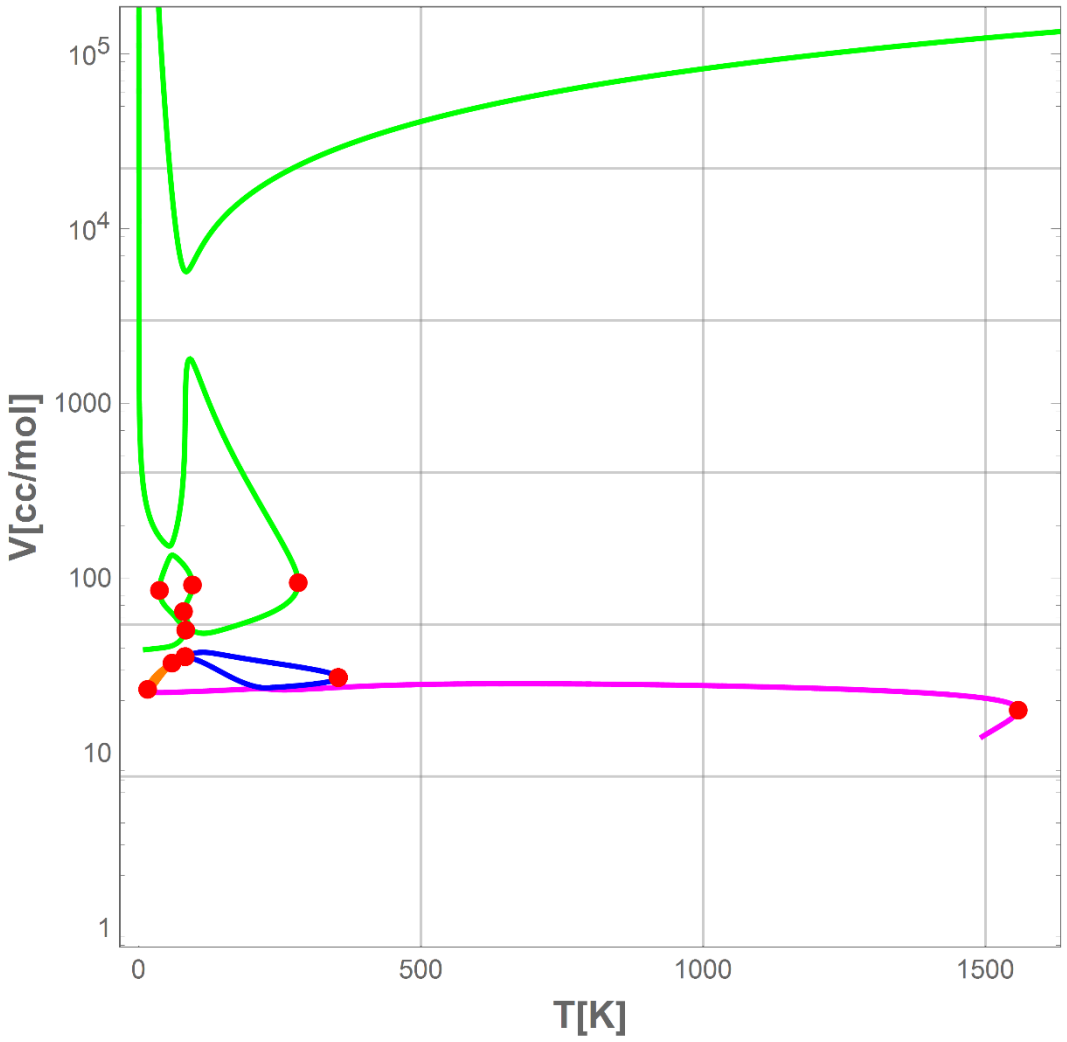


It is clear that the addition of the chain term lead to a non-realistic solution behavior where the physical branch has split into two branches. However, as the chain length increase, the two branches approach each other until they combine forming one physical branch. This can be observed by a simple comparison between the bifurcation diagrams of ethane, propane and octane as illustrated in **Figures 4.3**, **4.4** & **4.5** respectively.

**Figure 4.4: Bifurcation diagram of propane at 1atm for soft-SAFT equation of state.**

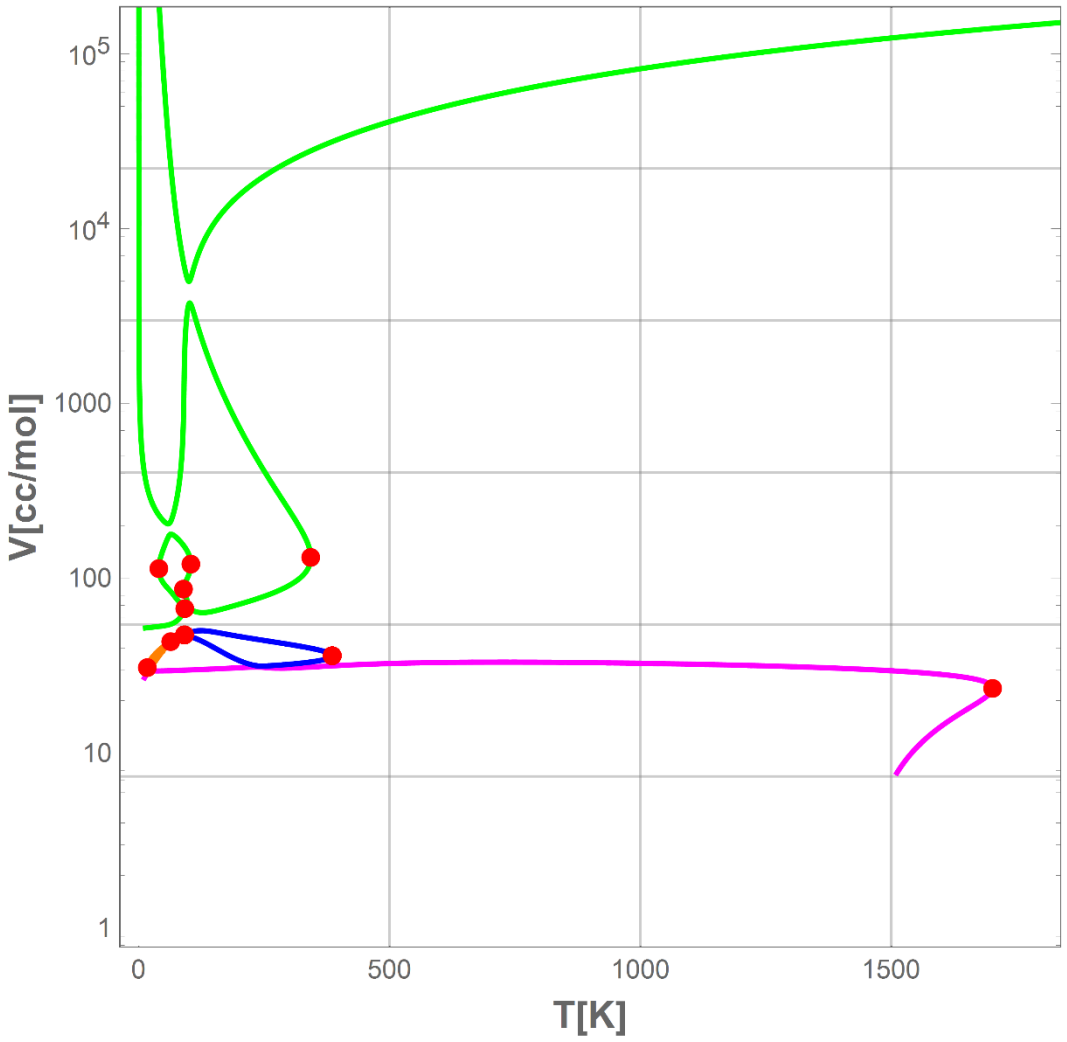

**Figure 4.5: Bifurcation diagram of octane at 1atm for soft-SAFT equation of state.**

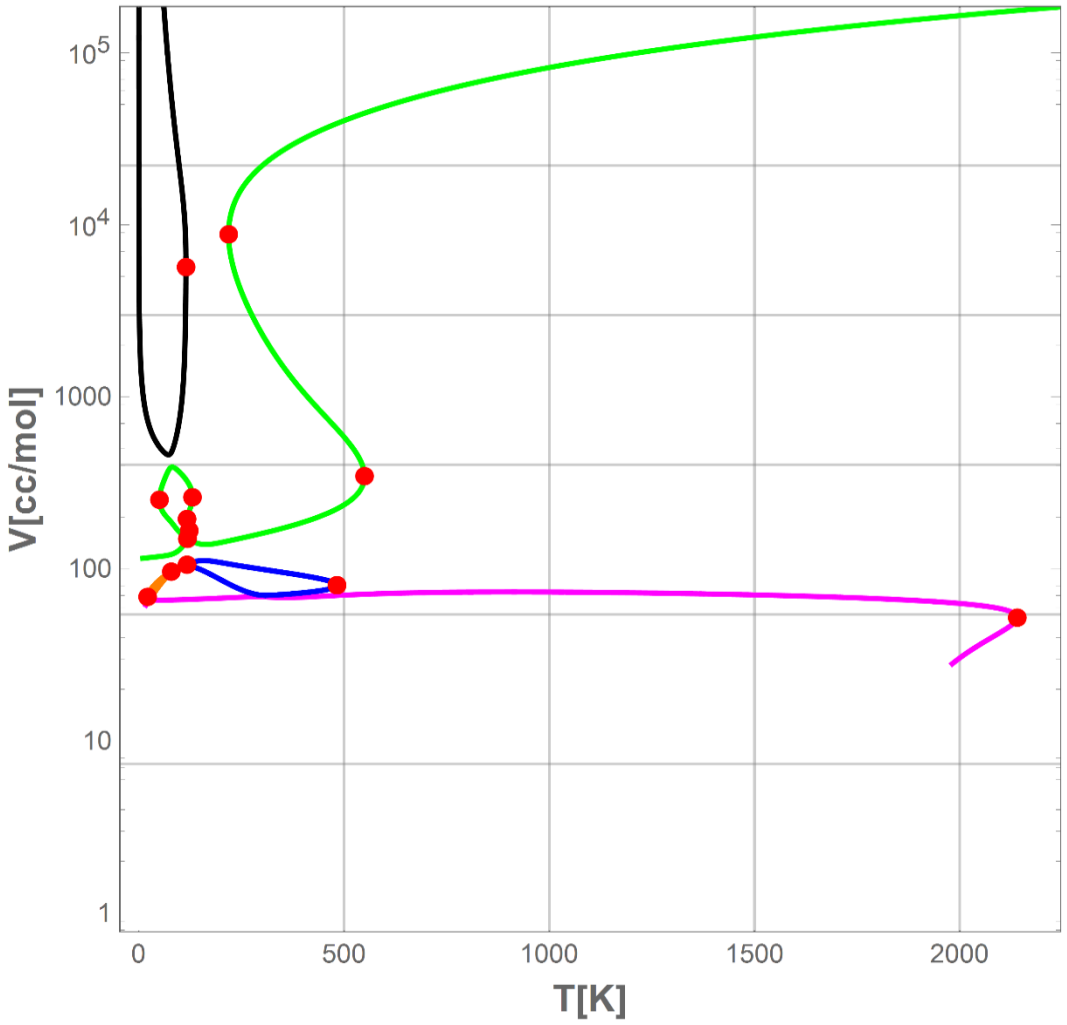


Furthermore, three more non-physical branches are found as shown in **Figures 4.3**, **4.4** & **4.5** for non-spherical components. This complex non-physical solution behavior exhibited by soft-SAFT equation of state for LJ chains suggests that the chain term is not well constructed and it should be revised. To make a valid conclusion about the chain term used in soft-SAFT, it has to be studied with another LJ reference. In the next section, the solution behavior of SAFT-LJ3 equation of state, which adopts the same chain term, is analyzed.

## 4.4 SAFT-LJ3

### 4.4.1 Spherical molecules

**Figure 4.6** shows the bifurcation diagram of methane at 1atm for SAFT-LJ3 equation of state. In general, the solution behavior of the physical branch is similar to that of the soft-SAFT where one non-physical two-phase region interferes with the actual two-phase region. The width of the non-physical two-phase region in SAFT-LJ3 is larger and more interfering with the actual two-phase region. However, the non-physical saturation temperature in SAFT-LJ3 is approximately 10 degrees less than soft-SAFT. This suggests that SAFT-LJ3 is safer in performing vapor-liquid equilibrium calculations for spherical components.

**Table 4.3** lists saturation temperatures for methane at 1atm and 5atm and their corresponding volume roots and fugacity coefficients. The non-physical branch in SAFT-LJ 3 is extended along the whole temperature range while soft-SAFT exhibits a cyclic non-physical branch that only exists below 250K. The gap between the non-physical branch and the physical branch is higher in SAFT-LJ3 than the gap in the soft-SAFT which indicates that the possibility of catching the non-physical root by mistake is less in SAFT-LJ3 equation of state. SAFT-LJ3 can give up to six roots for spherical components. Volume roots of methane at 1atm and 60K using SAFT-LJ3 are listed in **Table 4.4**.

**Figure 4.7** shows the bifurcation diagram of argon at 1atm. Generally speaking, all spherical components have the same solution behavior where a physical branch with two multi-phase regions co-exists with an extended non-physical branch resulting in a maximum of six volume roots.

**Figure 4.6: Bifurcation diagram of methane at 1atm for SAFT-LJ3 equation of state.**

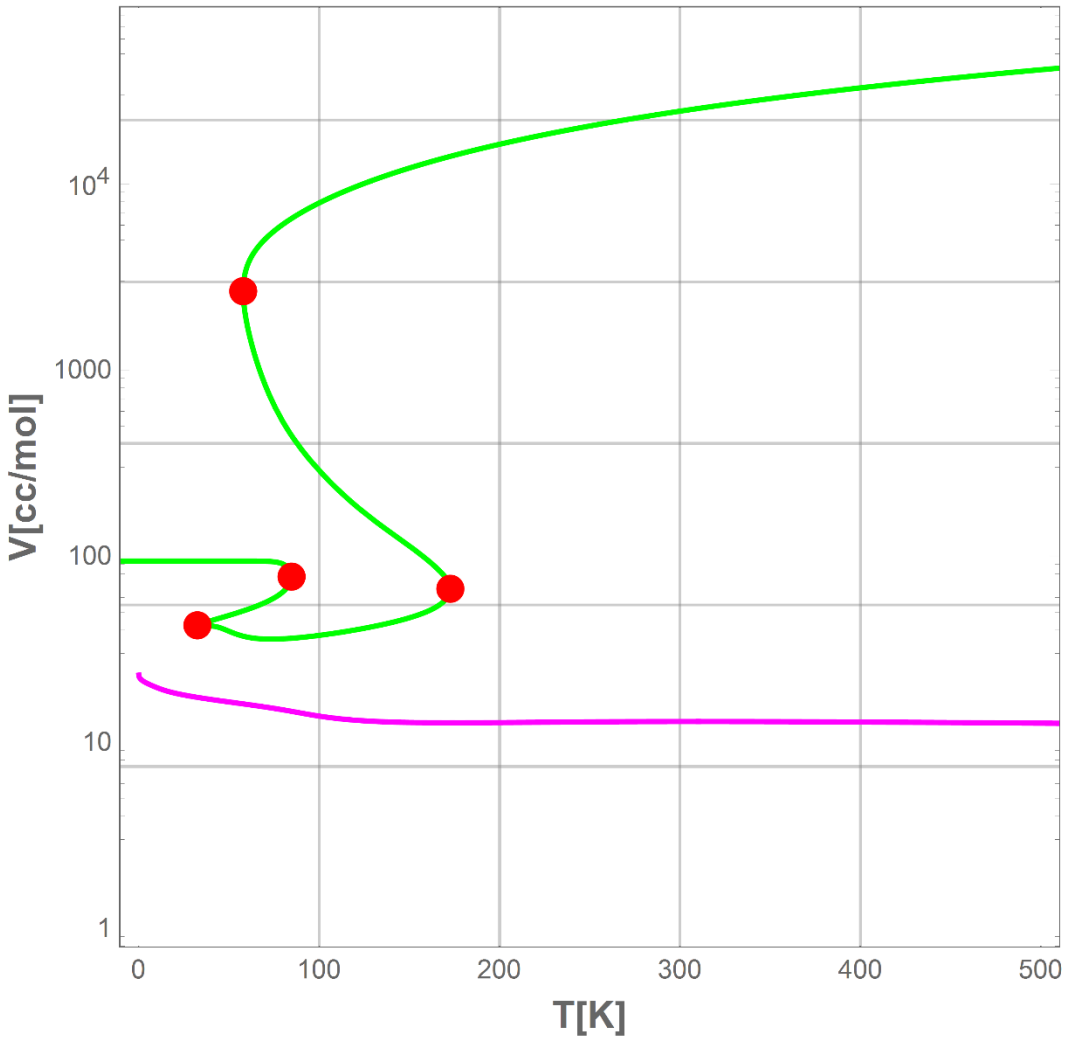

**Table 4.3: Saturation properties of methane at 1atm and 5atm using SAFT-LJ3.**

| P(atm) | Actual two-phase region | | | |
|---|---|---|---|---|
| | T(K) | $V_{liquid}$(cc/mol) | $V_{vapor}$(cc/mol) | Fugacity coefficient |
| 1 | 110.93 | 38.78 | 8847.71 | 0.9727 |
| 5 | 132.29 | 42.18 | 1970.24 | 0.9157 |
| P(atm) | Non-physical two-phase region | | | |
| | T(K) | $V_{liquid}$(cc/mol) | $V_{vapor}$(cc/mol) | Fugacity coefficient |
| 1 | 80.44 | 35.94 | 90.16 | 0.00759 |
| 5 | 80.41 | 35.92 | 90.13 | 0.00154 |

**Table 4.4: Volume roots (cc/mol) of methane at 1atm and 60K using SAFT-LJ3.**

| | |
|---|---|
| **V1** | 15.9 |
| **V2** | 36.7 |
| **V3** | 51.5 |
| **V4** | 94.0 |
| **V5** | 1761.6 |
| **V6** | 3591.8 |

**Figure 4.7: Bifurcation diagram of argon at 1atm for SAFT-LJ3 equation of state.**

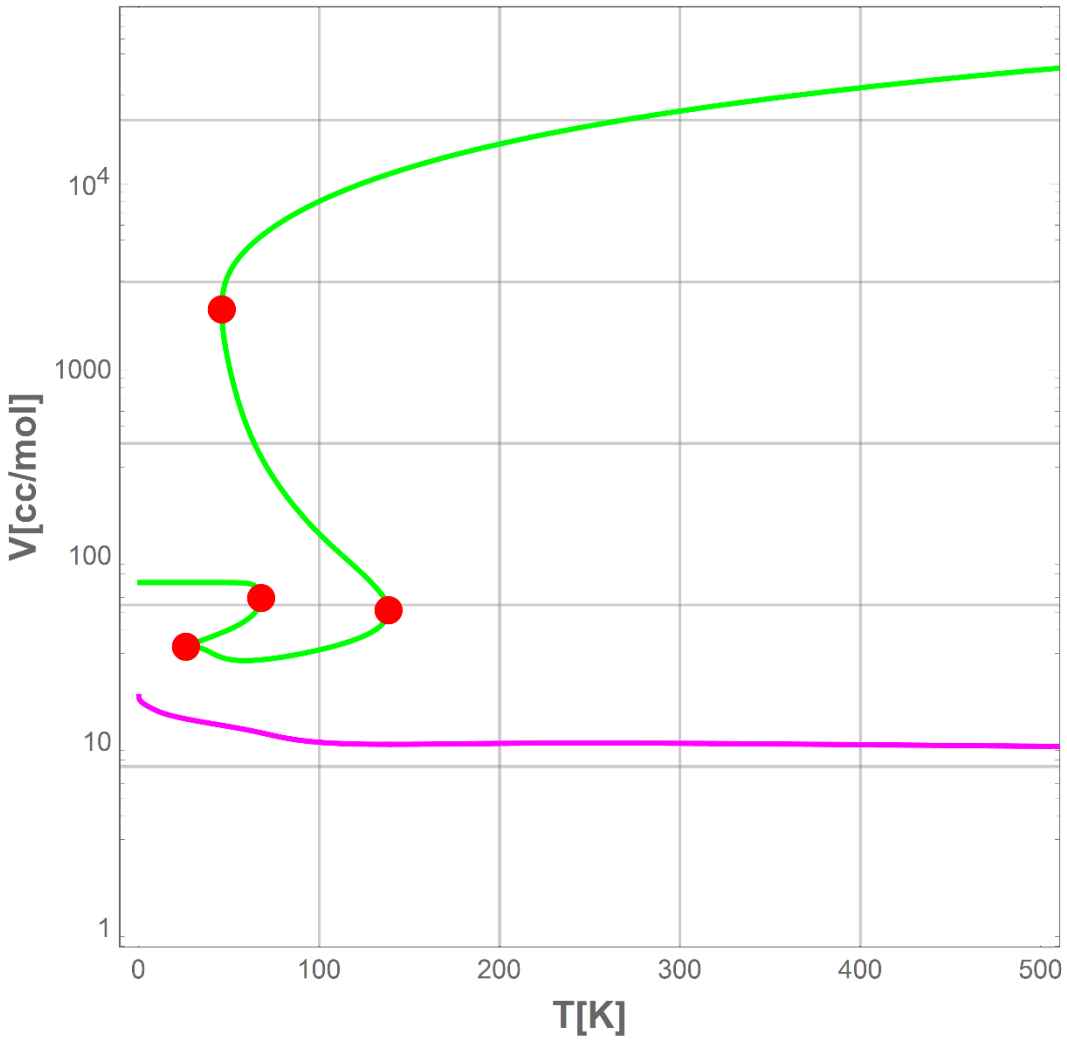


### 4.4.2 Non-spherical molecules

Since SAFT-LJ3 adopts the same chain term used in soft-SAFT (J. K. Johnson et al., 1994), the comparison of the bifurcation diagrams of non-spherical components using both models will give a valid conclusion about the effect of implementing this chain term on the PVT solution behaviour of LJ models. Bifurcation diagrams using SAFT-LJ3 for ethane, propane and octane at 1atm are shown in **Figures 4.8, 4.9** & **4.10**; respectively.

**Figure 4.8: Bifurcation diagram of ethane at 1atm for SAFT-LJ3 equation of state.**

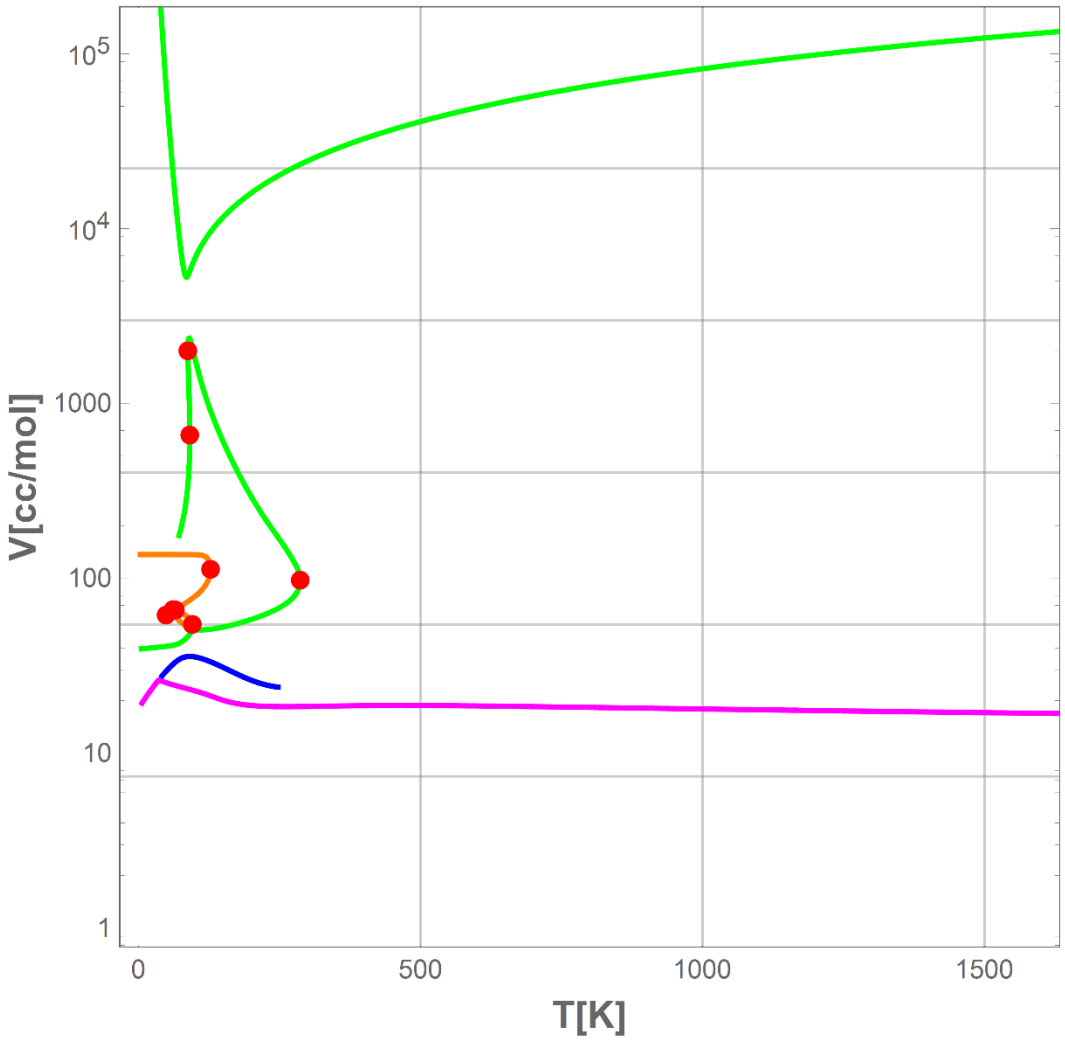


Similar to soft-SAFT, the addition of the chain term in SAFT-LJ3 has resulted in the appearance of several non-physical branches in the bifurcation diagram, especially at low temperature. Moreover, the bifurcation diagram of ethane shows the same behaviour of the physical branch where it is divided into two separate branches. As the chain length increases the two branches approach each other until they combine in one physical branch. This trend can be observed by comparing the bifurcation diagrams of ethane, propane and octane. From the analysis of the bifurcation diagrams of LJ-chains using soft-SAFT and

SAFT-LJ3, it can be concluded that the adopted chain term is not well constructed since it results in non-physical solution behaviour that makes these LJ models of limited use as they can easily give misleading results.

**Figure 4.9: Bifurcation diagram of propane at 1atm for SAFT-LJ3 equation of state.**

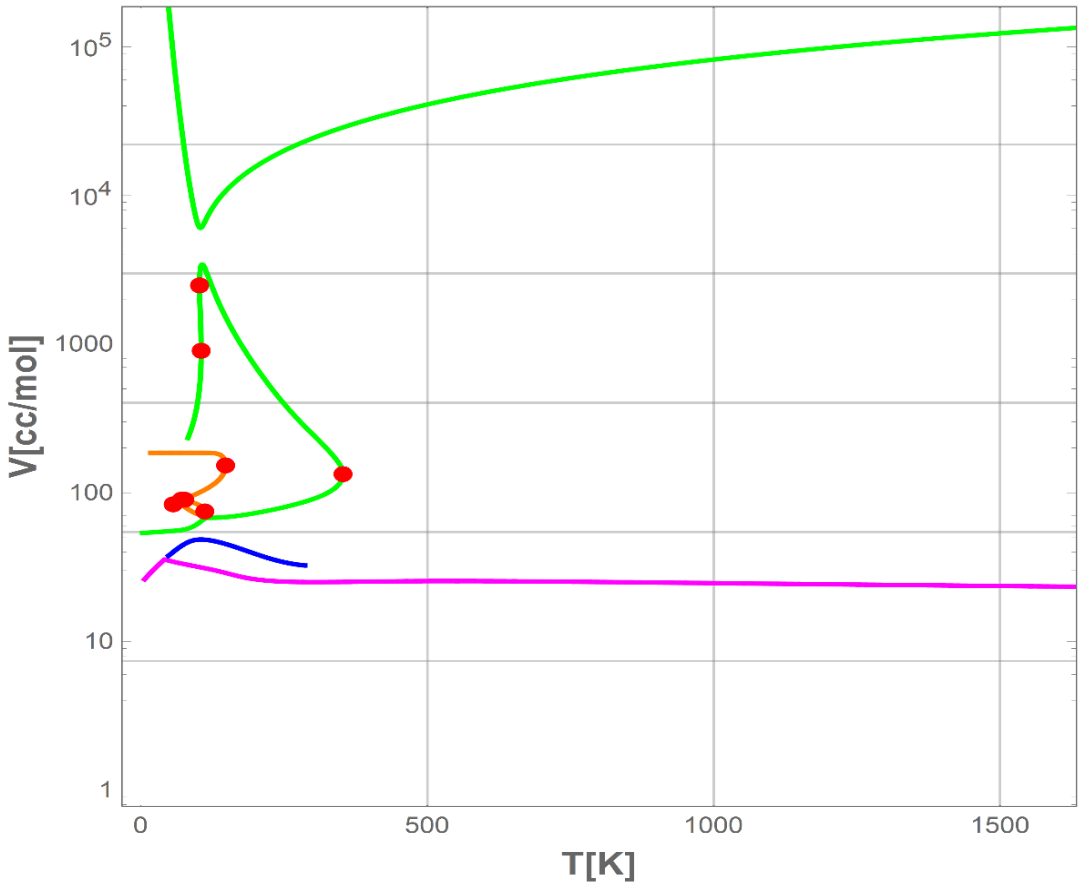

**Figure 4.10: Bifurcation diagram of octane at 1atm for SAFT-LJ3 equation of state.**

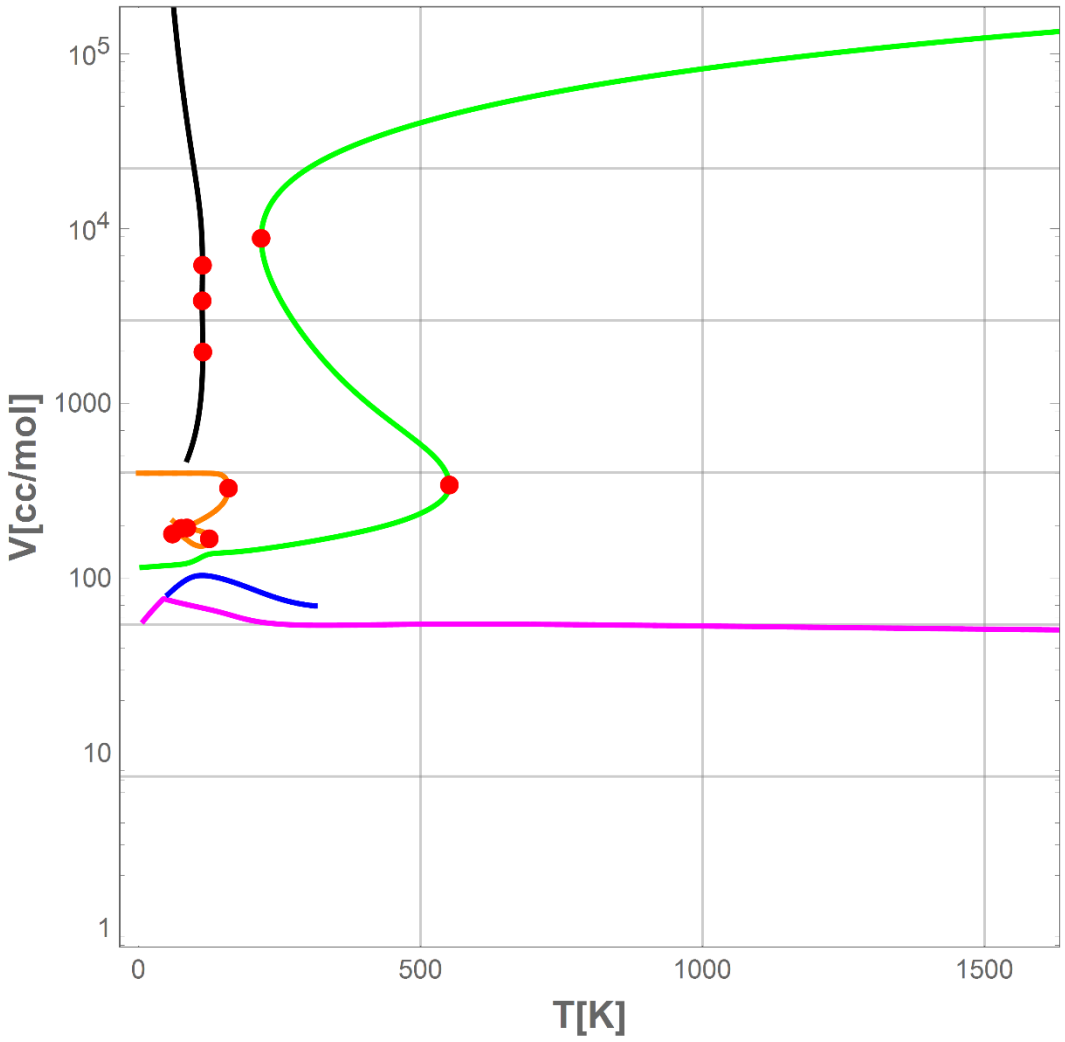


Finally, unlike soft-SAFT, the physical branch of non-spherical components in SAFT-LJ3 does not exhibit any non-physical multi-phase regions. This evidence supports the conclusion that SAFT-LJ3 is a better choice for vapor-liquid equilibrium calculations.

## 4.5 SAFT-VR Mie-LJ

### 4.5.1 Spherical molecules

In this section, the SAFT-VR Mie is utilized with forcing the repulsive and attractive exponents to be 12 and 6; respectively. Then, the adjustable parameters are obtained for several molecules. **Figure 4.11** shows the bifurcation diagram of methane at 1atm for SAFT-VR Mie-LJ equation of state. This bifurcation diagram exhibits four non-physical branches that are extended along wide range of temperature. SAFT-VR Mie-LJ can give up to eight volume roots. **Table 4.5** lists the volume roots of methane at 1atm and 130K using SAFT-VR Mie-LJ.

**Figure 4.11(a): Bifurcation diagram of methane at 1atm for SAFT-VR Mie-LJ equation of state.**

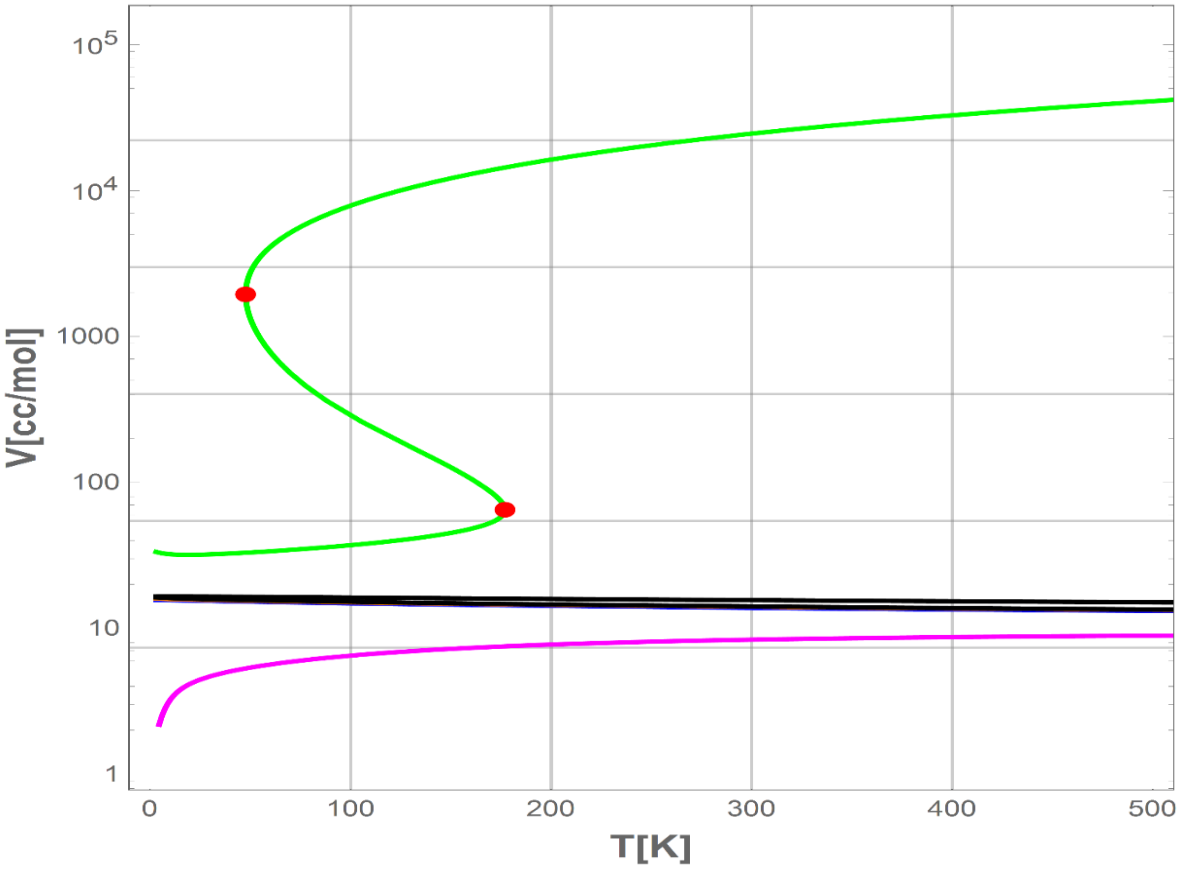

**Figure 4.11(b): Bifurcation diagram of methane at 1atm for SAFT-VR Mie-LJ equation of state (magnified region).**

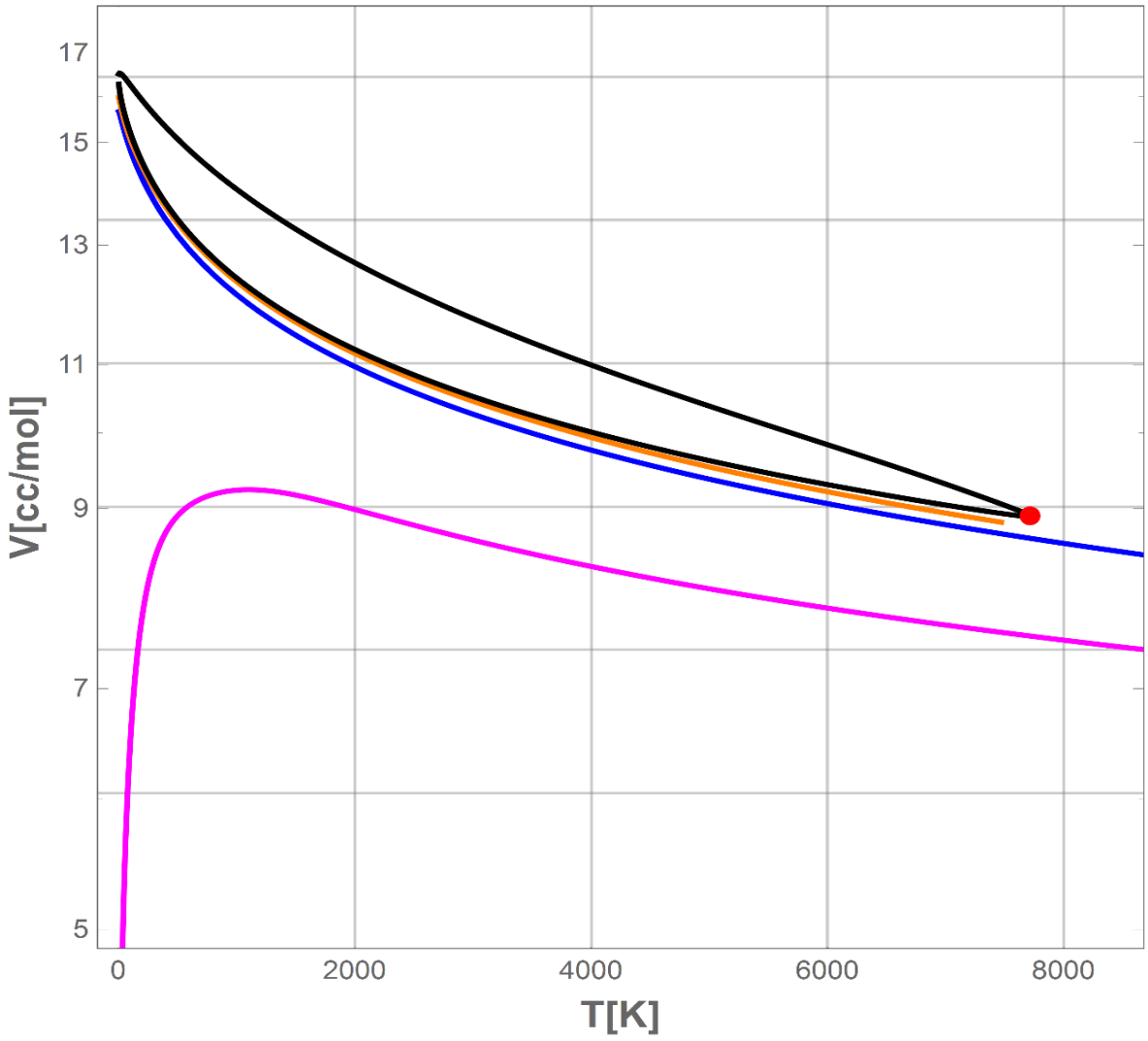

**Table 4.5: Volume roots (cc/mol) of methane at 1atm and 60K using SAFT-VR Mie-LJ.**

| | |
|---|---|
| **V1** | 6.974 |
| **V2** | 14.658 |
| **V3** | 14.887 |
| **V4** | 15.003 |
| **V5** | 16.152 |
| **V6** | 41.043 |
| **V7** | 175.005 |
| **V8** | 10465.100 |

Despite the fact that the number of non-physical volume roots is high, they are still far from the physical roots. Furthermore, it is clear that the first root is so small that it can be excluded immediately. On the other hand, the remaining non-physical volume roots are very close to each other in value. This suggests that these roots can be easily excluded since their range is very small, around 2 cc/mol. Unlike soft-SAFT and SAFT-LJ3, the bifurcation diagrams of spherical components using SAFT-VR Mie-LJ do not show any non-physical multi-phase regions.

**Figure 4.12(a): Bifurcation diagram of argon at 1atm for SAFT-VR Mie-LJ equation of state.**

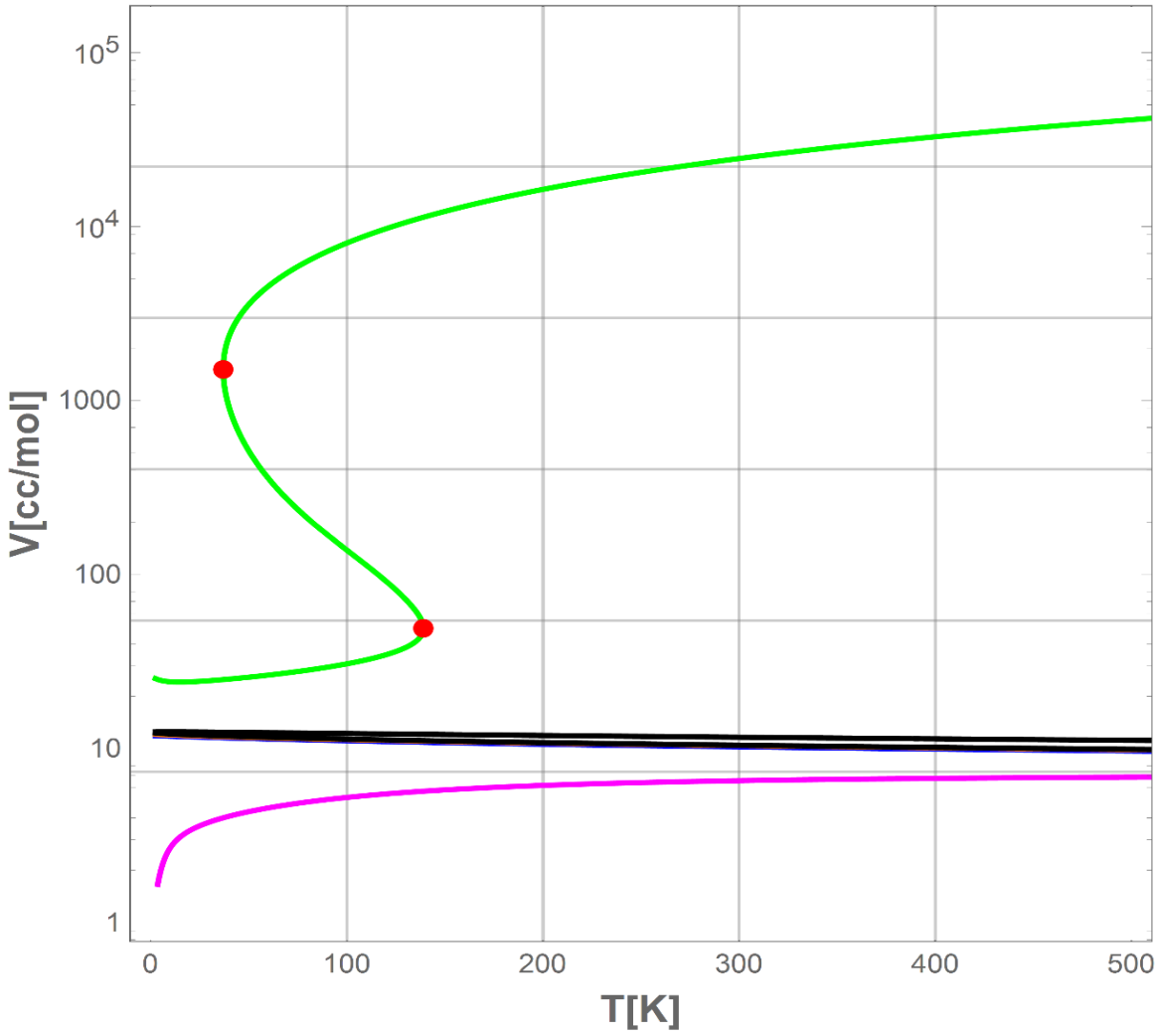

**Figure 4.12(b): Bifurcation diagram of argon at 1atm for SAFT-VR Mie-LJ equation of state (magnified region).**

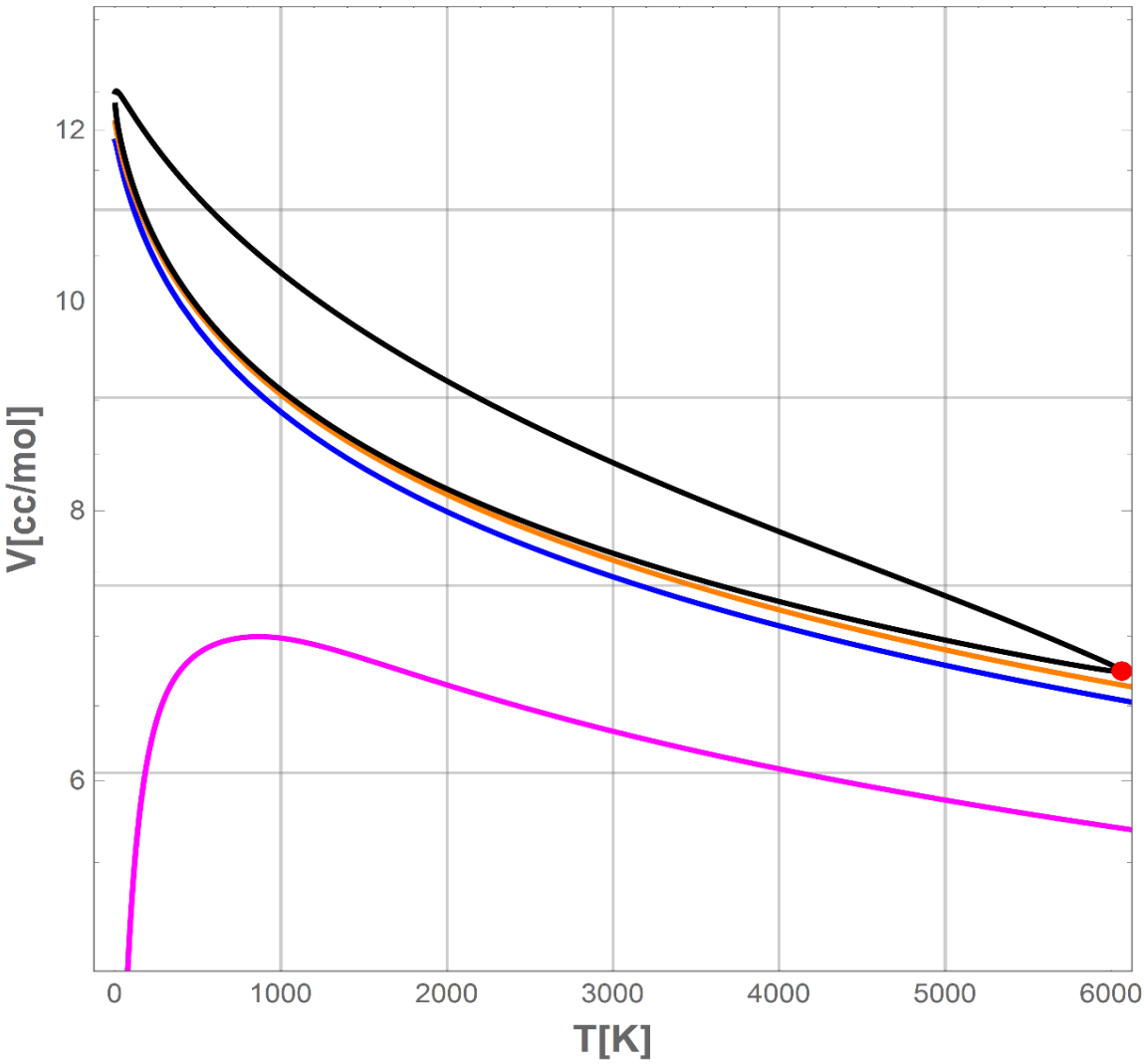


### 4.5.2 Non-spherical molecules

The bifurcation diagrams of ethane for SAFT-VR Mie-LJ equation of state is shown in **Figure 4.13**. This diagram exhibits two non-physical branches in addition to the physical branch. At low temperatures, the model could give up to six volume roots. It is clear that the addition of the chain term in SAFT-VR Mie-LJ, unlike soft-SAFT and SAFT-LJ3, has resulted in a more realistic PVT solution behavior since two non-physical branches have been omitted. However, the serious drawback of adding the chain term is the appearance

of a non-physical two-phase region at low temperature. In order to study the effect of the chain length on the solution behavior, the bifurcation diagram of octane at 1atm has been generated as shown in **Figure 4.14**. It is noticed that when the chain length increased, the PVT solution behavior maintained its structure unchanged. This advantage of having a stable solution behavior for LJ-chains can lead to a conclusion that SAFT-VR Mie-LJ is a safer choice, compared to soft-SAFT and SAFT-LJ3, for performing thermodynamic properties calculations.

**Figure 4.13: Bifurcation diagram of ethane at 1atm for SAFT-VR Mie-LJ equation of state.**

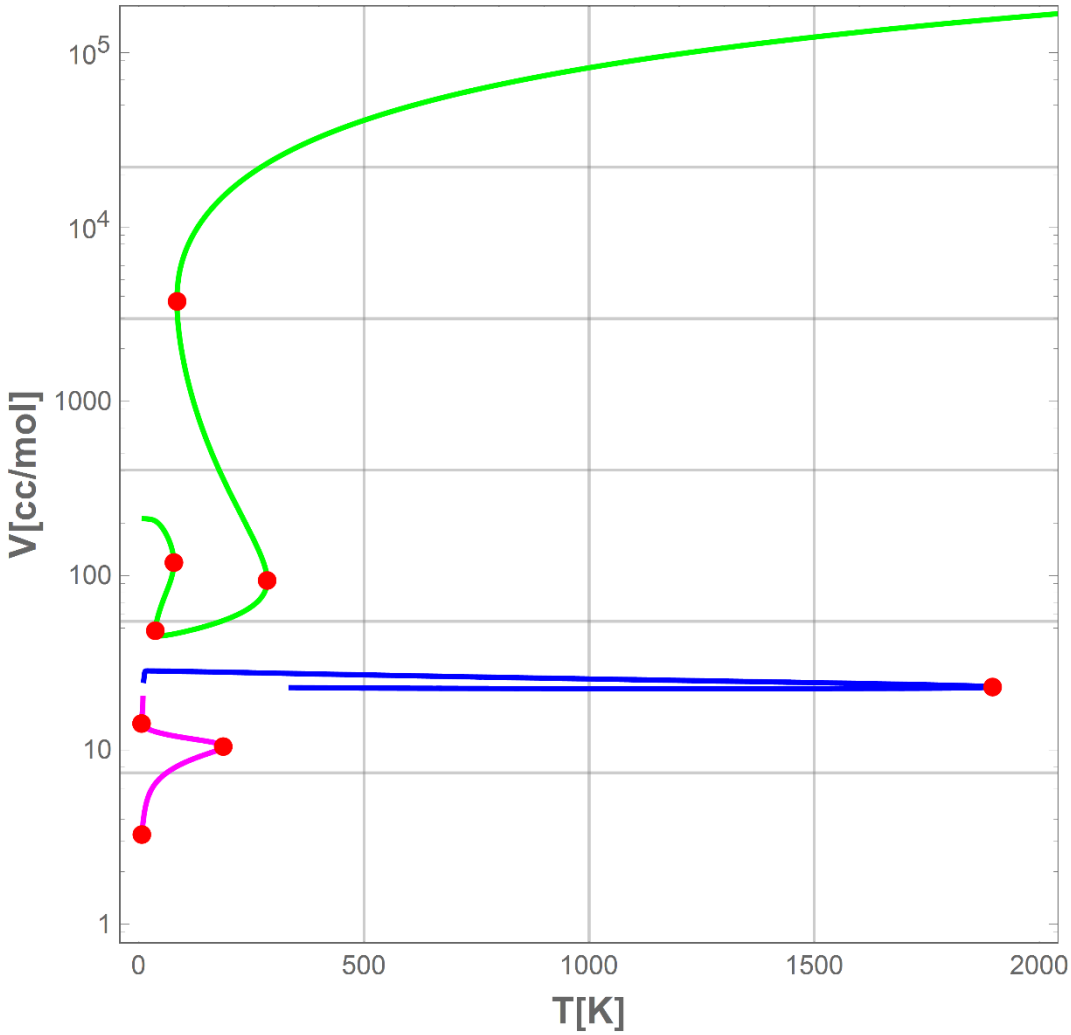

**Figure 4.14: Bifurcation diagram of octane at 1atm for SAFT-VR Mie-LJ equation of state.**

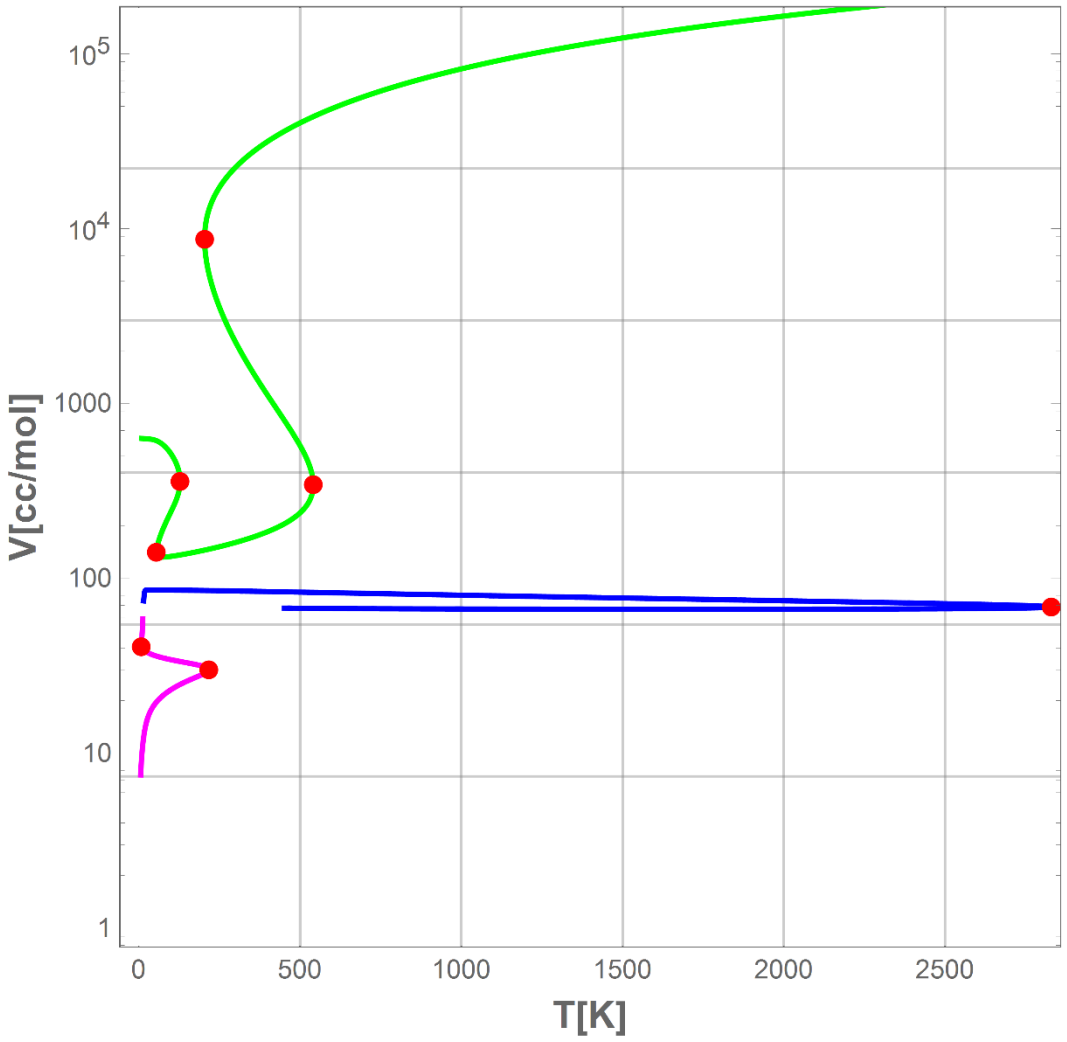


## 4.6 Effect of pressure

In general, as the pressure increases, the volume of the fluid at certain temperature decreases. For that reason, it is clear that the physical branch in a bifurcation diagram should shift down as the pressure increases. As the pressure approaches the critical pressure, the two-phase region gets narrower until the two turning points combine together forming the critical point. Moreover, increasing the pressure has the same effect of increasing the chain length on the solution behavior. This fact can be observed from the

bifurcation diagram of ethane at different pressures for soft-SAFT, **Figure 4.16**, where the two parts of the physical branch at 1atm get closer and combine at higher pressures. On the other hand, the non-physical branches are almost independent of pressure and this can be clearly noticed from **Figures 4.15** & **4.16**. **Tables 4.6** & **4.7** list the non-physical volume roots of methane and ethane at 100 K for SAFT-LJ3 and SAFT-VR Mie-LJ respectively. It is clear that these roots have almost the same values regardless of the pressure values

**Figure 4.15: Bifurcation diagram of methane at different pressures for soft-SAFT equation of state.**

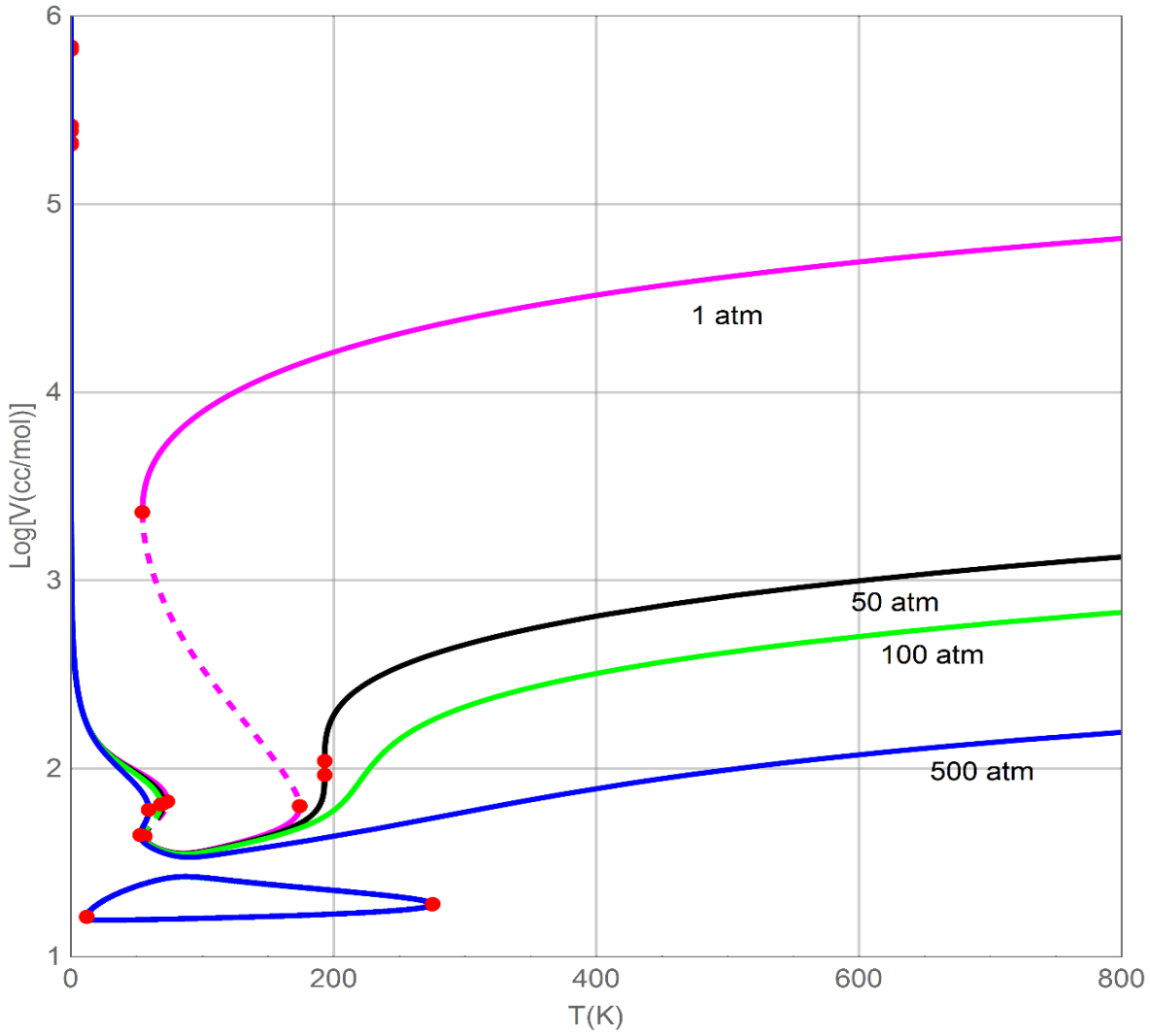

**Figure 4.16: Bifurcation diagram of ethane at different pressures for soft-SAFT equation of state.**

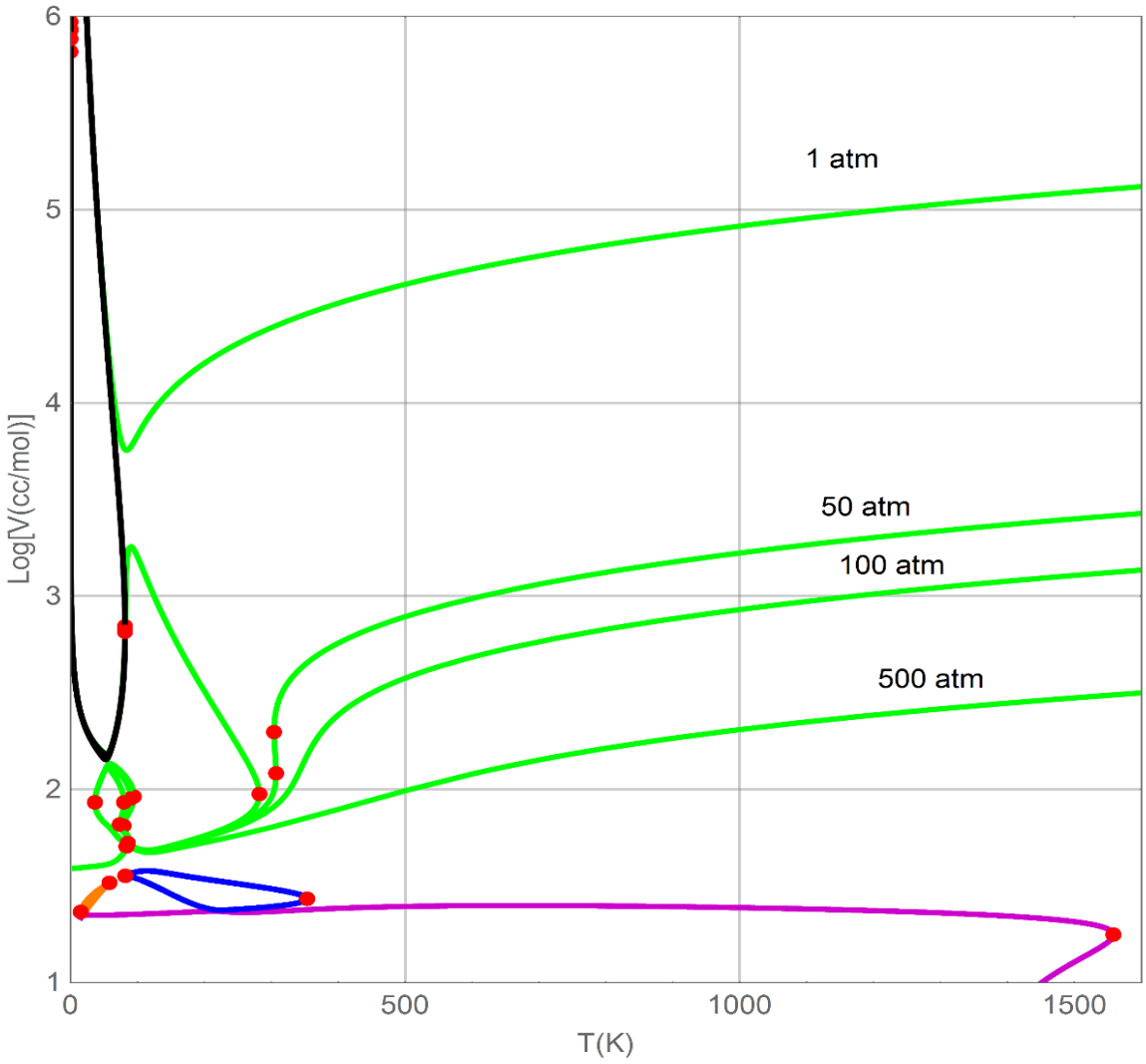


**Table 4.6: Non-physical volume roots of methane and ethane at 100K and different pressures using SAFT-LJ3.**

| P(atm) | T(K) | Methane | Ethane | | | | |
|---|---|---|---|---|---|---|---|
| | | V1(cc/mol) | V1(cc/mol) | V2(cc/mol) | V3(cc/mol) | V4(cc/mol) | V5(cc/mol) |
| 0.5 | 100 | 13.8027 | 22.7526 | 35.5586 | 50.863 | 79.1115 | 136.745 |
| 1 | 100 | 13.8027 | 22.7526 | 35.5586 | 50.8597 | 79.1123 | 136.745 |
| 10 | 100 | 13.8027 | 22.7526 | 35.5585 | 50.7999 | 79.1256 | 136.743 |
| 100 | 100 | 13.8025 | 22.7524 | 35.5583 | 50.263 | 79.2555 | 136.726 |
| 1000 | 100 | 13.8006 | 22.7507 | 35.5555 | 47.1534 | 80.2857 | 136.557 |

**Table 4.7: Non-physical volume roots of methane (cc/mol) and ethane at 100K and different pressures using SAFT-VR Mie-LJ.**

| P(atm) | T(K) | Methane | | | | | Ethane | | |
|---|---|---|---|---|---|---|---|---|---|
| | | V1 | V2 | V3 | V4 | V5 | V1 | V2 | V3 |
| 0.5 | 100 | 6.5011 | 14.8539 | 15.0705 | 15.2095 | 16.2569 | 8.42474 | 11.7708 | 28.2083 |
| 1 | 100 | 6.5011 | 14.8539 | 15.0705 | 15.2095 | 16.2569 | 8.42474 | 11.7708 | 28.2083 |
| 10 | 100 | 6.5011 | 14.8539 | 15.0705 | 15.2095 | 16.2569 | 8.42474 | 11.7708 | 28.2084 |
| 100 | 100 | 6.5011 | 14.8539 | 15.0705 | 15.2095 | 16.2569 | 8.42475 | 11.7708 | 28.2086 |
| 1000 | 100 | 6.50112 | 14.8539 | 15.0705 | 15.2095 | 16.2569 | 8.42476 | 11.7707 | 28.2114 |

# Chapter 5

# Solution behavior of SAFT-VR Mie EOS

## 5.1 INTRODUCTION

From the previous discussion of the PVT solution behavior of various LJ models, it was clear that SAFT-VR Mie-LJ equation of state has the most realistic PVT behavior among the discussed models. Due to its solution behavior as well as its high popularity and accuracy, the SAFT-VR Mie is investigated in this chapter. The bifurcation diagrams are generated for both spherical and non-spherical components. Because the only difference between SAFT-VR Mie and SAFT-VR Mie-LJ is the repulsive and attractive exponents, the analysis of the PVT behavior will demonstrate the effect of these two exponents. For most of the components, the attractive exponent ($\lambda a$) is usually fixed at Lennard-Jones value ($\lambda a = 6$). Finally, a simple technique for excluding non-physical volume roots is proposed based on the concept of maximum packing fraction of fluids.

## 5.2 Spherical molecules

Figures **5.1** to **5.4** show the bifurcation diagrams of methane at 1atm using SAFT-VR Mie with different repulsive exponents. From these bifurcation diagrams, it is clear that the effect of changing the repulsive exponent is limited to the non-physical branches. Although the general trend is that the SAFT-VR Mie exhibits five non-physical volume

roots for low repulsive exponents (close to 12) and four non-physical volume roots for high repulsive exponents, the solution behaviour can still change in a random manner even with a small change in the value of the repulsive exponent. For example, when $\lambda r = 12.650$, one of the non-physical branches exhibits two turning points resulting in seven non-physical volume roots as illustrated in **Figure 5.1(b)**.

**Figure 5.5** shows the bifurcation diagram of Perfluoromethane at 1atm. The obtained solution behavior confirms the conclusion that as the repulsive exponent increases, the number of non-physical volume roots decreases from five to four. Finally, SAFT-VR Mie equation of state does not exhibit any extra multi-phase region on the physical branch for molecular components.

**Figure 5.1(a): Bifurcation diagram of methane at 1atm for SAFT-VR Mie equation of state with $\lambda r = 12.650$.**

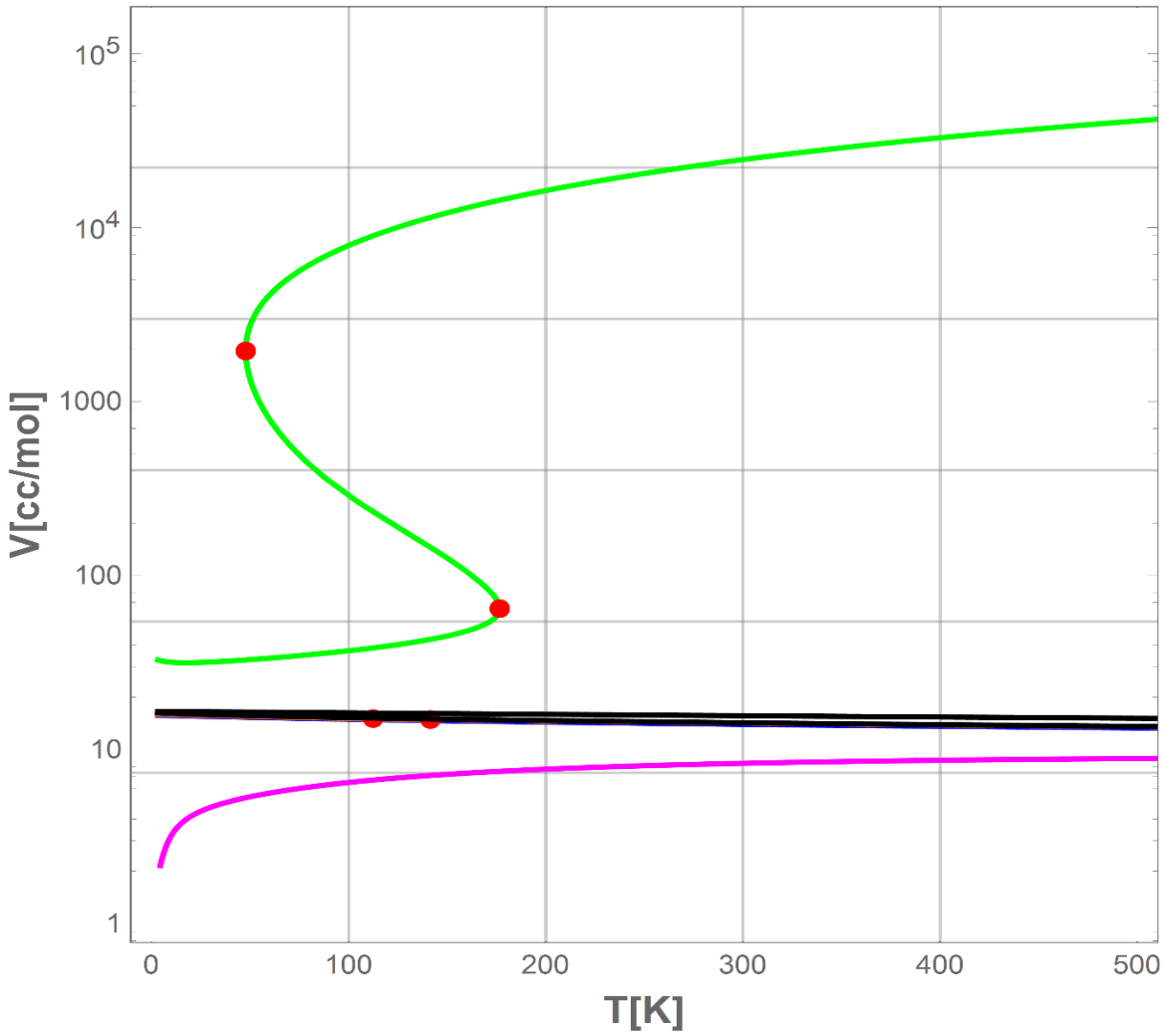

**Figure 5.1(b): Bifurcation diagram of methane at 1atm for SAFT-VR Mie equation of state with $\lambda r = 12.650$ (magnified region).**

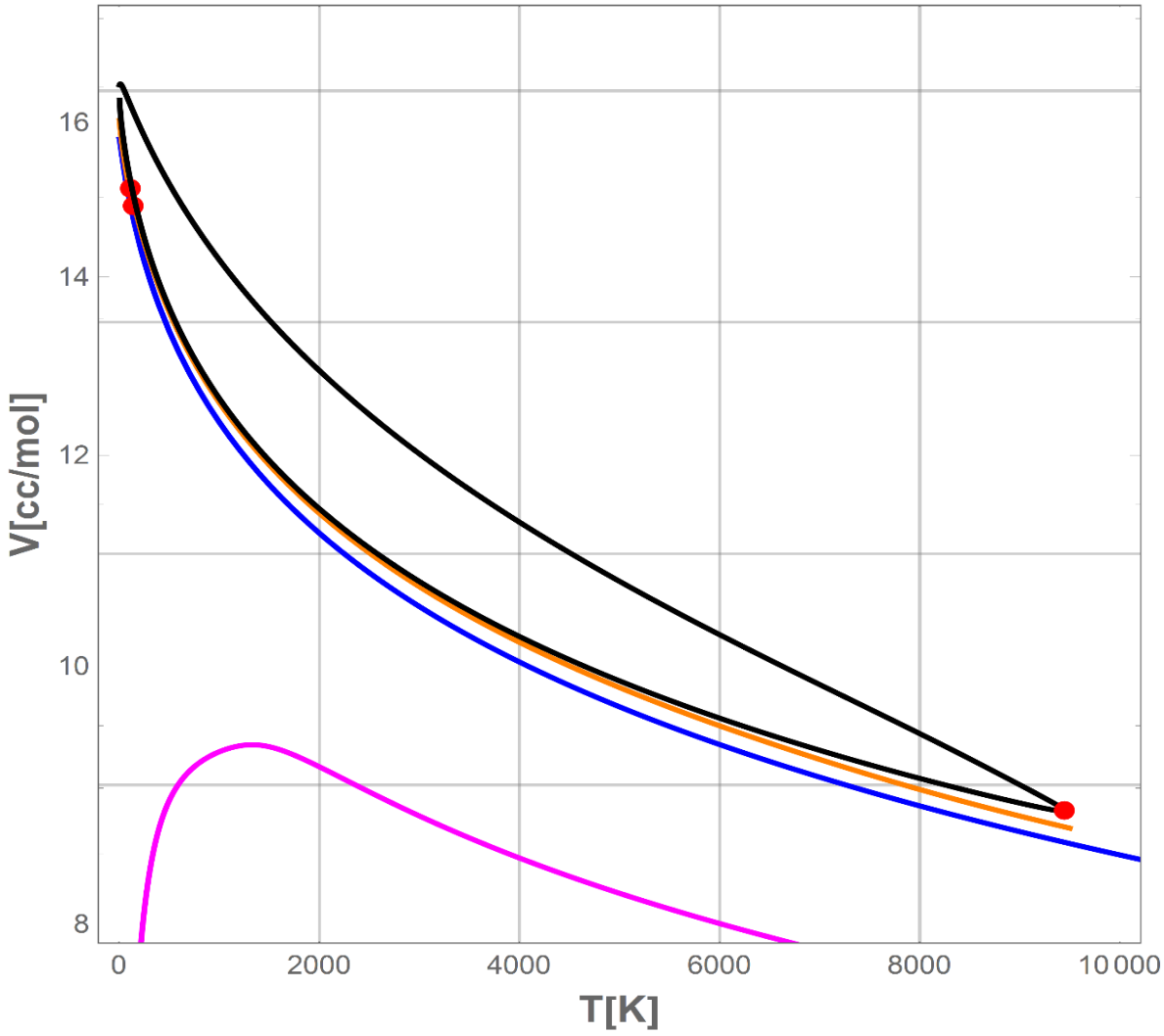

**Figure 5.2(a): Bifurcation diagram of methane at 1atm for SAFT-VR Mie equation of state with $\lambda r = 12$.**

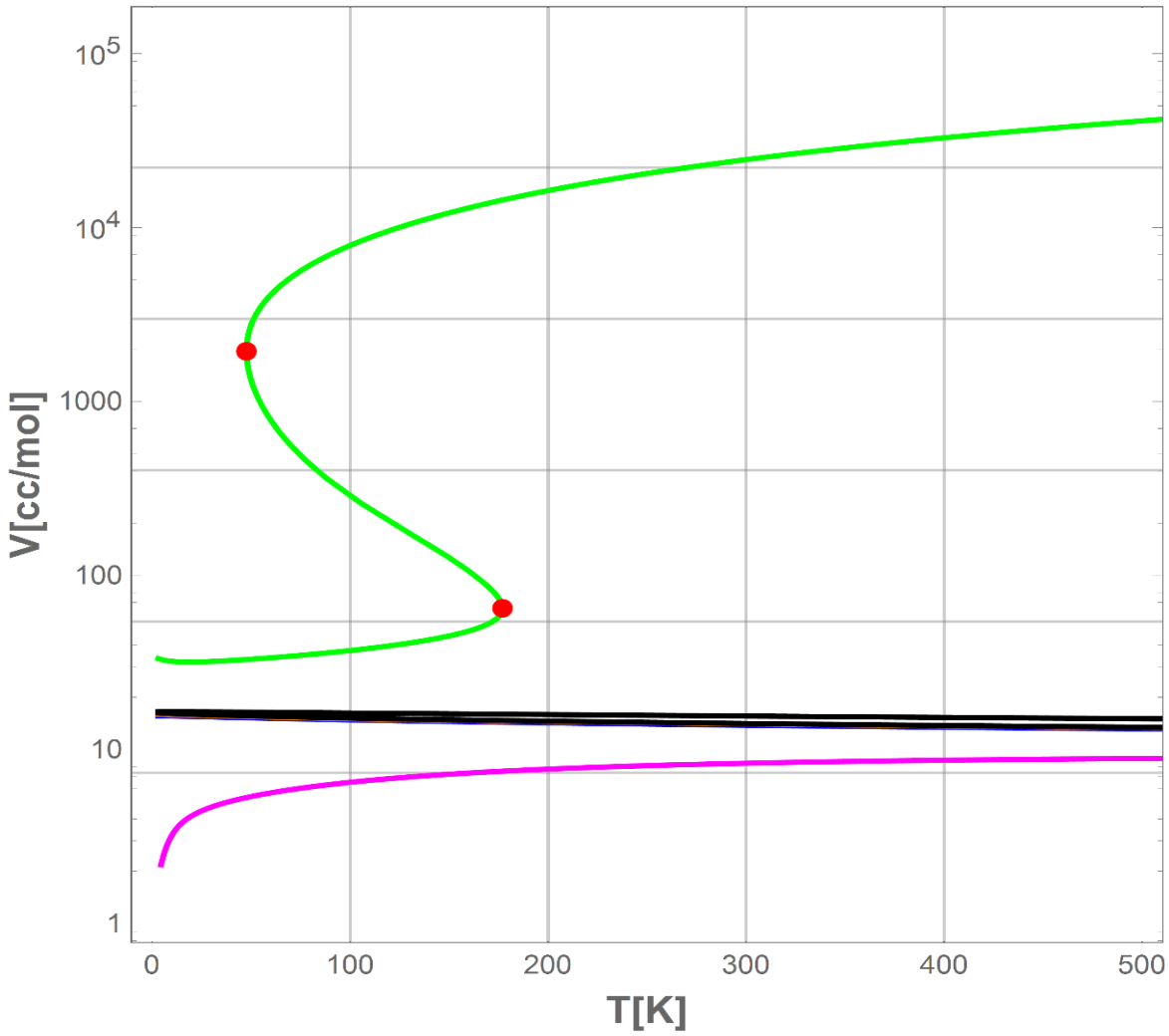

**Figure 5.2(b): Bifurcation diagram of methane at 1atm for SAFT-VR Mie equation of state with $\lambda r = 12$ (magnified region).**

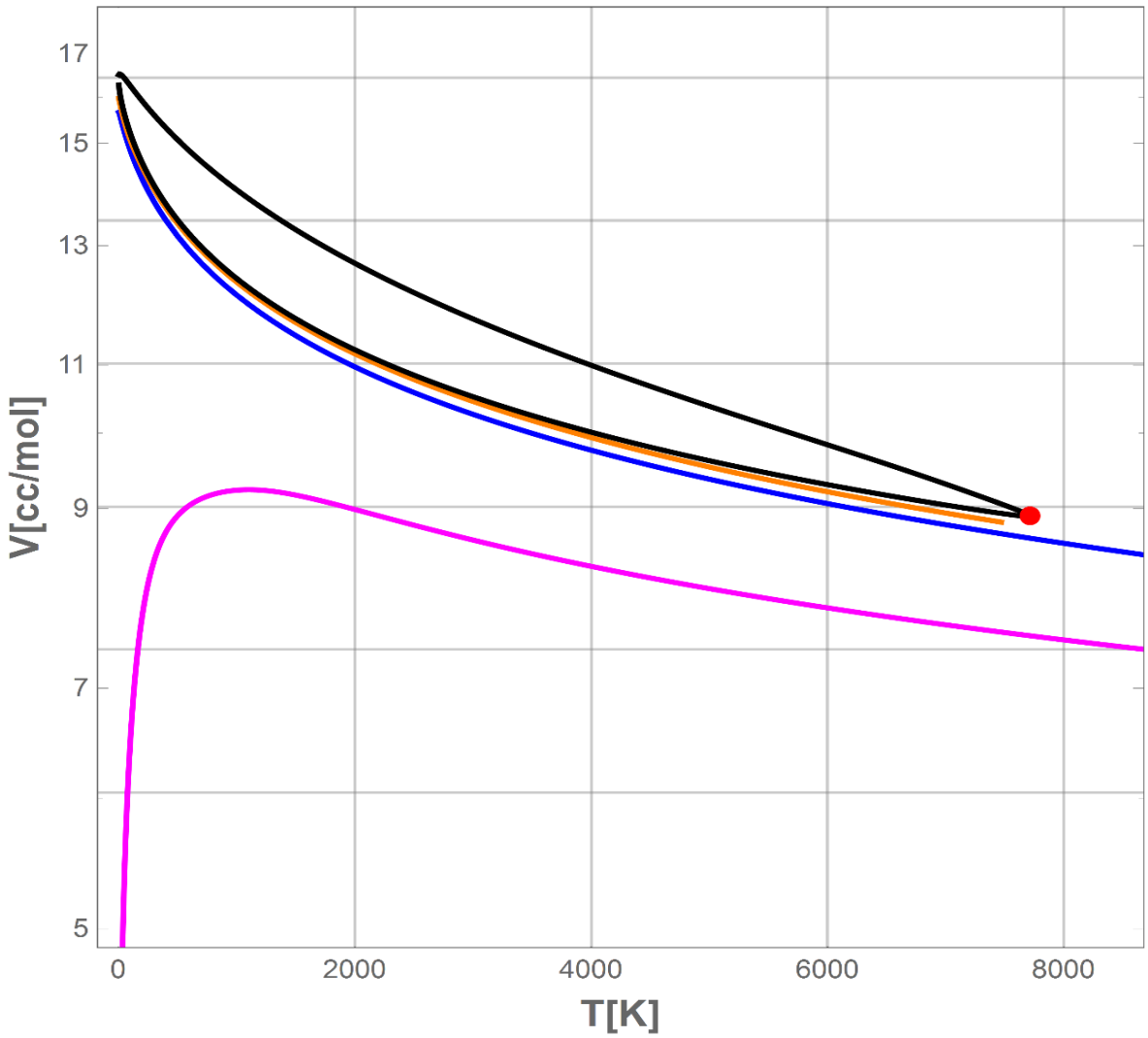

**Figure 5.3(a): Bifurcation diagram of methane at 1atm for SAFT-VR Mie equation of state with $\lambda r = 10$.**

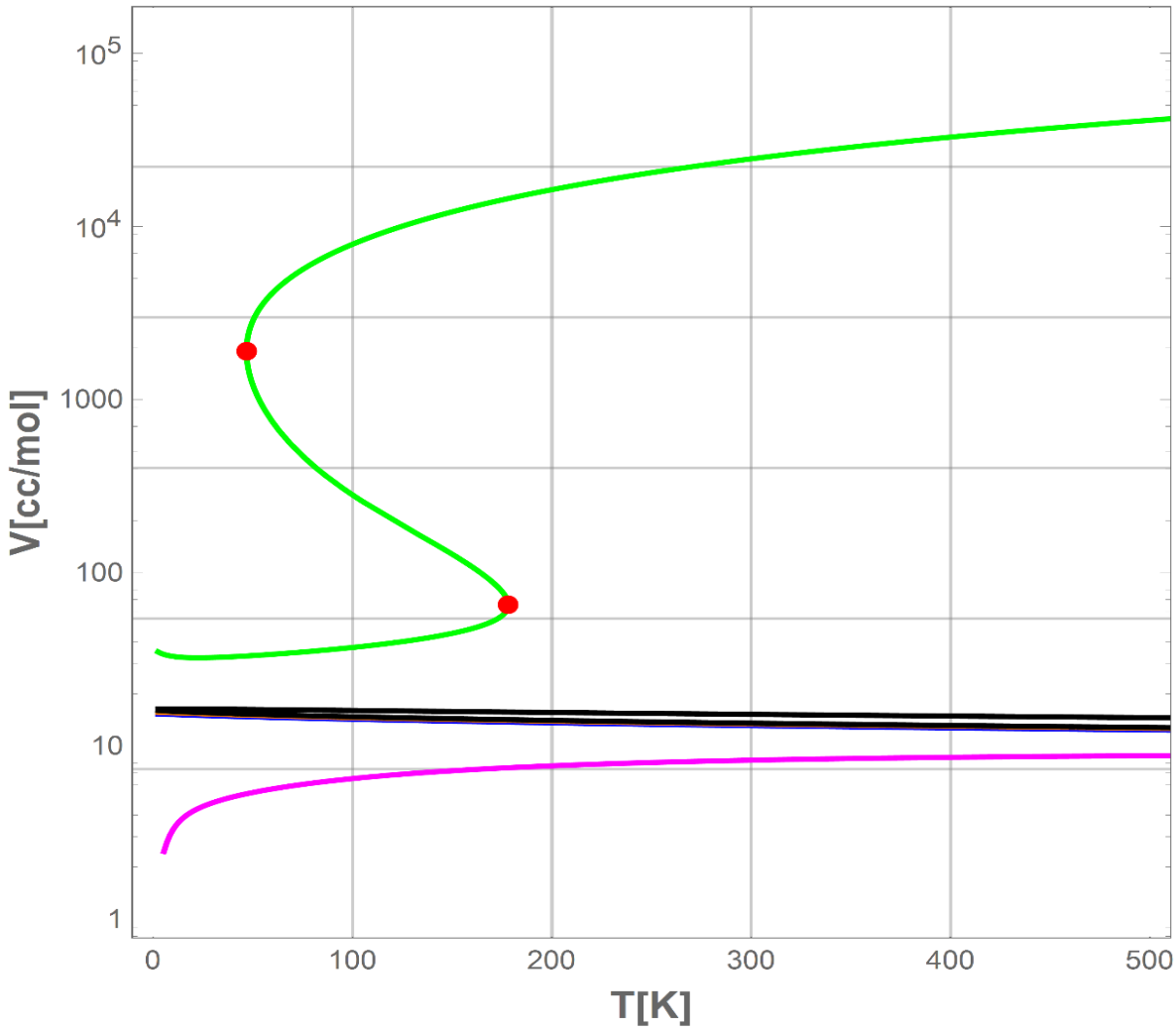

**Figure 5.3(b): Bifurcation diagram of methane at 1atm for SAFT-VR Mie equation of state with $\lambda r = 10$ (magnified region).**

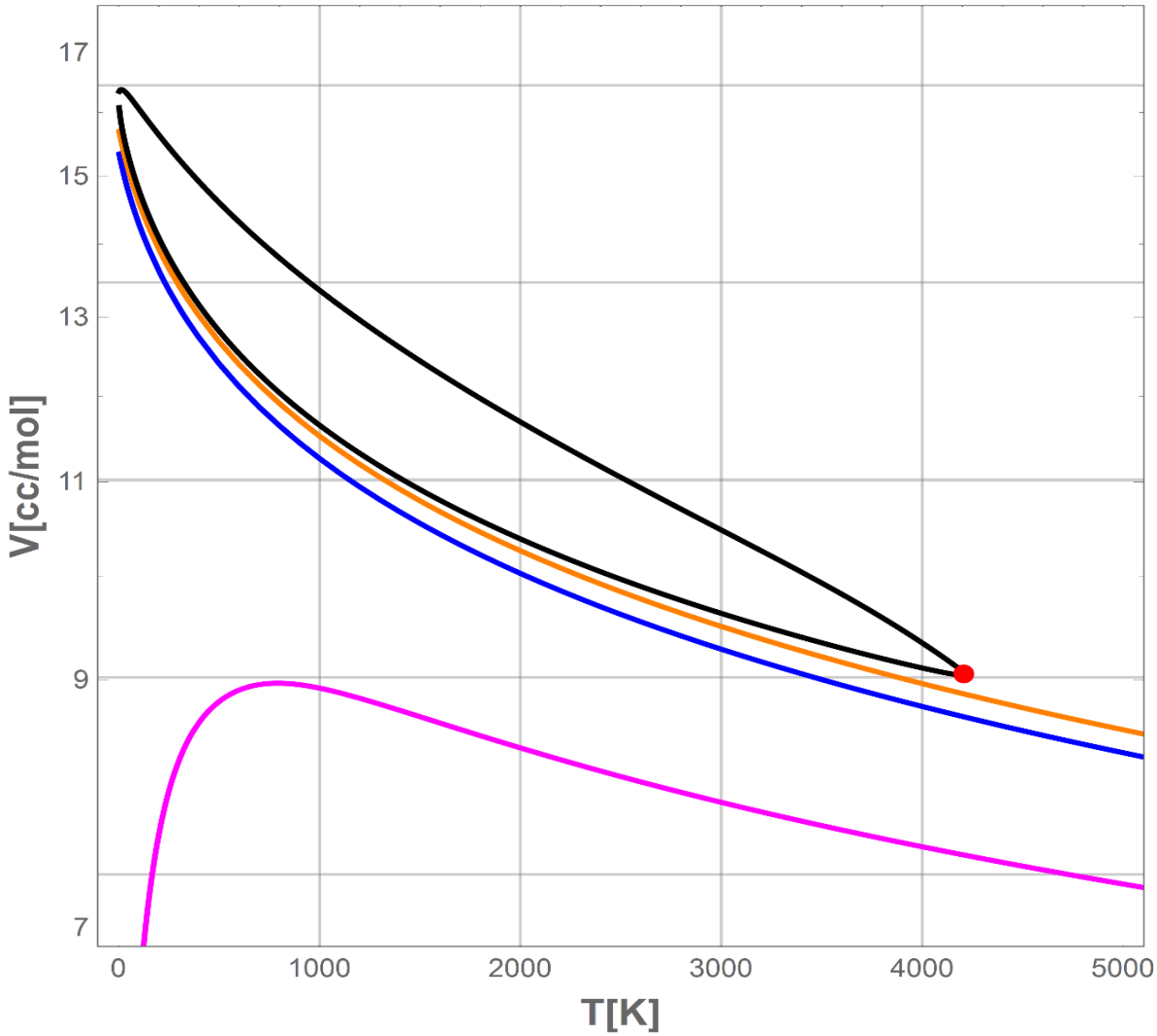

**Figure 5.4(a): Bifurcation diagram of methane at 1atm for SAFT-VR Mie equation of state with $\lambda r = 20$.**

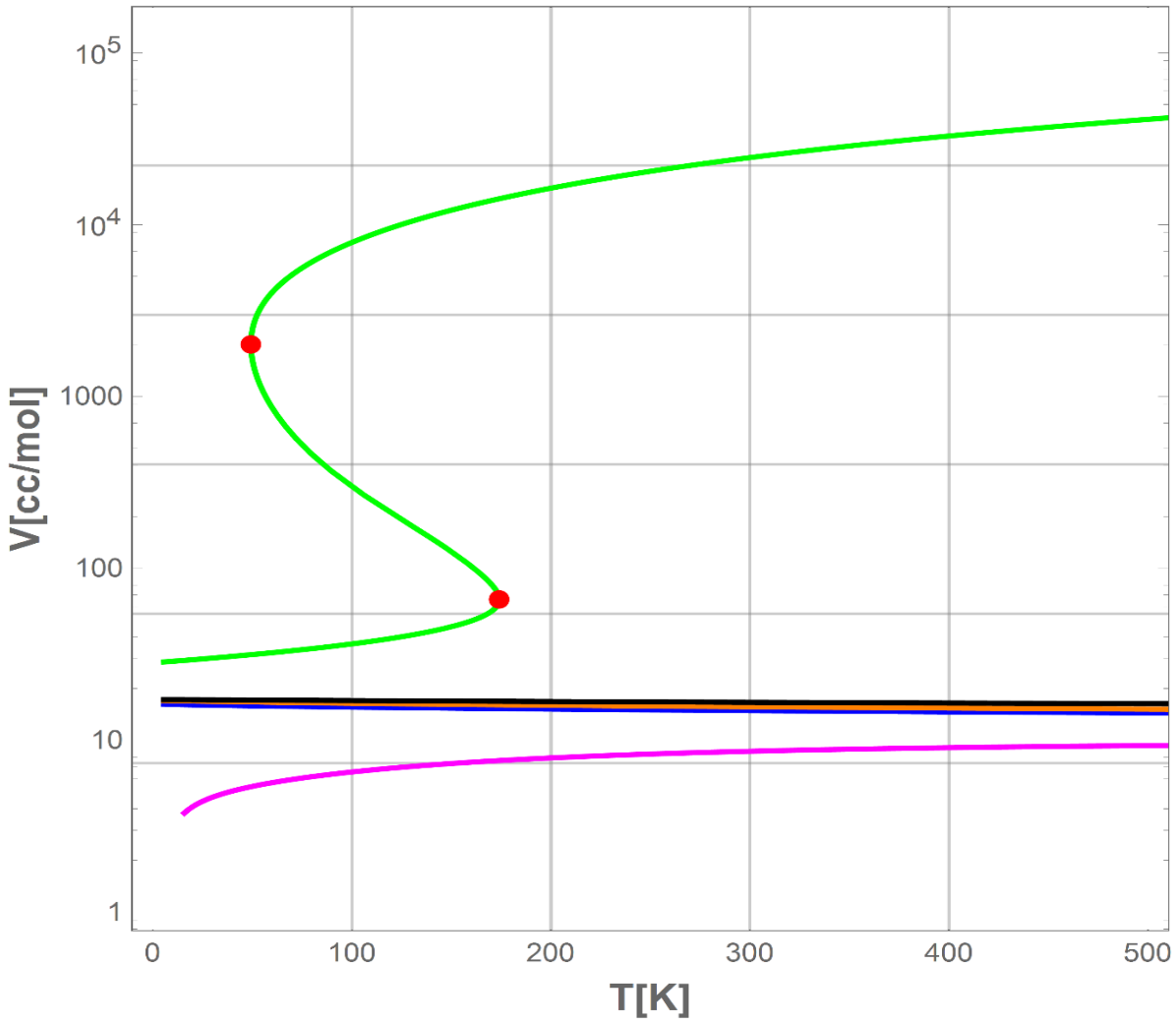

**Figure 5.4(b): Bifurcation diagram of methane at 1atm for SAFT-VR Mie equation of state with $\lambda r = 20$ (magnified region).**

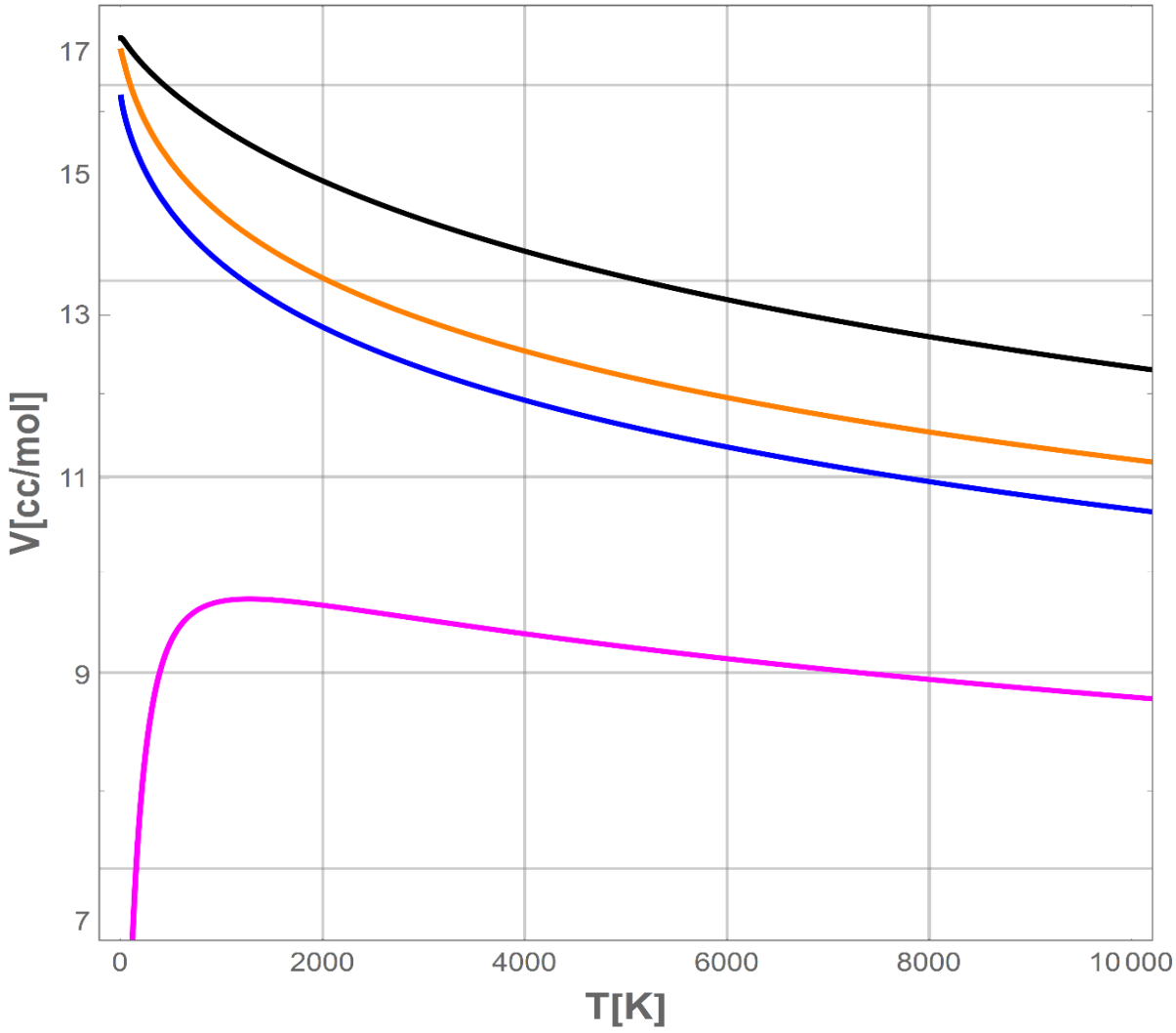

**Figure 5.5(a): Bifurcation diagram of Perfluoromethane at 1atm for SAFT-VR Mie equation of state with $\lambda r = 42.553$.**

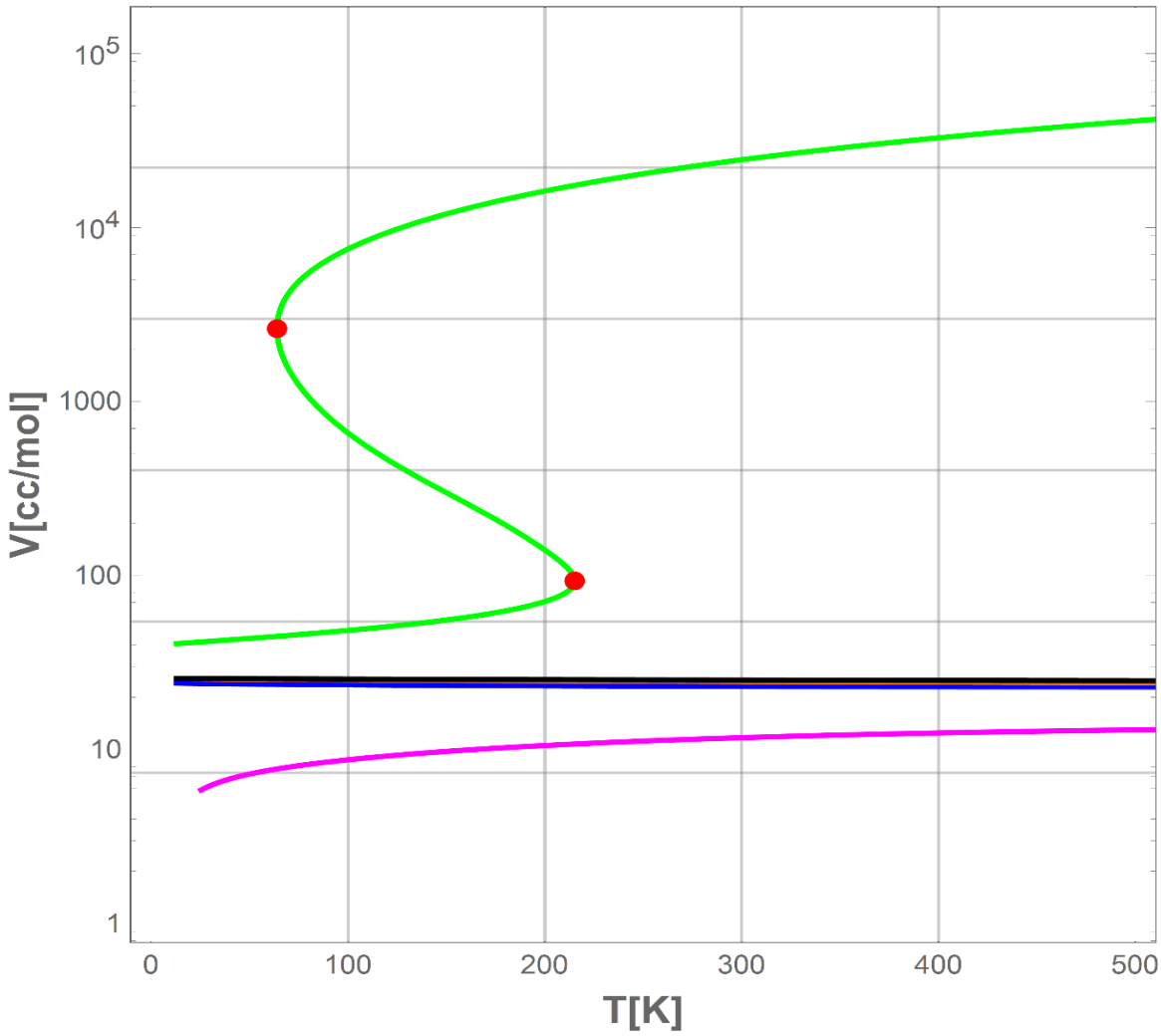

**Figure 5.5(b): Bifurcation diagram of Perfluoromethane at 1atm for SAFT-VR Mie equation of state with $\lambda r = 42.553$ (magnified region).**

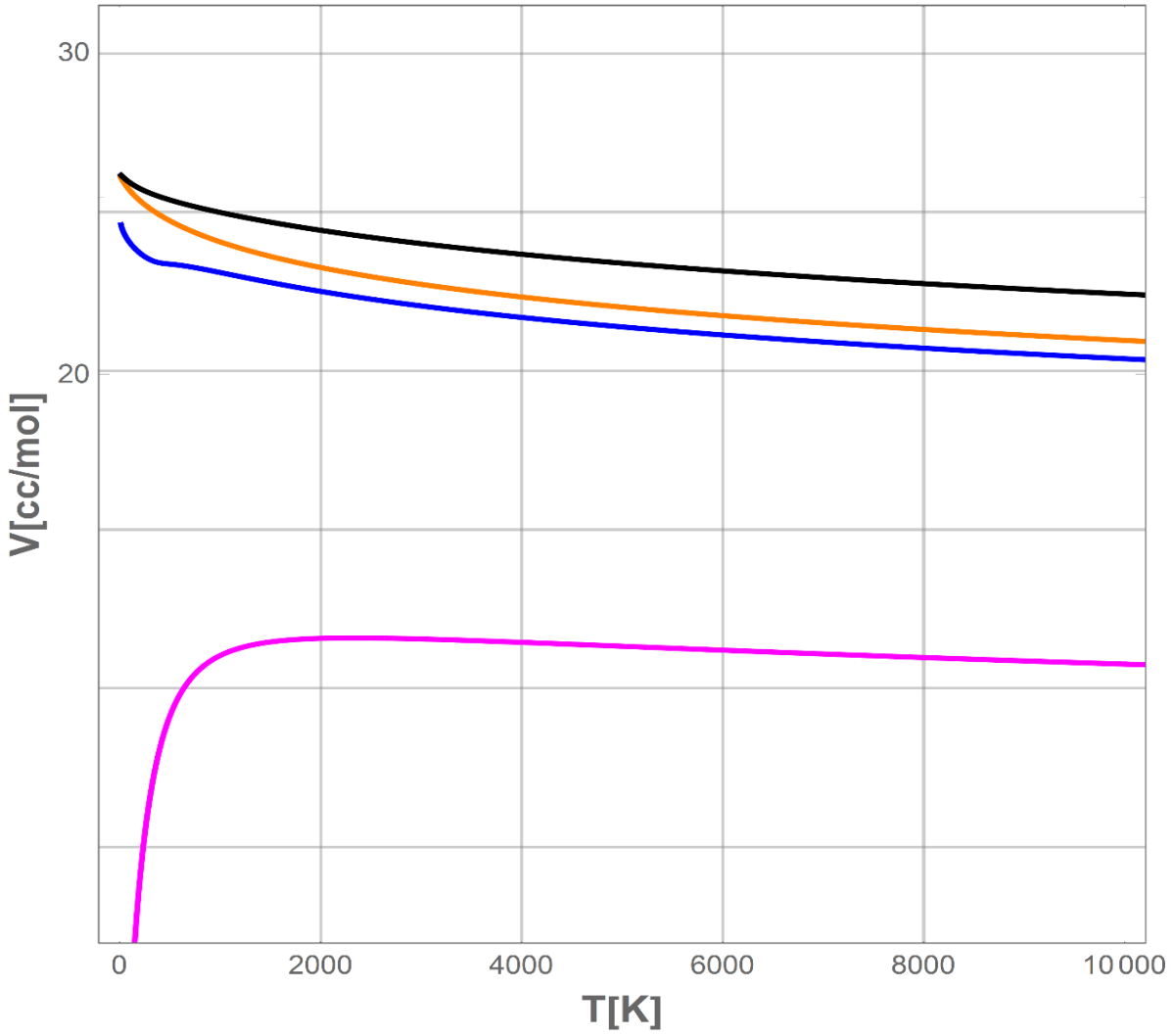

## 5.3 Non-spherical molecules

Figures **5.6** to **5.8** show the bifurcation diagrams of ethane, octane and decane respectively at 1atm using SAFT-VR Mie equation of state. It can be noticed that the non-physical branches in the bifurcation diagram of the short chains (ethane) is slightly different from those of longer chains (octane and decane). However, this change in the solution behaviour is not due to the change in the chain length because it has been concluded in the previous chapter that the chain length does not change the structure of the bifurcation diagram for SAFT-VR Mie-LJ. In fact, this change is most probably due to the increase in the repulsive exponent ($\lambda r = 12.400$, 17.378 and 18.885 for ethane, octane and decane respectively). This conclusion is confirmed by the fact that the bifurcation diagram of ethane (repulsive exponent close to LJ) is similar to that obtained for LJ chains using SAFT-VR Mie-LJ. On the other hand, it is clear that the non-physical multi-phase region is present for all non-spherical components. **Table 5.1** lists the saturation temperatures of ethane, octane and decane at 1atm using SAFT-VR Mie.

**Table 5.1: Saturation properties of ethane, octane and decane at 1atm using SAFT-VR Mie.**

| Component | Actual two-phase region | | | |
|---|---|---|---|---|
| | T(K) | $V_{liquid}$(cc/mol) | $V_{vapor}$(cc/mol) | Fugacity coefficient |
| Ethane | 184.553 | 55.414 | 14745.4 | 0.974458 |
| Octane | 398.362 | 187.59 | 31413.8 | 0.962751 |
| Decane | 446.901 | 237.301 | 35078.3 | 0.95869 |
| **Component** | **Non-physical two-phase region** | | | |
| | **T(K)** | **$V_{liquid}$(cc/mol)** | **$V_{vapor}$(cc/mol)** | **Fugacity coefficient** |
| Ethane | 61.2996 | 45.8588 | 175.631 | $7.7663 \times 10^{-11}$ |
| Octane | 123.159 | 137.712 | 576.502 | $6.7874 \times 10^{-15}$ |
| Decane | 132.946 | 167.892 | 718.678 | $8.7752 \times 10^{-17}$ |

**Figure 5.6: Bifurcation diagram of ethane at 1atm for SAFT-VR Mie equation of state.**

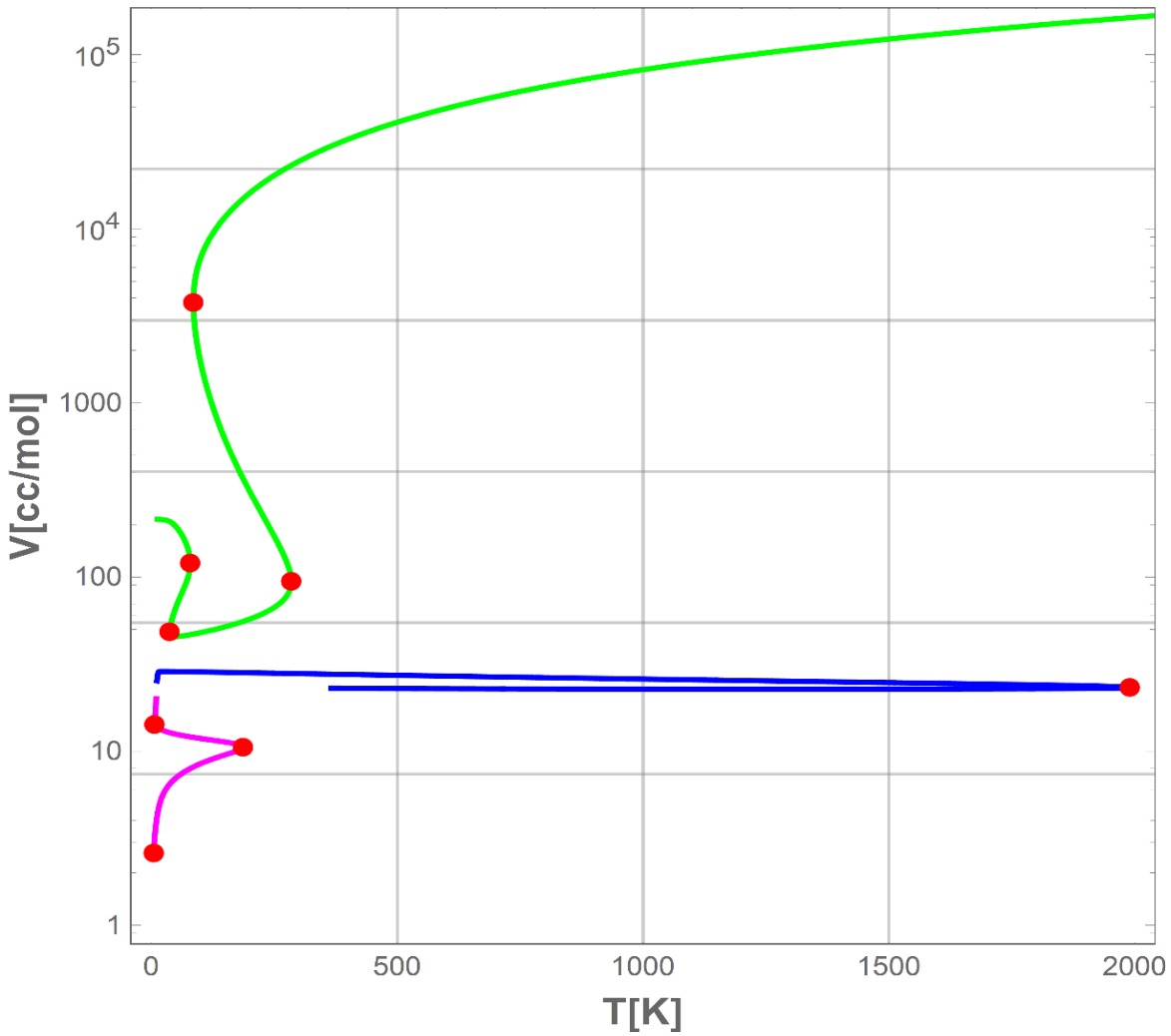

**Figure 5.7: Bifurcation diagram of octane at 1atm for SAFT-VR Mie equation of state.**

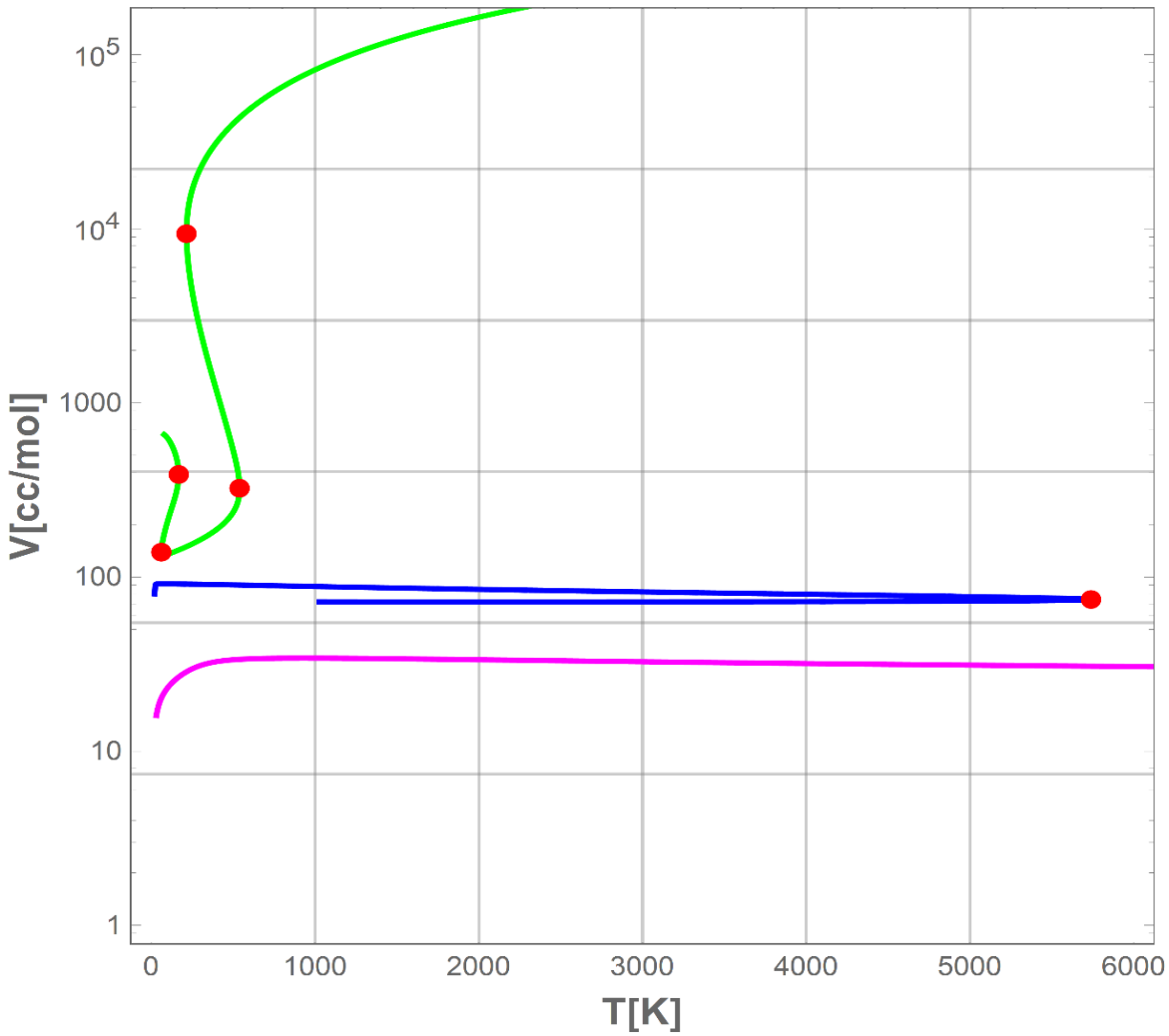

**Figure 5.8: Bifurcation diagram of decane at 1atm for SAFT-VR Mie equation of state.**

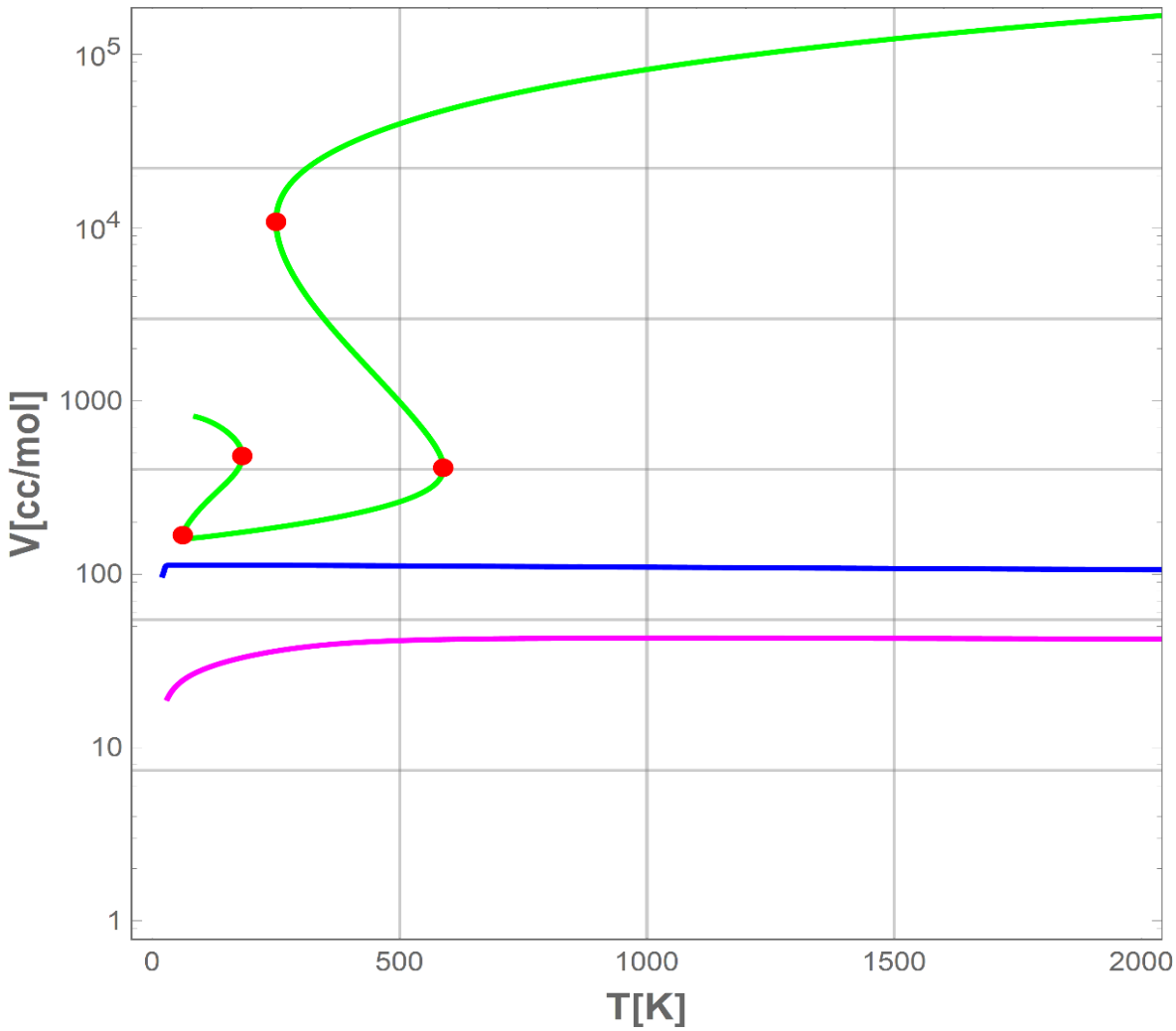

## 5.4 A systematic method to exclude non-physical roots

One of the main challenges associated with the application of SAFT equations of state in simulators is the long computation time needed to examine the stability of the obtained volume roots in order to determine the physical one. These tedious calculations become more difficult as the number of volume roots increases. One of the main advantages of the PVT solution behaviour of SAFT-VR Mie equation of state, compared to soft-SAFT and SAFT-LJ3, is that all non-physical branches exceed the maximum packing fraction of fluids ($\eta = 0.494$). This feature is demonstrated by plotting the bifurcation diagrams of several components along with the minimum allowable volume for fluids (figures **5.9** to **5.12**). In this way, the volume roots are examined by calculating the packing fraction:

$$\eta = \frac{\pi\, N_{av} m_s d}{6\, V} \quad (5.1)$$

where $d$ is the diameter, $N_{av}$ is the Avogadro's number, $m_s$ is the chain length and $V$ is the molar volume. If the packing fraction exceeds the limit of fluids (0.494), the volume root is immediately rejected. This method will significantly reduce the time and cost of computation and simplify the implementation of SAFT-VR Mie equation of state in simulators.

**Figure 5.9: Bifurcation diagram of methane at 1atm for SAFT-VR Mie equation of state with physical limit.**

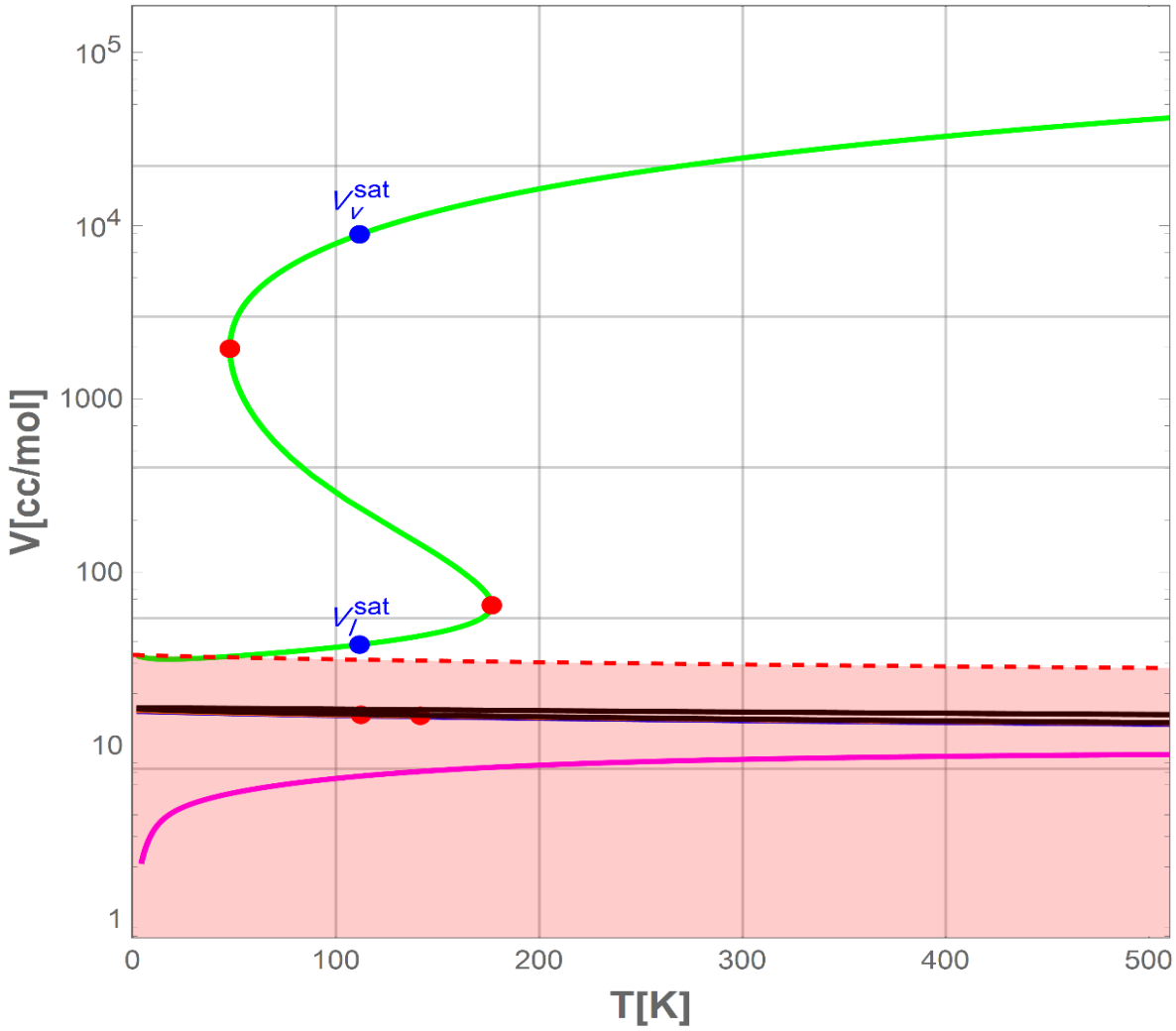

**Figure 5.10: Bifurcation diagram of ethane at 1atm for SAFT-VR Mie equation of state with physical limit.**

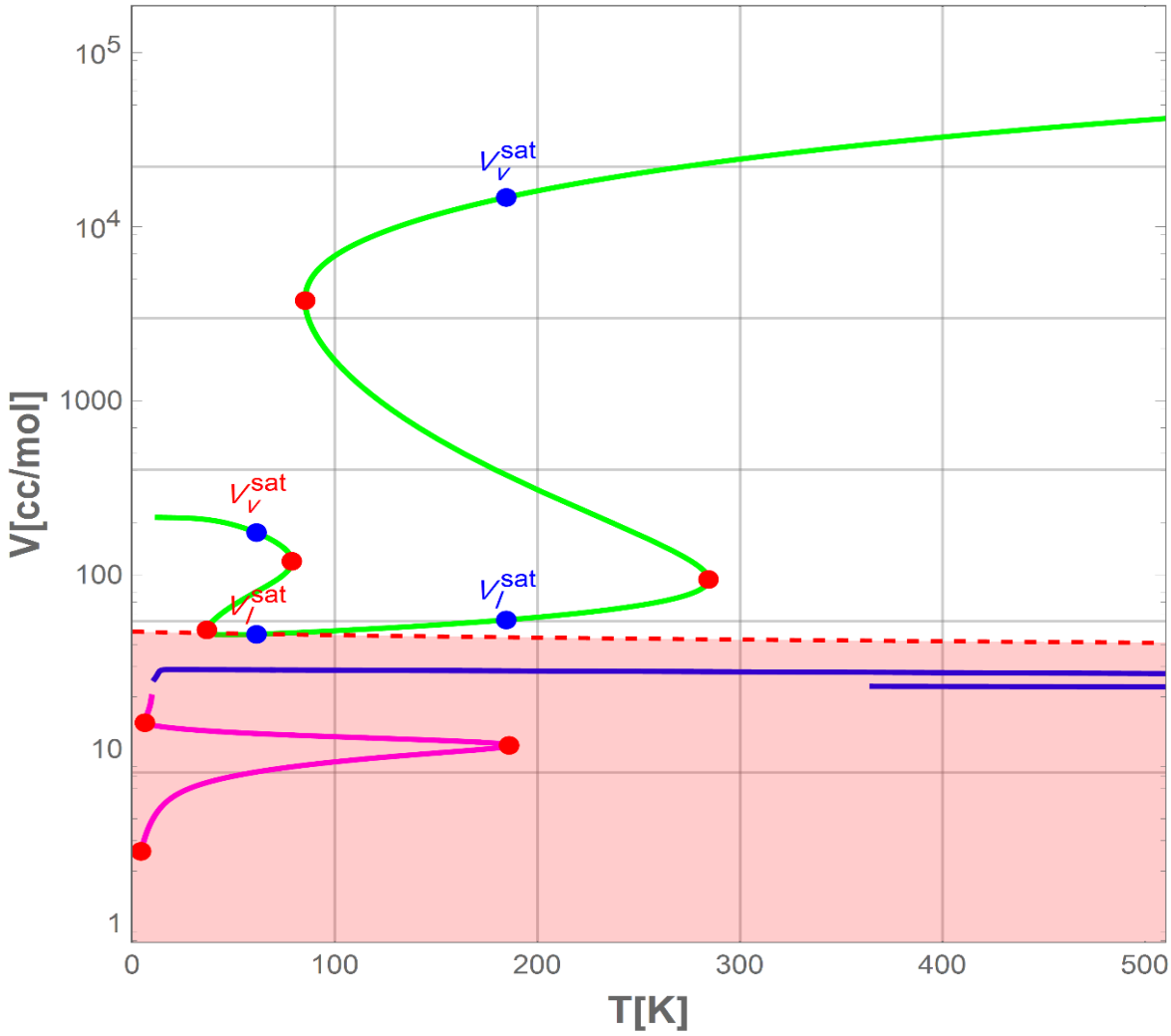

**Figure 5.11: Bifurcation diagram of octane at 1atm for SAFT-VR Mie equation of state with physical limit.**

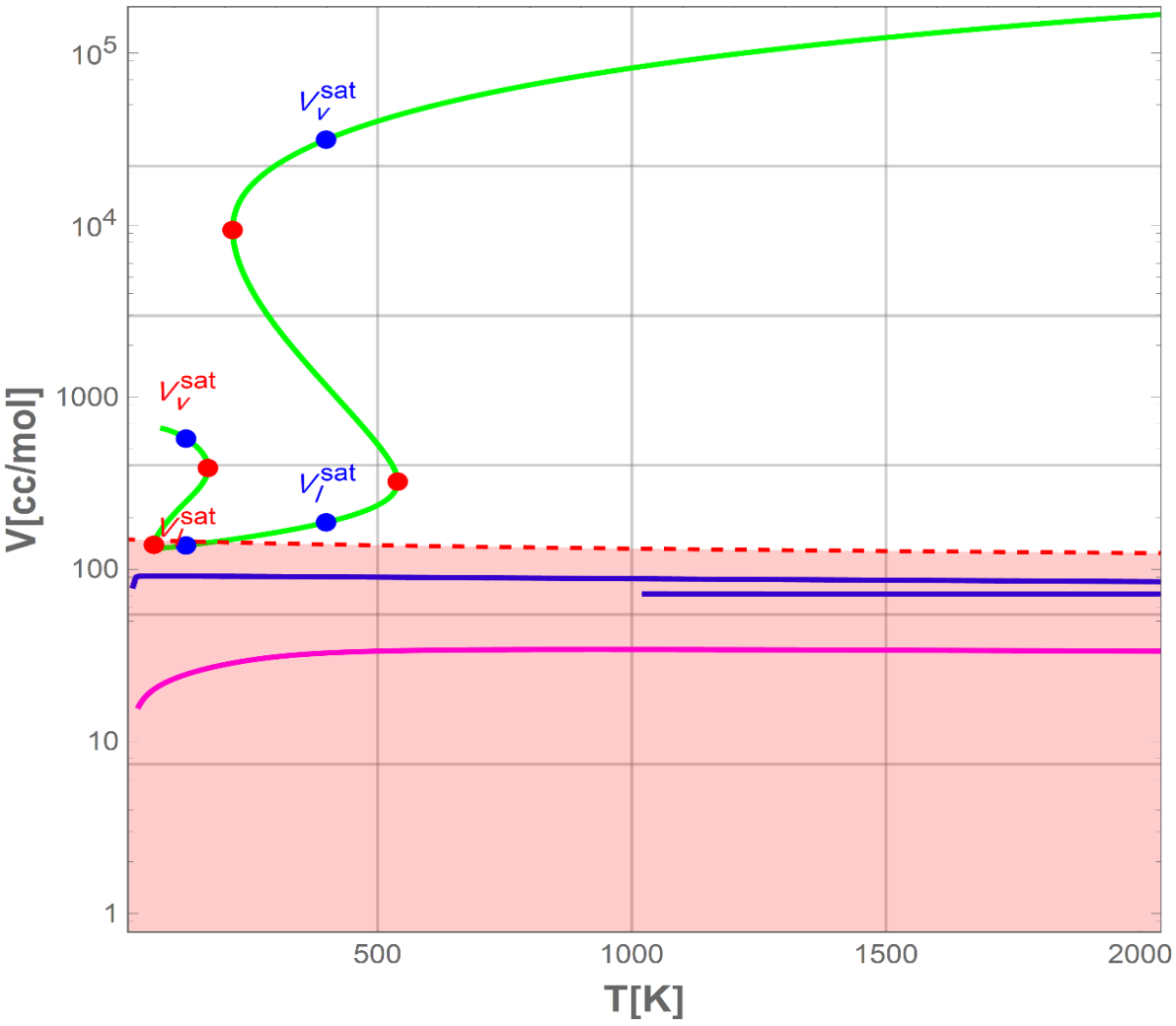

**Figure 5.12: Bifurcation diagram of decane at 1atm for SAFT-VR Mie equation of state with physical limit.**

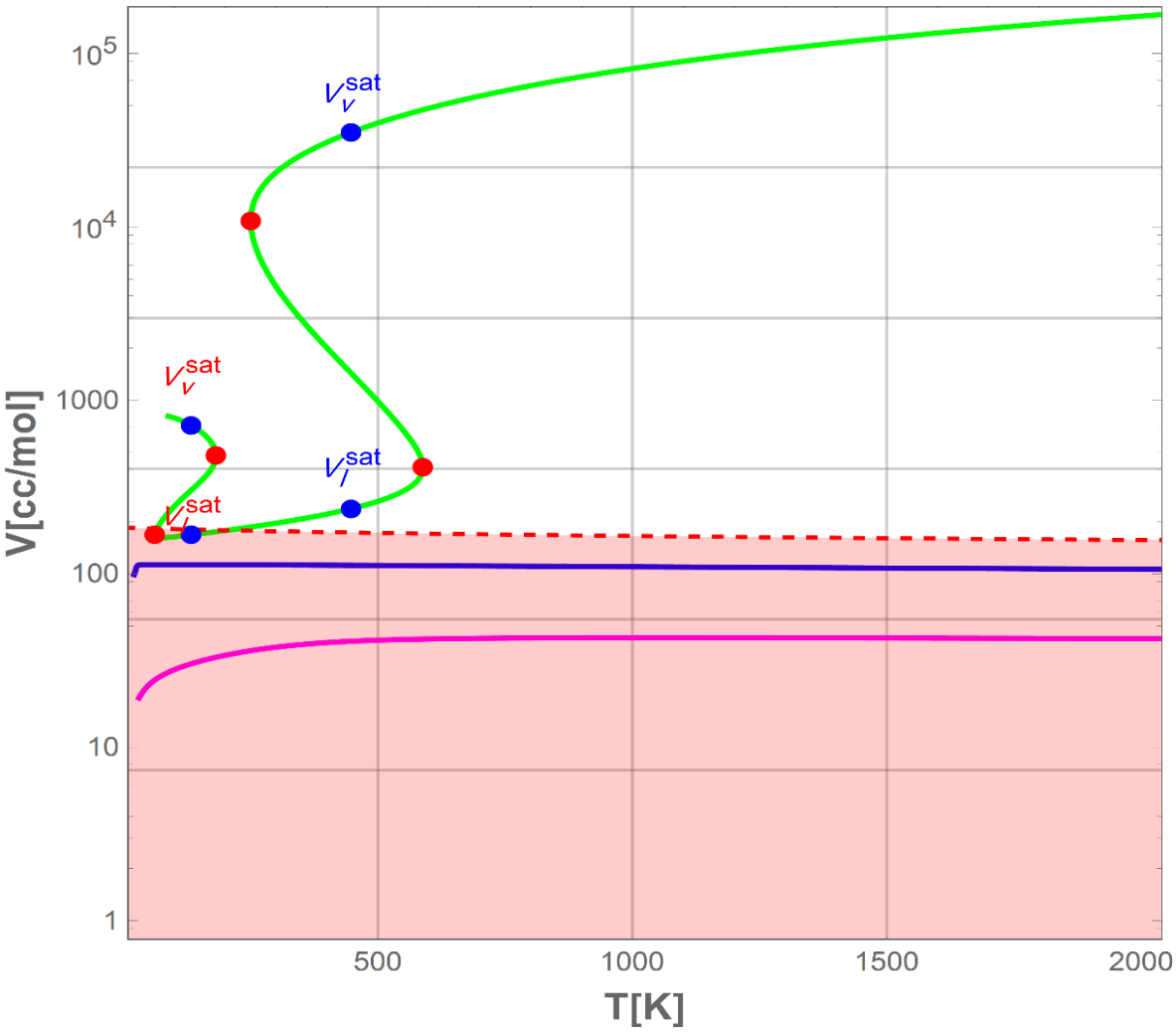

# Chapter 6

# Conclusions and recommendations

## 6.1 Conclusions

In this work, various references and perturbation terms of Wertheim's first order thermodynamic perturbation theory were evaluated by investigating their PVT solution behavior. The work was focused on Lennard-Jones and Mie potentials. In particular, the soft-SAFT, SAFT-LJ3 and SAFT-VR Mie equations of state were analyzed by studying the loci of their PVT solutions. Both the soft-SAFT and SAFT-LJ3 equations of state are based on Lennard-Jones potential while SAFT-VR Mie is based on Mie potential. The reason for selecting these models in this work is the fact that Lennard-Jones and Mie potentials accurately describe the real interactions between molecules. Since Lennard-Jones potential is a special case of Mie potential, the SAFT-VR Mie equation of state can be considered as a Lennard-Jones model (SAFT-VR Mie-LJ) if the repulsive and attractive exponents are fixed at 12 and 6; respectively.

In this study, the volume roots loci of all models were obtained by bifurcation diagrams in which the temperature is selected as the bifurcation parameter while the pressure is fixed. Bifurcation diagrams are generated with the aid of arc-length continuation method as well as Wagon's method for finding all the roots. The Wagon's method was proved to be a reliable technique to locate all volume roots.

The PVT solution behaviors of the three Lennard-Jones models (soft-SAFT, SAFT-LJ3 and SAFT-VR Mie-LJ) were studied and compared. While the soft-SAFT and SAFT-

LJ3 were mainly empirically constructed by fitting molecular simulation data in their dispersion terms as well as their pair-correlation functions at contact, the SAFT-VR Mie-LJ was developed on more sound theoretical ground. This fact is clearly reflected on the solution behavior of these models. Both the soft-SAFT and SAFT-LJ3 equations of state exhibit non-physical behavior especially for short chains. The non-physical behavior is most probably due to the chain term implemented in the soft-SAFT and SAFT-LJ3 equations of state (K. Johnson et al., 1994).

Despite the fact that these models are equivalent in terms of accuracy (Felipe J. Blas & Vega, 1998), their solution behaviors are quite different. The SAFT-LJ3 equation of state was found to be less problematic than soft-SAFT in conducting vapor-liquid equilibrium calculations since it does not exhibit any non-physical multi-phase regions on its physical branch for non-spherical components. Nonetheless, none of these two models, the soft-SAFT and SAFT-LJ3 equations of state, was free from exhibiting high number of volume roots. Indeed, these non-physical volume roots are unfortunately close in value to the stable roots. The reason behind this non-physical behavior is the empirical mathematical structure of the dispersion and chain terms.

On the other hand, the SAFT-VR Mie-LJ equation of state, exhibits a more physical PVT behavior. Although non-physical volume roots do exist in the SAFT-VR Mie-LJ equation of state, their values are far enough from the real ones so they can be distinguished easily. These results gave a good reason to investigate the complete form of the SAFT-VR Mie.

The study of the SAFT-VR Mie equation of state considered various factors including the effect of the repulsive exponent in the Mie potential on the locus of the PVT

solution. All the non-physical volume roots exhibited by the SAFT-VR Mie equation of state were found beyond the limit of maximum packing fraction of fluids (0.494). This unique feature of the solution behavior of the SAFT-VR Mie equation of state can be utilized to build an efficient algorithm for finding stable volume roots. However, the study revealed that the SAFT-VR Mie is not free form exhibiting multiple phase separation regions although (Lafitte et al., 2013) claimed that the model is free from this deficiency. Because this additional phase separation region was found without a critical point, it could be considered as a liquid-solid demixing region.

## 6.2 Recommendations

The analysis of the PVT solution behavior of various versions of the SAFT equations of state led to some suggestions and recommendations for improving the solution behavior of these models and simplifying their implementation in solvers and process simulators. First of all, the radial distribution function at contact adopted in the soft-SAFT and SAFT-LJ3 equations of state has either to be replaced or re-constructed because its impact on the PVT solution behavior is very misleading. Another technique for improving the solution behavior of these models, which depend on fitting of molecular simulation data, is to avoid polynomial fitting and replace it with simpler mathematical forms. Regarding the SAFT-VR Mie equation of state, it is recommended to develop a solver that implements the modified Wagon's method, presented in this work, limiting the search interval between the fluid limit (packing fraction equals 0.494) and the volume of ideal gas. This technique ensures catching all the physical volume roots and excluding all the non-physical ones.

# Bibliography


Allgower, E. L., & Georg, K. (1990). *Numerical continuation methods : an introduction*. Berlin ; New York: Springer-Verlag.

Barker, J. A., & Henderson, D. (1967). Perturbation Theory and Equation of State for Fluids: The Square-Well Potential. *THE JOURNAL OF CHEMICAL PHYSICS, 47*(8), 2856-2861.

Blas, F. J., & Vega, L. F. (1997). Thermodynamic behavior of Homonuclear and Heteronuclear Lennard-Jones Chains with Association Sites from Simulation and Theory. *Molecular Physics, 92*, 135-150.

Blas, F. J., & Vega, L. F. (1998). Prediction of binary and ternary diagrams using the statistical associating fluid theory (SAFT) equation of state. *Industrial & Engineering Chemistry Research, 37*(2), 660-674 %@ 0888-5885.

Button, J., & Gubbins, K. (1999). SAFT prediction of vapour-liquid equilibria of mixtures containing carbon dioxide and aqueous monoethanolamine or diethanolamine. *Fluid Phase Equilibria, 158*, 175-181.

Byun, H.-S., Hasch, B., & McHugh, M. (1996). Phase behavior and modeling of the systems CO 2-acetonitrile and CO 2-acrylic acid. *Fluid Phase Equilibria, 115*(1), 179-192.

Carnahan, N. F., & Starling, K. E. (1969). Equation of State of non-attracting Rigid Spheres. *Journal of Chemical Physics, 51*, 635-636.

Chandler, D. (1978). Structures of molecular liquids. *Annual Review of Physical Chemistry, 29*(1), 441-471 %@ 0066-0426X.

Chapman, W. G., Gubbins, K. E., Jackson, G., & Radosz, M. (1989). SAFT: Equation- of-State Solution Model for Associating Fluids. *Fluid Phase Equilibria, 52*, 31-38.

Chapman, W. G., Gubbins, K. E., Jackson, G., & Radosz, M. (1990). New reference equation of state for associating liquids. *Industrial and Enginering Chemistry Research, 29*, 1709.

Chapman, W. G., Jackson, G., & Gubbins, K. E. (1988). Phase equilibria of associating fluids - Chain molecules with multiple bonding sites. *Molecular Physics, 65*, 1057.

Chen, S. J., Economou, I. G., & Radosz, M. (1992). Density-tuned polyolefin phase equilibria. 2. Multicomponent solutions of alternating poly (ethylene-propylene) in subcritical and supercritical olefins. Experiment and SAFT model. *Macromolecules, 25*(19), 4987-4995.

Clements, P. J., Zafar, S., Galindo, A., Jackson, G., & McLure, I. A. (1997). Thermodynamics of ternary mixtures exhibiting tunnel phase behaviour Part 3.—Hexane–hexamethyldisiloxane–perfluorohexane. *Journal of the Chemical Society, Faraday Transactions, 93*(7), 1331-1339.

Economou, I. G., & Donohue, M. D. (1992). Equation of state with multiple associating sites for water and water-hydrocarbon mixtures. *Industrial & Engineering Chemistry Research, 31*(10), 2388-2394.

Economou, I. G., Gregg, C. J., & Radosz, M. (1992). Solubilities of solid polynuclear aromatics (PNA's) in supercritical ethylene and ethane from statistical associating fluid theory (SAFT): toward separating PNA's by size and structure. *Industrial & Engineering Chemistry Research, 31*(11), 2620-2624.

Fu, Y. H., & Sandler, S. I. (1995). A simplified SAFT equation of state for associating compounds and mixtures. *Industrial and Engineering Chemistry Research, 34*, 1897-1909.

Gil-Villegas, A., Galindo, A., Whitehead, P. J., Jackson, G., & Burgess, A. N. (1997). Statistical Associating Fluid Theory for Chain Molecules with Attractive Potentials of Variable Range. *Journal of Chemical Physics, 106*(10), 4168-4186.

Goldman, J. I., & White, J. A. (1988). Equation of state for the hard-sphere gas. *Chemical Physics, 89*(10), 6403.

Gregg, C. J., Stein, F. P., Chen, S. J., & Radosz, M. (1993). Phase equilibria of binary and ternary n-alkane solutions in supercritical ethylene, 1-butene, and ethylene+ 1-butene. Transition

from type A through LCST to U-LCST behavior predicted and confirmed experimentally. *Industrial & Engineering Chemistry Research, 32*(7), 1442-1448.

Gross, J., & Sadowski, G. (2001). Perturbed-chain SAFT: An equation of state based on a perturbation theory for chain molecules. *Industrial and Engineering Chemistry Research, 40*, 1244-1260.

Gross, J., & Sadowski, G. (2002). Application of the Perturbed-Chain SAFT Equation of State to Associating Systems. *Industrial and Engineering Chemistry Research, 41*, 5510-5515.

Huang, S., & Radosz, M. (1991). Phase behavior of reservoir fluids V: SAFT model of CO 2 and bitumen systems. *Fluid Phase Equilibria, 70*(1), 33-54.

Huang, S. H., & Radosz, M. (1990). Equation of State for Small, Large, Polydisperse and Associating Molecules. *Industrial and Engineering Chemistry Research, 29*, 2284.

Huang, S. H., & Radosz, M. (1990). Equation of state for small, large, polydisperse, and associating molecules. *Industrial & Engineering Chemistry Research, 29*(11), 2284-2294.

Huang, S. H., & Radosz, M. (1991). Equation of state for small, large, polydisperse, and associating molecules: extension to fluid mixtures. *Industrial and Engineering Chemistry Research, 30*(8), 1994-2005.

Isa, A. A. (2015). *Bifurcation and Stability Analysis of Multiple Molar Volume Roots for Statistical Associating Fluid Theory.* (Master), King Fahd University of Petroleum and Minerals.

Johnson, J. K., Mueller, E. A., & Gubbins, K. E. (1994). Equation of state for Lennard-Jones chains. *The Journal of Physical Chemistry, 98*(25), 6413-6419 %@ 0022-3654.

Johnson, J. K., Zollweg, J. A., & Gubbins, K. E. (1993). The Lennard-Jones equation of state revisited. *Molecular Physics, 78*(3), 591-618 %@ 0026-8976.

Johnson, K., Muller, E. A., & Gubbins, K. E. (1994). Equation of state for Lennard–Jones chains. *The Journal of Physical Chemistry, 98*, 6413-6419.

Khoshkbarchi, M. K., & Vera, J. H. (1997). A simplified hard-sphere equation of state meeting the high and low density limits. *Fluid Phase Equilibria, 130*(1-2), 189–194.

Kolafa, J., & Nezbeda, I. (1994). The Lennard-Jones fluid: An accurate analytic and theoretically-based equation of state. *Fluid Phase Equilibria, 100*, 1-34 %@ 0378-3812.

Kraska, T., & Gubbins, K. E. (1996). Phase equilibria calculations with a modified SAFT equation of state. 1. Pure alkanes, alkanols, and water. *Industrial & Engineering Chemistry Research, 35*(12), 4727-4737 %@ 0888-5885.

Lafitte, T., Apostolakou, A., Avendaño, C., Galindo, A., Adjiman, C. S., Müller, E. A., & Jackson, G. (2013). Accurate statistical associating fluid theory for chain molecules formed from Mie segments. *THE JOURNAL OF CHEMICAL PHYSICS, 139*(15), 154504.

Lafitte, T., Bessieres, D., Piñeiro, M. M., & Daridon, J.-L. (2006). Simultaneous estimation of phase behavior and second-derivative properties using the statistical associating fluid theory with variable range approach. *THE JOURNAL OF CHEMICAL PHYSICS, 124*(2), 024509 %@ 020021-029606.

Lee, S.-H., LoStracco, M. A., & McHugh, M. A. (1994). High-Pressure, Molecular Weight-Dependent Behavior of (Co) polymer-Solvent Mixtures: Experiments and Modeling. *Macromolecules, 27*(17), 4652-4658.

Lisal, M., Aim, K., Mecke, M., & Fischer, J. (2004). Revised equation of state for two-center Lennard–Jones fluids. *International Journal of Thermophysics, 25*, 159-173.

Liu, W.-B., Li, Y.-G., & Lu, J.-F. (1999). A new equation of state for real aqueous ionic fluids based on electrolyte perturbation theory, mean spherical approximation and statistical associating fluid theory. *Fluid Phase Equilibria, 158*, 595-606.

Liu, Z.-P., Li, Y.-G., & Chan, K.-Y. (2001). Equation of state for nonpolar, polar, chain, and associating fluids based on the dipolar Yukawa potential. *Industrial & Engineering Chemistry Research, 40*(3), 973-979.

Malijevsky, A., & Veverka, J. (1999). New equations of state for pure and binary hard-sphere fluids. *Physical Chemistry Chemical Physics, 1*, 4267-4270.

Mansoori, G., & Canfield, F. (1969). Variational approach to the equilibrium thermodynamic properties of simple liquids. I. *THE JOURNAL OF CHEMICAL PHYSICS, 51*(11), 4958-4967.

Mecke, M., Müller, A., Winkelmann, J., Vrabec, J., Fischer, J., Span, R., & Wagner, W. (1996). An accurate van der Waals-type equation of state for the Lennard-Jones fluid. *International Journal of Thermophysics, 17*(2), 391-404 %@ 0195-0928X.

Müller, E. A., & Gubbins, K. E. (2000). 12 Associating fluids and fluid mixtures. *Experimental Thermodynamics, 5*, 435-477.

Pan, C., & Radosz, M. (1999). Modeling of solid–liquid equilibria in naphthalene, normal-alkane and polyethylene solutions. *Fluid Phase Equilibria, 155*(1), 57-73.

Peng, D. Y., & Robinson, D. B. (1976). A New Two-constant Equation of State. *Industrial & Engineering Chemistry Fundamentals, 15*, 58-64.

Percus, J. K., & Yevick, G. J. (1958). Analysis of classical statistical mechanics by means of collective coordinates. *Physical Review, 110*(1), 1.

Polishuk, I. (2010). About the numerical pitfalls characteristic for SAFT EOS models. *Fluid Phase Equilibria, 298*(1), 67-74 %@ 0378-3812.

Pradhan, D., Chen, C.-k., & Radosz, M. (1994). Fractionation of polystyrene with supercritical propane and ethane: Characterization, semibatch solubility experiments, and SAFT simulations. *Industrial & Engineering Chemistry Research, 33*(8), 1984-1988.

Privat, R., Conte, E., Jaubert, J.-N., & Gani, R. (2012). Are safe results obtained when SAFT equations are applied to ordinary chemicals? Part 2: Study of solid–liquid equilibria in binary systems. *Fluid Phase Equilibria, 318*, 61-76 %@ 0378-3812.

Privat, R., Gani, R., & Jaubert, J.-N. (2010). Are safe results obtained when the PC-SAFT equation of state is applied to ordinary pure chemicals? *Fluid Phase Equilibria, 295*(1), 76-92 %@ 0378-3812.

Rambaldi, S., Salustri, G., & Benedetti, C. (2006). Hard sphere gas state equation. *Physica A, 361*(1), 180–194.

Rasaiah, J., & Stell, G. (1970). Upper bounds on free energies in terms of hard-sphere results. *Molecular Physics, 18*(2), 249-260.

Sandler, S. I. (2010). *An introduction to applied statistical thermodynamics*: John Wiley & Sons.

Soave, G. (1972). Equilibrium Constants from a Modified Redlich-Kwong Equation of State. *Chemical Engineering Science, 27*, 1197-1203.

Tang, Y., & Lu, B. C. (1997). Analytical description of the Lennard-Jones fluid and its application. *AIChE Journal-American Institute of Chemical Engineers, 43*(9), 2215-2226.

Tang, Y., Tong, Z., & Lu, B. C. Y. (1997). Analytical equation of state based on the Ornstein-Zernike equation. *Fluid Phase Equilibria, 134*(1), 21-42 %@ 0378-3812.

Wagon, S. (2010). *Mathematica® in Action: Problem Solving Through Visualization and Computation*: Springer Science & Business Media.

Wang, X. Z. (2002). van der Waals–Tonks-type equations of state for hard-disk and hard-sphere fluids. *Physical Review E, 66*(3), 31203

Weeks, J. D., Chandler, D., & Andersen, H. C. (1971). Role of Repulsive Forces in Determining the Equilibrium Structure of Simple Liquids. *THE JOURNAL OF CHEMICAL PHYSICS, 54*(12), 5237-5247.

Wertheim, M. S. (1984a). Fluids with Highly Directional Attractive Forces. I. Statistical Thermodynamics. *Journal of statistical physics, 35*, 19.

Wertheim, M. S. (1984b). Fluids with Highly Directional Attractive Forces. II. Thermodynamic Perturbation Theory and Integral Equations. *Journal of statistical physics, 35*, 35.

Wertheim, M. S. (1986a). Fluids with Highly Directional Attractive Forces. III. Multiple Attraction Sites. *Journal of statistical physics, 42*, 459.

Wertheim, M. S. (1986b). Fluids with Highly Directional Attractive Forces. IV. Equilibrium Polymerization. *Journal of statistical physics, 42*, 477.

Wu, C.-S., & Chen, Y.-P. (1994). Calculation of vapor-liquid equilibria of polymer solutions using the SAFT equation of state. *Fluid Phase Equilibria, 100*, 103-119.

Xu, G., Brennecke, J. F., & Stadtherr, M. A. (2002). Reliable Computation of Phase Stability and Equilibrium from the SAFT Equation of State. *Industrial and Engineering Chemistry Research, 41*, 938-952.

Yelash, L., Müller, M., Paul, W., & Binder, K. (2005). Artificial multiple criticality and phase equilibria: an investigation of the PC-SAFT approach. *Physical Chemistry Chemical Physics, 7*(21), 3728-3732.

Yelash, L. V., & Kraska, T. (2001). A generic equation of state for the hard-sphere fluid incorporating the high density limit. *Physical Chemistry Chemical Physics, 3*(15), 3114-3118.

# Nomenclature

| | |
|---|---|
| $a$ | Helmholtz free energy |
| $Z$ | Compressibility factor |
| B | Second virial coefficient |
| d | Effective hard sphere dimeter |
| g | Pair correlation function at contact |
| k | Boltzmann's constant |
| $\varepsilon$ | Dispersion energy |
| $m, m_s$ | Chain length |
| $N_{Av}$ | Avogadro's number |
| λa | Attractive exponent |
| λr | Repulsive exponent |
| T | Temperature |
| $\sigma$ | Segment diameter |
| $\eta$ | Packing fraction |
| V | Volume |
| T* | Reduced temperature |
| $\rho$ | Density |
| $\rho^*$ | Reduced density |

**Subscripts**

| | |
|---|---|
| Mie | Mie potential |
| LJ | Lennard-Jones potential |
| res | Residual |
| disp | Dispersion |
| assoc | Association |

# Vitae


| | |
|---|---|
| Name | : MOHAMMED FAHAD AL KHATER |
| Nationality | : Saudi |
| Date of Birth | : 20/09/1990 |
| Email | : m.f.alkhater@gmail.com |
| Address | : Jubail, King Faisal North St. |
| Academic Background | : Chemical Engineering |